THE UNIVERSITY
of EDINBURGH

Declaration

This is to certify that the work contained within has been composed by me and is entirely my own work. No part of this thesis has been submitted for any other degree or professional qualification.

Signed:

Nicole Elizabeth Lennon Sime

Abstract

Sushi, von Willebrand factor type A, epidermal growth factor and pentraxin domain containing 1 (SVEP1) is an extracellular matrix protein which may bind to cell surface molecules such as integrins. A non-synonymous single amino acid polymorphism in the Svep1 gene is associated with a 14% increased risk of coronary heart disease, a 13% higher risk of type 2 diabetes and a 1mmHg increase in systolic blood pressure. Expression of the SVEP1 gene is increased in the kidney in the Cyp1a1mRen2 rat model of diabetes and hypertension previously developed in our lab. SVEP1 is also known to be upregulated in human diabetic nephropathy and is upregulated in rodent models of renal fibrosis. I hypothesized that Svep1 played a role in renal fibrosis, diabetes and blood pressure. Hence, the primary goal of this thesis was to investigate the role of SVEP1 and in the pathogenesis of diabetes, hypertension and renal fibrosis.

Svep1 gene expression is increased in the kidney in the DOCA-salt-angII-uninephrectomy model of hypertension and following UUO. SVEP1 hemizygous mice showed no differences in expression of pro-fibrotic genes after UUO compared to wildtype littermates. No overt metabolic phenotype was exhibited by the Svep1 hemizygous mice, however there was a significant decrease in fat depot weights after high fat diet (HFD) and a significant increase in blood glucose concentrations during the glucose tolerance test at the 12 week time point in hemizygous Svep1 mice compared with wild-type controls. After telemetry analysis of blood pressure no difference was seen in blood pressure but SVEP1$^{+/-}$animals had an increased heart rate of 100 beats per minute compared to wildtype animals.

Svep1 expression is increased in the kidney in models of hypertension and fibrosis, however loss of one Svep1 allele did not alter the severity of fibrosis in the UUO model or significantly alter glucose tolerance after high fat diet. However, the high fat diet experiment was a pilot study and should be repeated with a larger number of animals.

In addition, generation of a mouse with the human point mutation could determine the mechanisms by which this extracellular matrix protein confers risk of diabetes and hypertension.

Lay Summary

This thesis was undertaken to study a little known gene- SVEP1 and its role in diabetes and kidney injury. Small inherited changes in the Svep1 structure are associated with increased risk of heart disease, diabetes and high blood pressure in humans. Expression of the SVEP1 gene was increased in the kidney in a rat model of diabetes and hypertension. I wished to determine the mechanisms by which Svep1 might alter risk of kidney disease, diabetes and high blood pressure.

A mouse model of high blood pressure was developed to assess whether Svep1 gene expression was increased in the kidney by high blood pressure. A mouse which had only one copy of the SVEP1 gene (hemizygous mice) rather than the usual two copies (wild-type mice) was employed to determine if a reduction in SVEP1 changed the risk of diabetes or high blood pressure. Calorie usage, activity, food intake and body weight were measured in both hemizygous and wild-type mice to determine if any differences existed. Blood glucose and insulin were also measured to determine whether the hemizygous mice were more prone to diabetes. Blood pressure was measured in the mice to determine if a reduction in SVEP1 caused a difference in blood pressure.

SVEP1 expression was shown to be increased in kidney tissue from mice with high blood pressure. In mice with scarred kidneys SVEP1 expression was also increased. Similarly, SVEP1 expression was increased in the kidney in patients with diabetic nephropathy. No differences in kidney scarring were seen between mice which had only one copy of SVEP1 compared with mice with the normal two copies. Mice with one copy of the SVEP1 gene tended to have higher blood sugar levels and smaller fat depots. However, to be certain that the trends observed were valid, further studies employing a larger number of mice will need to be performed to assess the role of the Svep1 gene in the development of type 2 diabetes.

Acknowledgements

Firstly I owe an immense amount of thanks and gratitude to my primary supervisor Bryan for his constant encouragement, teaching and mentoring. Your ability to guide me and support me has been second to none and I thank you for the hours you have dedicated to developing my scientific endeavours. At every hurdle you were there with support, encouragement and a fresh outlook on the project. I would also like to thank my second supervisor John. Thank you John for believing in me (when I most likely didn't believe in myself). Thank you for asking the questions which made me think and helped develop my scientific knowledge and ability to critique both my own work and the work of others. You are a wealth of knowledge and direction. I am truly grateful to have had such excellent supervision during my PhD and could not have asked for a greater supervisory committee. I am also immensely grateful to Prof Nik Morton for his guidance which was essential to my metabolism work. Thanks go to the BHF for my financial support of my BHF studentship.

I am grateful to have had the best lad support available- Carolynn there are not words for how immensely helpful you have been- both in lab technical advice and general life management. You are a very special person and this thesis has greatly improved from your sound technical advice. Thank you for all the time you have spent with me explaining and demonstrating. Marie-Louise thanks for being a great lab partner. Julie Litterfair (McNairn) thank you for the coffee and support throughout this project. To past and present Hughes lab- a big thank you for your support- Boris, Peng, Fiona and of course Prof Hughes, thank you for your support and input to my project.

To the molecular physiology group: thank you for your help and assistance and great banter in the lab. Audrey thank you for all your assistance mainly in finding things I didn't know we had or something I had lost!

To my office and honorary office buddies: Seb, Scott and Emma- thanks for the coffee and life chats and the ability to bounce my scientific ideas off you all at lunch or on coffee break. Charlotte, Jess, Morag, Adrienne and Cristina don't know what I would do without you.

Finally, thank you to my family for endless love and support. My school girls for being there to listen and brighten my weekends. Jamie, Kieran and Aramis thanks for being there when I needed you, for distraction when I needed it most and for being the best boys- I am lucky to have you.

Table of Contents

List of Figures

List of Tables

Chapter 1: Introduction

1.1 Kidneys in Health

The kidneys are a key organ in regulating homeostasis in the body. They filter the blood, removing the waste products and control total body salt and water content thereby playing a leading role in blood pressure regulation. In addition, they regulate electrolyte concentration, maintain acid-base balance, activate vitamin D and promote erythropoiesis through production of erythropoeitin.

The functional unit in the kidney is the nephron, there are approximately 1 million nephrons in each adult human kidney. The nephron is comprised of the glomerulus, which harbours the filtering apparatus of kidney, and the tubule, which is lined by specialized cells that are responsible for reabsorption of water and small molecules from urine into the peritubular capillaries and secretion of waste from the blood to the urine. Approximately 125mls of plasma is filtered every minute (180 L/day), with the vast majority of filtered electrolytes and water being reabsorbed in the tubules.

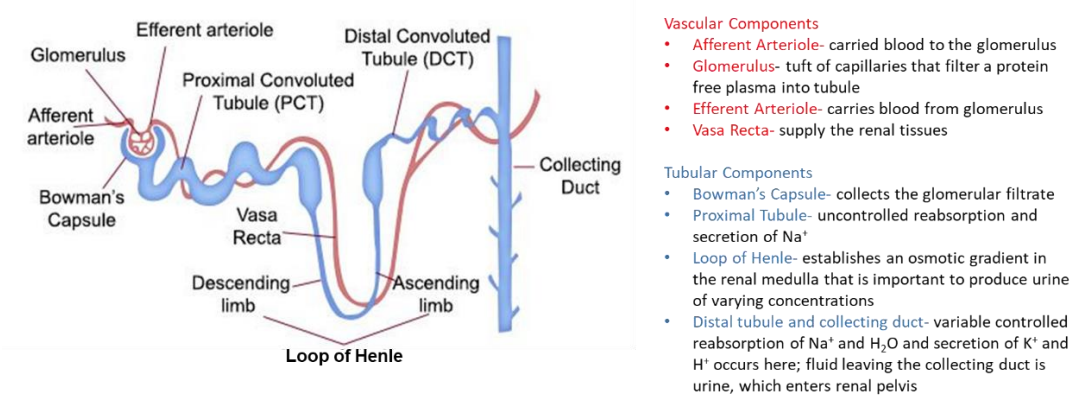

Figure 1 1 Schematic of a nephron detailing the vascular components and the tubular components adapted from (Sherwood, 2010)***.***

The kidneys main function is to maintain homeostasis in extracellular fluid (ECF) and produce urine and the nephron is the functional unit that facilitates this. There is both a vascular and tubular component (Figure 1.1) (Sherwood, 2010). The vascular component begins with the afferent arteriole which supplies blood to the glomerulus.

The glomerulus is a tuft of capillaries through which water and solutes are filtered from passing blood. The filtered fluid passes onto the tubule where it will eventually be converted to urine. Glomerular capillaries join the efferent arterioles where blood that is not filtered in the tubular component leaves and joins the peritubular capillaries supplying the renal tissues with oxygenated blood. The tubular component is formed by a single layer of epithelial cells. The tubular component begins with the Bowman's capsule which collects filtered fluid from the glomerular capillaries and delivers filtered fluid to the proximal tubules located in the cortex of the kidney, this then leads to the loop of Henle located in the medulla of the kidney. The loop of Henle transfers the fluid through the juxtaglomerular apparatus which leads onto the distal tubule which empties into the collecting duct which is responsible for the delivery of urine to the renal pelvis for excretion.

Three basic renal processes occur in the nephron- glomerular filtration, tubular reabsorption and tubular secretion (Sherwood, 2010). Glomerular filtration is the first step in urine formation, blood flows through the glomerular capillaries and the protein-free plasma filters through the glomerulus to the Bowman's capsule. This process is indiscriminate- water, nutrients, electrolytes and waste products enter the tubule lumen (Sherwood, 2010). When the filtered fluid flows through the tubule, tubular reabsorption occurs where substances of value are reabsorbed and returned to the peritubular capillaries (Sherwood, 2010). Tubular secretion also occurs to eliminate substances from the plasma. Tubular reabsorption and secretion are highly discriminate and work on filtrate to return to the blood a fluid of composition and volume necessary to maintain homeostasis of internal fluid environment (Table 1.1) (Sherwood, 2010) (Zacchia, 2018). Tubular reabsorption occurs through transepithelial transport and active transport through the Na^+-K^+ ATPase pump (Sherwood, 2010).

Substance	Average % of filtered substance reabsorbed	Average % of filtered substance excreted
Water	99	1
Sodium	99.5	0.5
Glucose	100	0
Urea	50	50
Phenol	0	100

Table 1 1 Table of the fates of various substances filtered by the kidneys (Sherwood, 2010)**.**

The kidneys are controlled both hormonally and by sympathetic nerve activity. Sympathetic nerve fibres innervate the renal vasculature, tubules and juxtaglomerular granular cells. Specific adrenoreceptors relay renal sympathetic nerve activity which in turn decreases renal blood flow and glomerular filtration rate (GFR), increases renal tubular sodium and water reabsorption and increases renin release (Johns *et al,*. 2011).

An important hormonal modulator of blood pressure homeostasis is the renin-angiotensin aldosterone system (RAAS). A fall in blood pressure results in renal secretion of the hormone renin which promotes sodium chloride retention in the kidney, through angiotensin and aldosterone secretion (Figure 1.2). The RAAS is key in regulating sodium- the granular cells of the juxtaglomerular apparatus secrete renin into the blood in response to a fall in NaCl/ECF/blood pressure (Sherwood, 2010). An increase in renin is an indication for the need to expand plasma volume- to return arterial pressure to normal (Sherwood, 2010). An increase in renin causes increased Na^+ absorption via the distal and collecting tubules. Salt retention osmotically promotes H_2O retention thus helps restore plasma volume rendering it an important long-term control of blood pressure.

Renin works as an enzyme to activate angiotensinogen (always present in the plasma) into angiotensin I (ANG I), on passing through the lungs via the pulmonary circulation, ANG I is converted to angiotensin II (ANG II) by angiotensin converting enzyme (ACE) which is abundant in pulmonary capillaries (Sherwood, 2010). ANG II is the main stimulus for the secretion of aldosterone (Crowley *et al.*, 2006). Aldosterone

works on the principal cells of the distal and collecting tubules (Sherwood, 2010). Aldosterone increases the reabsorption of Na^+ and K^+ secretion, through insertion of additional Na^+channels into the luminal membranes and additional Na^+ K^+ ATPase pumps in the basolateral membranes (Crowley *et al.*, 2006). This leads to a greater passive and active inward flux of Na^+ out of cells and into the plasma, which leads to salt retention, water retention and an increase in blood pressure. The RAAS is an example of a negative feedback loop as it works to alleviates factors which triggered the release of renin, once this has been achieved renin release ceases. In normal homeostasis renin secretion is inhibited (Sherwood, 2010).

Renin causes increased levels of ANG II into circulation (Weir and Dzau, 1999). ANG II is a potent vasoconstrictor which directly increases blood pressure by increasing total peripheral resistance through constriction of systemic arterioles (Crowley *et al.*, 2006). It also stimulates thirst and vasopressin (a hormone that increases water retention by the kidneys) which works to increase plasma volume expansion and increase blood pressure (Weir and Dzau, 1999).

1.2 The Kidney in Disease

Kidney disease can broadly be described as acute or chronic.

Acute kidney injury (AKI) is most commonly the result of a complication of another serious illness, such as autoimmune diseases or shock due to sepsis, trauma, or cardiac failure (Nie *et al.*, 2017). It may also be caused by nephrotoxins or a blockage of the urinary tract. Persons who are most susceptible to AKI include those aged over 65, and those with existing chronic kidney disease (CKD), diabetes, liver or heart failure (Nie *et al.*, 2017). Diagnosing AKI can be achieved through blood tests and measuring urine volume. A reduced urine volume would be indicative of AKI as would rises in creatinine, a product of muscle metabolism that is excreted by the kidneys. It is important to diagnose and treat the cause of AKI quickly in order to avoid further renal injury and the renal damage in AKI is potentially reversible if the cause is promptly treated (Nie *et al.*, 2017).

Chronic kidney disease (CKD) derives from various pathologies which have a negative impact on kidney function such as hypertension, diabetes, recurrent infection, glomerulonephritis, polycystic kidney disease, blockage of urine flow (kidney stones or prostatic hypertrophy) and long term use of some medications such as lithium and non-steroidal anti-inflammatories (NSAIDS) (Zoccali *et al.*, 2017).

CKD is often asymptomatic until renal function is severely reduced and is typically diagnosed through blood and urine tests (Lloyd *et al.*, 2010). Serum creatinine is measured to estimate the glomerular filtration rate (eGFR) which is a commonly used clinical readout of kidney function. Urine is collected to determine the albumin: creatinine ratio as elevated urinary albumin concentration is the hallmark of disease affecting the glomerular filtration barrier.

CKD can be categorized into stages 1-5. In stage 1 and stage 2 the eGFR is normal (>90 or >60ml/min/1.73m^2, respectively) but other assessments detect kidney damage (such as albuminuria or multiple cysts detected on ultrasound scan). In stage 3 and stage 4 CKD the eGFR is reduced to between 30-59 or 15-29 ml/min/1.73m^2, respectively). Patients with stage 5 CKD have an eGFR less than 15ml/min/1.73m^2 which shows kidneys have lost almost all their function, therefore this is known as end-stage renal disease (ESRD) (Zoccali *et al.*, 2017).

Stage	GFR (ml/min normalised to an average surface area of 1.73m^2	Description	Treatment
1	90+	Normal kidney function, albuminuria/structural abnormalities or genetic predisposition to kidney disease	Observation, control blood pressure.
2	60-89	Mildly reduced kidney function and finding as described in stage 1 suggesting kidney disease	Observation, control of blood pressure and other risk factors.
3A 3B	45-59 30-44	Moderately reduced kidney function	Observation, control of risk factors.
4	15-29	Severely reduced kidney function	Planning of end-stage renal failure treatment and treating complications such as anaemia and renal bone disease.
5	<15 or on dialysis	Very severe or endstage kidney failure	Monitoring, dialysis or kidney transplant.

Table 1 2 Classification of CKD stages- adapted from the Renal Association website (http://www.renal.org/information-resources/the-uk-eckd-guide/ckd-stages#sthash.bA12bcEW.1sC5BgRE.dpbs)

The prevalence of CKD is almost 1 in 10 in England, and this prevalence rises with age in those aged over 75 years and above (Aitken *et al.*, 2014). Hence, with an aging

population the number of people developing CKD will continue to increase. Patients with CKD are more susceptible to cardiovascular disease (CVD) - indeed, they are more likely to die from a cardiac event than progress to ESRD (Zoccali *et al.*, 2017). Therefore, it is essential that we study cardiovascular and renal disease in conjunction to better understand the pathophysiology of the condition so that we can develop new treatments.

Treatment of CKD is limited and there is no cure. Progression of CKD can be slowed by adopting a healthy diet and lifestyle and controlling the injurious stimuli; however, once the disease has progressed to stage 5, transplant or dialysis are the only long-term treatment options (National Kidney Foundation, 2002). Some patients with multiple co-morbidities would not survive transplant surgery and they may elect not to undergo dialysis as it may not substantially improve their prognosis (O'Connor and Kumar, 2012).

1.3 Regulation of Blood Pressure

Blood pressure homeostasis is determined by the kidneys through the regulation of sodium chloride excretion and the impacts of this on the extracellular fluid volume (ECFV). When arterial pressure is increased there is an increase in urine volume (pressure diuresis) and also an increase in the amount of sodium chloride excreted by the kidneys (pressure natriuresis) to return the arterial pressure to normal (Guyton *et al.*, 1972). This is a system of infinite feedback gain described by Guyton *et al* 1984, who proposed that the kidneys are the predominant regulator of blood pressure homeostasis (Guyton *et al.*, 1972). The kidneys also regulate blood pressure through controlled release of renin from specialised cells in the juxtaglomerular apparatus. A fall in blood pressure results in renal secretion of the hormone renin which activates the angiotensin-aldosterone system to promote sodium retention and vasoconstriction (Figure 1 1).

The RAAS system has been a target for anti-hypertensive medications such as angiotensin converting enzyme (ACE) inhibitors which act to inhibit the conversion of angiotensin I to angiotensin II or angiotensin II receptor antagonists, which prevent the action of angiotensin on target organs (Figure 1 1).

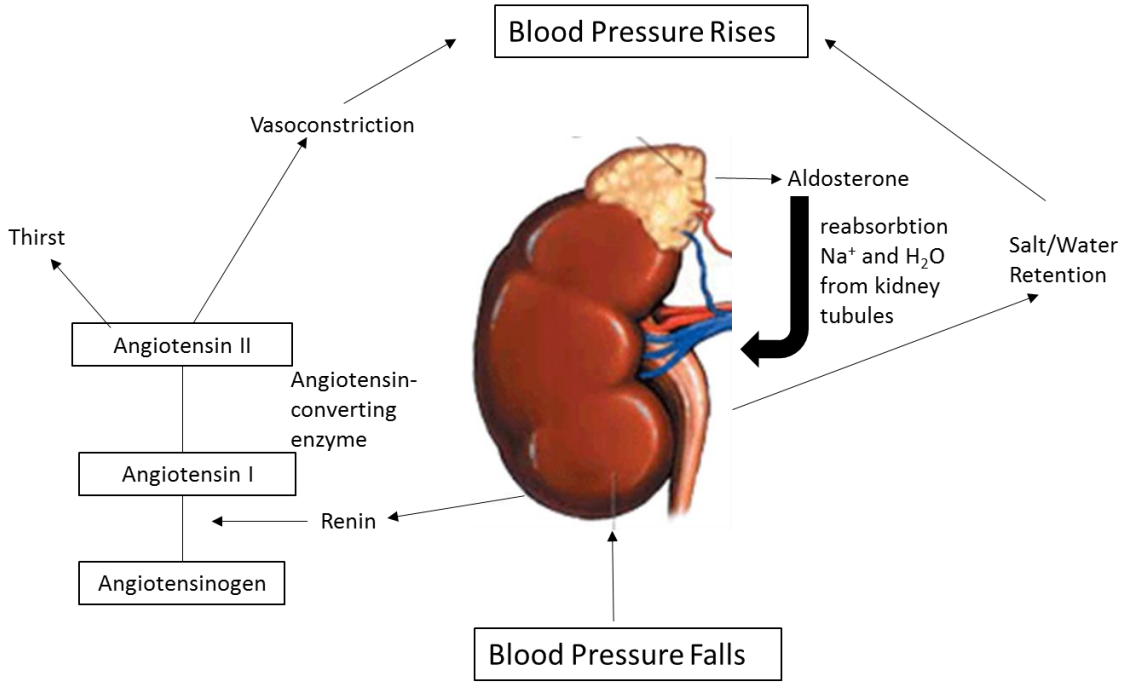

Figure 1 2 Regulation of blood pressure adapted from Davidsons Principals and Practice of Medicine.

1.4 Hypertension

Hypertension is a major contributor to cardiovascular and chronic kidney disease (Nahas and Bello, 2010). The World Health Organisation (WHO) presents hypertension as one of the leading causes of premature death worldwide. In Scotland one third of the adult population has high blood pressure- this has remained constant since 2003(http://www.scotpho.org.uk/clinical-risk-factors/high-blood-pressure/data/prevalence). Hypertension is defined as chronically elevated blood pressure of above 140/90mmHg (Mancia *et al.*, 2013).

Category	Systolic (mmHg)	Diastolic (mmHg)
Normal	Less than 120	Less than 80
Pre-hypertensive	120-139	80-89
Hypertensive	>140	>90

Table 1 3 Regulation of blood pressure adapted from Davidsons Principals and Practice of Medicine.

Hypertension is a powerful cardiovascular risk factor leading to adverse cardiovascular events such as ischemic heart disease and stroke(Tirschwell *et al.,* 2001). It is reported that an increase of 20/10mmHg in blood pressure doubles the risk of cardiovascular disease (Lewington *et al.,* 2002). Therefore small increments in blood pressure can cause lasting damage. High blood pressure has been shown to increase progression of almost all forms of kidney disease (Turner *et al.*, 1998).

In a minority of cases, hypertension is secondary to a specific kidney, endocrine, vascular or genetic disorder (Omuru *et al.,* 2004), but in approximately 95% of patients, there is no known cause and this is known as 'essential hypertension' (Mancia *et al.*, 2013). The pathophysiology of essential hypertension is complex due to the many interactions including neural, hormonal and paracrine mechanisms that interact to regulate cardiovascular and renal function (Navar, 2005).

There are a variety of mechanisms attributed to the development of hypertension reported in the literature such as kidney disease leading to salt and water retention, increase in vascular resistance, genetic susceptibility and environmental factors such as dietary salt intake(Ohta *et al.*, 2010) .

The RAAS systems plays a significant role in salt and water retention in kidney disease along with vascular resistance (Ghazi and Drawz, 2017). ANG II has a direct effect on renal vascular smooth muscle cells which causes vasoconstriction of both the afferent and efferent arterioles which causes glomerular capillary hypertension and reduced

renal blood flow (RBF). The effect at the medullary level is enhanced reabsorption of salt and water stimulated by multiple nephron segments (Mennuni *et al.*, 2014). ANG II directly promotes salt and water retention in the proximal tubule and stimulates secretion of aldosterone which causes reabsorption of sodium and water from the distal tubule. It also promotes expression of renal endothelin-1 (ET-1) which is a potent vasoconstrictor peptide with pro-inflammatory and pro-fibrotic actions (Mennuni *et al.*, 2014).

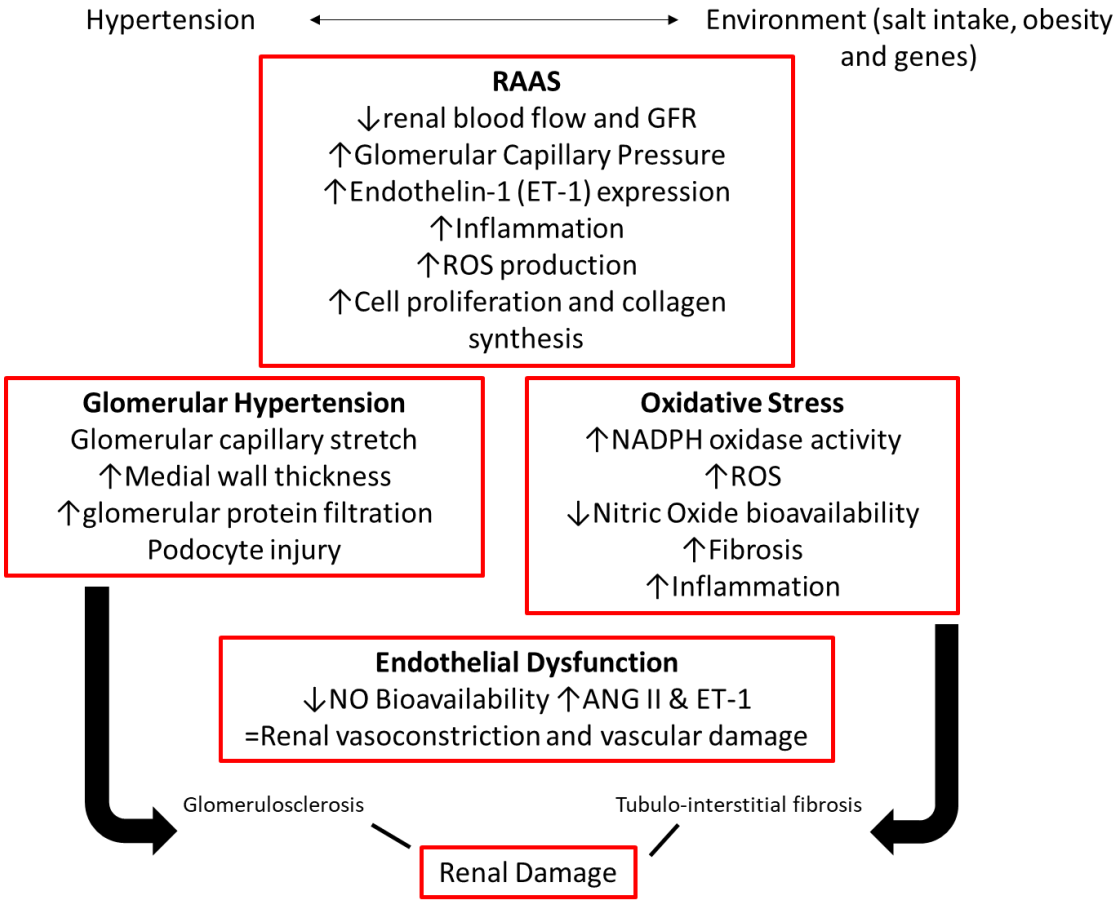

Figure 1 3 Schematic representation of mechanisms involved in development of hypertensive renal injury- adapted from Mennuni et al 2013 (Mennuni et al. 2013).

Genetic traits can attribute to hypertension- salt sensitivity is characterised by blood pressure increases after salt loading and blood pressure decrease after salt depletion. Salt sensitivity (SS) is reported as a cardiovascular risk factor independent of blood pressure (Laffer *et al.*, 2016). SS affects a quarter of the normotensive adult population and more than half of all hypertensive patients (Weinberger *et al.*, 1986). One opinion

on the pathophysiology of SS is that individuals with SS require a higher to maintain salt balance via pressure natriuresis, due to a defect in single or multiple physiological natriuretic systems (Laffer *et al.*, 2016). However, the possibility that a shift in pressure natriuresis depends on defective renal sodium (Na^+) excretion has not been proven with any certainty (Laffer *et al.*, 2016). The hemodynamic pattern of SS hypertension is one of relative vasoconstriction, or impaired vasodilation in response to normal salt-induced increase in cardiac output(Sullivan *et al.*, 1987). SS is associated with elevation of forearm vascular resistance and attenuation of the microcirculation- subjects with SS hypertension had lower conjunctival capillary density compared with normotensive salt resistant (SR) individuals (Sullivan *et al.*, 1987).

Rarely hypertension can be caused by Mendelian mutations which cause defects in renal sodium handling and mainly effect the nephron. Syndromes such as Liddle, glucocorticoid-remediable aldosteronism (GRA) and hypertension exacerbated in pregnancy are caused by genetic defects which mainly affect the mineralocorticoid receptor (Lifton, Gharavi and Geller, 2001). This receptor is the main regulator of ENaC activity and is activated by aldosterone. GRA is an autosomal dominant trait which results in early onset hypertension (Lifton, Gharavi and Geller, 2001). Exogenous glucocorticoid completely suppresses aldosterone secretion. The mutation effects the gene which encodes aldosterone synthase- the rate limiting enzyme for aldosterone synthesis- this leads to expanded plasma volume and hypertension. Liddle syndrome describes an autosomal dominant mutation which is associated with early onset hypertension (Lifton, Gharavi and Geller, 2001). It presents with hypokalemic alkalosis, suppressed plasma renin activity and low plasma aldosterone levels. Hypertension exacerbated in pregnancy is a mutation in the ligand binding domain of the mineralocorticoid receptor which gives an autosomal dominant form of hypertension (Lifton, Gharavi and Geller, 2001). This mutation causes hypertension to be markedly accelerated during pregnancy.

Hypertension has also been linked to lifestyle factors such as salt consumption and a close relationship has been established between dietary intake of sodium and high blood pressure (Mozaffarian *et al.*, 2014). The optimal daily intake of sodium salt

(NaCl) is thought to be 6-7g (Lawrence *et al.*, 1997). Dahl *et al* were one of the first to observe the evidence for the role of sodium chloride intake and human hypertension(Dahl and Love, 1954). Previously salt intake has been linked to experimental models of hypertension. Dahl *et al* notes that hypertension was not evident in primitive groups such as Greenland Eskimos and Australian Aboriginals which had relatively low salt diets compared to western society which adds large quantities of salt to food (Dahl and Love, 1954). Restricting salt intake has also been reported to reduce blood pressure (Ohta *et al.*, 2010). Historically salt intake was roughly one-twentieth of that consumed today in developed countries (Mancilha *et al*,. 1989). Prevention of sodium loss may have previously conferred a selective advantage in salt-poor environments, and the enrichment for sodium-preserving genes may contribute to hypertension in the salt-rich environment of western society today. Insulin has also been reported to play a role in retaining sodium by suppressing sodium loss in urine via the renal tubules (DeFronzo, 1981).

In hypertension the system has been reset so that the arterial pressure norm is higher therefore the kidneys work to keep blood pressure within the elevated range (Andresen and Yang, 1989). The kidneys are protected from fluctuations in blood pressure by auto-regulatory glomerular afferent arteriole contraction which occurs by myogenic responses and tubuloglomerular feedback (Mennuni *et al.*, 2014). The extent of the kidney damage due to hypertension is proportional to the degree of arterial pressure transmission to the renal microvasculature and therefore the control of the microvasculature tone is important (Mennuni *et al.*, 2014). The mechanisms by which high blood pressure mediates hypertensive renal injury remains unknown, but may involve increased cyclical cell stretch or shear stress thereby activating pro-fibrotic pathways, promoting inflammation or increasing oxidative stress (Mennuni *et al.*, 2014).

Hypertension can cause the initiation of a vicious cycle of injury where the injury to the kidney causes a further increase in blood pressure (Townsend, 2015) (Calhoun *et al.*, 2008).

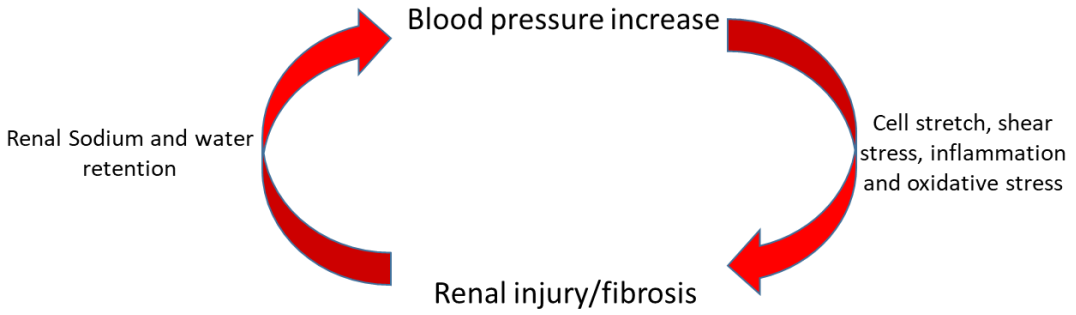

Figure 1 4 Hypertension initiates a vicious cycle where renal injury is caused by high blood pressure and this injury causes further hypertension due to inadequate renal salt excretion.

Hypertension frequently causes kidney injury. The injury caused can range from low grade injury to malignant nephropathy. The severity of injury may be influenced by several factors such as individual susceptibility, degree and duration of hypertension, and the aetiology of the underlying kidney disease (Mennuni *et al.*, 2014). Nephrosclerosis is observed in the majority of patients with longstanding hypertension. It ranges from early focal ischemic glomerular obsolescence to progressive nephron loss over time (Bidani and Griffin, 2004). Malignant nephrosclerosis occurs with very severe hypertension, with the renal phenotype presenting as acute disruptive vascular and glomerular injury with prominent fibrinoid necrosis and thrombosis (Bidani and Griffin, 2004).

1.5 Treatment of Hypertension

The treatment of hypertension can be complex requiring multiple anti-hypertensive medications. It has been reported that 30% of adults in the USA have hypertension but in only half of this group has target blood pressure achieved through intervention (Edwards *et al.*, 2014). The first anti-hypertensive agents were developed in the 1950s and were the β-blockers and diuretic agents. In a large study comparing pharmacological agents and blood pressure control- ALLHAT study- thiazide diuretics were found to be "superior" to ACE inhibitors and calcium channel blockers in preventing one or more major forms of cardiovascular disease in high risk patients with hypertension or hypertension accompanied by diabetes (Edwards *et al.*, 2014). Thiazide diuretics are well tolerated and relatively inexpensive and are therefore the first line in treatment of hypertension. Thiazides work by inhibiting sodium chloride

transport in the distal convoluted tubule by binding and inhibiting the sodium chloride cotransporter. This causes an increase in the excretion of sodium and water helping to reduce blood pressure.

Angiotensin converting enzyme (ACE) inhibitors are commonly used in patients with proteinuria and patients with diabetes and microalbuminuria (James *et al.*, 2014). They work to competitively inhibit the conversion of angiotensin I to angiotensin II, a potent vasoconstrictor. They prevent the compensatory angiotensin II mediated vasoconstriction of glomerular efferent arterioles that takes place in order to maintain glomerular perfusion pressure, and hence selectively reduce glomerular pressure beyond their generic blood pressure-lowering effect (Regulski *et al.*, 2015).

However, treatments currently available are unable to address the renal fibrosis caused by hypertension.

1.6 Regulation of Blood Glucose

Glucose metabolism is critical to normal physiological functioning and is the fundamental cellular energy source. Dietary sugars are digested and the glucose released is absorbed through the gut wall and then distributed throughout the body, with excess being stored as glycogen in the liver which is available for rapid release into the circulation in the fasting state (Sherwood, 2010). The liver is the major metabolic regulatory organ, with 85% of endogenous glucose production being derived from the liver by glycogenolysis (glycogen to glucose) and gluconeogenesis (glucose formation from non-carbohydrate sources) which contributes equal to the basal rate of hepatic glucose production (Sherwood, 2010). The liver does not require insulin to facilitate glucose uptake, it does need insulin to regulate glucose output. If insulin concentration is low, hepatic glucose output rises.

The kidney has the ability to release glucose into the blood- plasma glucose continuously passes through the kidney and must be reabsorbed to prevent loss. The kidney reabsorbs glucose at the proximal tubule and allows the elimination of excess glucose by facilitating excretion in urine (Sherwood, 2010).

Blood glucose is maintained mainly by hormones and the central and peripheral nervous system to meet metabolic requirement. Insulin and glucagon are the most relevant hormones. Insulin is produced in the Islets of Langerhans by the beta cells of the pancreas. Secretion of insulin controls the metabolism of carbohydrates, proteins and lipids, and it is tightly regulated by feedback systems which enable stable control (Mathieu, Gillard and Benhalima, 2017). On intake of food, beta cells sense increased blood glucose levels through import of glucose through glucose transporter type 2 (GLUT2) receptors on their surface, and this stimulates the release insulin into the blood (Mathieu, Gillard and Benhalima, 2017). Glucagon is produced by the alpha cells in the Islets of Langerhans in the pancreas. Glucagon is produced in response to low normal glucose levels or hypoglycaemia. It works to increase glucose levels by accelerating glycogenolysis and promoting gluconeogenesis (Sherwood, 2010).

Insulin works to reduce blood glucose by accelerating transport of glucose into insulin sensitive cells and facilitating its conversion to storage compounds via glycogenesis (conversion of glucose to glycogen) and lipogenesis (fat formation). Conversely, it also suppresses endogenous (primarily hepatic) glucose production. Basal insulin secretion maintains metabolism in an anabolic state (Mathieu, Gillard and Benhalima, 2017).

Major glucose uptake (>80%) in peripheral tissue occurs in the muscle (Bouzakri and Zierath, 2005). Skeletal muscle cannot release glucose into the circulation but is able to uptake glucose which is critical for dealing with sudden increases in plasma glucose (Bouzakri and Zierath, 2005). Adipose tissue helps maintain total body glucose homeostasis by regulating the release of free fatty acids (which increase gluconeogenesis) from stored triglycerides, influencing insulin sensitivity in muscle and liver (Goossens, 2008).

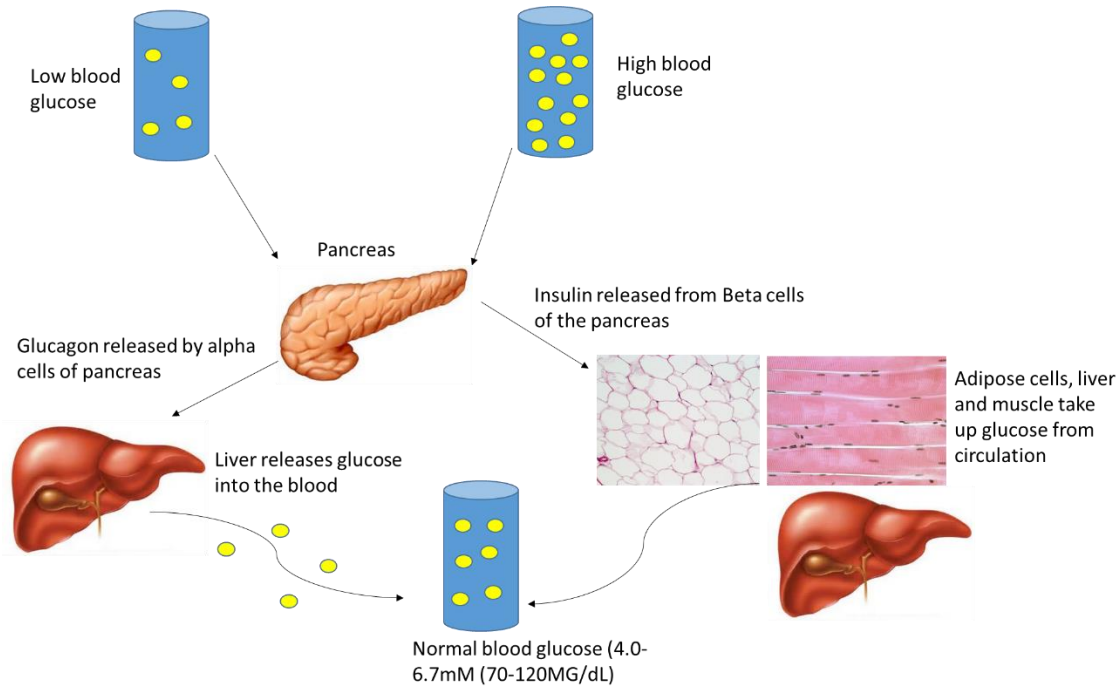

Figure 1 5 Schematic representation of the regulation of blood glucose adapted from Davidson's Principals and Practice of Medicine.

1.7 Diabetes

Diabetes can be described as chronic hyperglycemia due to inadequate insulin secretion (deficiency) or diminished tissue response to insulin (resistance) - these factors frequently coexist. Diabetes can be separated into type 1, type 2 and maturity onset of diabetes in the young (MODY). When beta cell secretion of insulin becomes insufficient for the glucose load hyperglycemia ensues characterizing diabetes. Genetic factors can influence whether an individual is susceptible to either type 2 diabetes or type 1 diabetes (Rich, 2006). Obesity is an influential factor in the type 2 diabetes epidemic faced by the western world (Yaturu, 2011).

Type 1 diabetes is commonly diagnosed in children or young adults, and comprises only ~10% of patients in the UK with the disease (Daneman, 2006). Type 1 diabetes is an autoimmune disorder where the insulin-producing pancreatic beta cells are destroyed by the immune system. Therefore, regulating blood glucose concentrations is hindered by lack of insulin secretion. This can result in chronic hyperglycemia and glucotoxicity leading to kidney injury and predisposes to CVD in the form of microvascular and macrovascular complications (Daneman, 2006).

Type 2 diabetes is typified by a gradual decline of beta cell function and mass occurring over time which causes impaired insulin secretion (Meigs *et al.*, 2003). Major contributors in beta cell loss of function are glucotoxicity, lipotoxicity, proinflammatory cytokines, leptin and islet cell amyloid (Triplett *et al*,.2012). Reduced insulin secretion is often aggravated by insulin resistance which is typified by the incapacity of insulin to decrease plasma glucose levels through reduction of hepatic glucose production and stimulation of glucose utilisation in skeletal muscle and adipose tissue (Meigs *et al.*, 2003).

Development of type 2 diabetes is heterogeneous between patients but normally begins with insulin resistance and early phase impaired insulin secretion (Meigs *et al.*, 2003). Transition from normal to impaired glucose tolerance begins with a reduction in insulin sensitivity to about 27% of normal, with chronic hyperglycaemia resulting from a further deterioration of insulin sensitivity and secretion by 51% (Weyer *et al.*, 2001). Increased hepatic glucose output can also play a role. Insulin is normally secreted into the portal vein and taken up by the liver and suppresses hepatic glucose output. When hepatic insulin sensitivity is impaired it continues to release inappropriately high amounts of glucose into the bloodstream which causes hyperglycemia (Gupta *et al.*, 2003).

Adipocyte dysfunction also plays a role in type 2 diabetes development (Hajer, Van Haeften and Visseren, 2008). Adipocytes become resistant to insulin's antilipolytic effect which results in chronically elevated plasma free fatty acid levels which stimulates gluconeogenesis, induces hepatic and muscle insulin resistance and impairs insulin secretion (Hajer, Van Haeften and Visseren, 2008). Furthermore, adipocyte necrosis causes adipose tissue macrophages to release inflammatory cytokines, which promote further adipocyte damage(Feng *et al.*, 2011). Adipocytes then fail to secrete normal amounts of insulin-sensitizing adipokines, such as adiponectin.

Maturity onset diabetes of the young (MODY) is a rare form of diabetes which is strongly familial (Tattersall, 1974). It is generally diagnosed in children and young adults under 25 years of age (Hattersley and Patel, 2017). It is not insulin dependent and is shown to be autosomal dominant in inheritance (Tattersall, 1974). MODY represents between 1.2-3% of diabetes diagnosed in children in a predominantly white

European population (Hattersley & Patel 2017). It is caused by a gene mutation, most commonly in glucokinase (GCK); hepatic nuclear factor 1 alpha, hepatic nuclear factor 4 alpha and hepatic nuclear factor 1 beta (Horikawa *et al.*, 1997). GCK MODY presents with stable raised fasting glucose, whereas transcription factor MODY presents with a deterioration of glucose over time (Hattersley & Patel 2017). Patients with transcription factor MODY also present with glycosuria, fetal macrosomia and neonatal hypoglycaemia (Hattersley and Patel, 2017).

1.8 Diabetic nephropathy

Diabetic nephropathy (DN) is the most common cause of end stage renal disease in the USA (https://www.usrds.org/), and UK (www.renalreg.org/reports). The peak incidence for DN normally occurs in patients who have had diabetes for 10-20years. Patients with DM often develop hypertension and are at a high risk of other comorbidities such as coronary artery disease and obesity(Dinneen and Gerstein, 1997). Hyperglycaemia is thought to play a key role in damaging small blood vessels including in the kidney (American Diabetes Association, 2010). DN therefore often presents in combination with other microvascular complications such as diabetic retinopathy and neuropathy (American Diabetes Association, 2010).

Diabetic nephropathy (DN) is characterised by persistent albuminuria, elevated blood pressure and a progressive decline in glomerular filtration rate (Gross *et al.*, 2005). The earliest pathological change in the kidney is a thickening of the glomerular basement membrane, followed by mesangial expansion due to increased matrix production or impaired matrix degradation due to glycation and cross-linkage of matrix proteins (Alsaad and Herzenberg, 2007). Finally overt glomerular sclerosis will be evident, sometimes including classical nodular glomerulosclerosis (Kimmelstiel-Wilson nodules) (Alsaad and Herzenberg, 2007). The severity of DN can be estimated by the thickness of the basement membrane and the degree of mesangial matrix expansion (Alsaad and Herzenberg, 2007).

Hemodynamic alterations occur in patients with DN (Soldatos and Cooper, 2008). The first evidence is loss of nocturnal dipping which precedes and predicts albuminuria (Empar *et al,*. 2002). This progresses to systemic hypertension, which is an adverse development as it will accelerate progression of renal disease. Independent of

systemic hypertension there is increased intraglomerular pressures induced by haemodynamic effects of hyperglycaemia on the renal vasculature (Fioretto *et al,*. 1992).

Treatment of DN is focused on: i. gaining glycaemic control through blood glucose monitoring and if necessary administering insulin or oral therapy such as metformin; ii. controlling hypertension by reducing dietary salt intake and administration of an antihypertensive medication, with the first choice of agent for those with albuminuria being an inhibitor of the RAAS and iii. minimising cardiovascular risk factors through lifestyle changes (e.g. stopping smoking, losing weight, increasing exercise) and prescription of statins to reduce cholesterol. Salt restriction has been reported to slow the progression of diabetic kidney disease to a similar extent as single drug therapy (Anderson *et al.*, 2009). In advanced cases it may also be important to reduce phosphate and potassium intake. When patients' progress to end stage renal disease (ESRD), renal replacement therapy such as dialysis or transplant is required if this is appropriate taking into account their co-morbidities and life expectancy (Fullerton *et al.*, 2016).

1.9 Renal Fibrosis

Renal fibrosis is common end point in the majority of renal pathologies. There is a strong correlation between the degree of interstitial fibrosis and subsequent loss of renal function (Eddy *et al.*, 2012). Understanding of the mechanisms by which renal fibrosis occurs should enable the development of new therapies to reduce the number of people progressing to CKD and eventually end-stage renal disease (ESRD).

Common presentations of renal fibrosis are glomerulosclerosis and tubulointerstitial fibrosis (Efstratiadis *et al.*, 2009). Glomerulosclerosis causes loss of the surface area in the glomerulus available for filtration, leading to a reduction in the glomerular filtration rate however, this pathophysiology has been better correlated with interstitial fibrosis (Fukagawa *et al.*, 1999). Interstitial fibrosis interferes with the normal function of the tubules, preventing secretion of toxins and the passage of nutrients from the circulation (Duffield, 2014). Arterioles also undergo fibrosis- known as arteriolosclerosis which results in the loss of autoregulation of blood flow and reduced

perfusion, which may exacerbate renal hypoxia and promote further renal injury (Duffield 2014).

Renal fibrosis can be described as an excessive accumulation and deposition of extracellular matrix and is both cellular and molecular in mechanism (Duffield, 2014). It is thought to derive from a wound healing response that does not resolve (Farris and Colvin, 2013). The chronic fibrogenic cellular process is thought to be detrimental to the nephron and surrounding vasculature, independently from the deposition of pathological matrix(Duffield, 2014). Renal fibrosis can be described in four phases: cellular activation and injury phase, fibrogenic signalling phase, fibrogenic phase and lastly destructive phase (Eddy, 2000).

Renal injury can cause tubular insults which lead to the production and release of pro-inflammatory and injurious molecules that cause interstitial inflammation (Eddy *et al.*, 2012). This inflammation is thought to activate cells to become myofibroblasts, which are thought to be the key cell type that generate matrix in the kidney. In CKD myofibroblasts express markers such as alpha-smooth muscle actin and they may be seen in the interstitium around renal tubules and arterioles (Duffield, 2014). The matrix these myofibroblasts deposit is rich in collagen I and III (Farris and Colvin, 2013). The source of interstitial myofibroblasts is controversial at present. Potential sources of include: activation of mesangial cells, pericytes, and quiescent fibroblasts, influx from a pool of circulating fibrocytes and tubular-mesenchymal and endothelial-mesenchymal transition (Lin *et al.*, 2008). Recent fate mapping studies cast doubt on the origin of myofibroblasts coming from injured tubules through tubular-mesenchymal transition (Humphreys *et al.*, 2010).

1.10 Models of Renal Fibrosis

In order to study renal fibrosis both *in vitro* and *in vivo* models which are able to mimic the human pathology are required. This can be challenging as disease onset and progression can be difficult to model robustly, however modelling certain aspects *in vitro* and *in vivo* can inform future studies and give vital information in understanding the mechanisms of renal injury and fibrosis.

1.10.1 In vitro models of renal fibrosis

Mimicking fibrosis in an *in vitro* setting is difficult to establish and does not encompass the complex environment of fibrosis *in vivo* but creates a starting point to look at the cellular mechanisms of fibrosis. The complete picture of fibrogenesis *in vivo*, requires the deposited collagen to form a fibrillar matrix that becomes cross-linked and can be remodelled and resorbed. The key choices in attempting to replicate this in an *in vitro* model include the nature of the cell type(s) and the injurious or fibrotic stimulus employed.

1.10.2 TGFβ1 role in models of renal fibrosis

TGFβ1 is a prototypic profibrotic cytokine and is known to be a major driver of glomerular and tubulointersitial fibrosis in most forms of human chronic kidney disease (CKD) (Böttinger and Bitzer, 2002). TGFβ activation triggers transcription of genes encoding extracellular matrix proteins, inhibitors of matrix-degrading enzymes and matrix-binding integrin receptors. TGFβ is the most important cytokine for accumulation of matrix in renal fibrosis (Strutz *et al.*, 2001). It also promotes transformation of fibroblasts into myofibroblasts; transdifferentiation of tubular epithelial cells into myofibroblasts; and chemotaxis of fibroblasts and monocytes (Eddy *et al.*, 2012).

The blockage of TGFβ1 in animal models of kidney disease has been shown to reduce fibroblast activation and collagen deposition, while its overexpression induces fibrosis (Leask and Abraham, 2004). It works both through a Smad-based (canonical) and non-Smad-based signalling pathway (Leask and Abraham, 2004) . The canonical signalling pathway involves phosphorylation and activation of Smad 2 and 3 by TGFβ receptor 1 (Feng & Derynck 2015). Smad4 binds Smad2/3 enabling the complex to translocate to the nucleus to activate pro-fibrotic gene expression.

TGFβ1 has been described in the literature as a model of fibrosis *in vitro*. TGFβ directly acts on fibroblasts and mesangial cells to induce proliferation, migration, activation and transcription of profibrotic molecules such as collagens, fibronectins and plasminogen activator inhibitor-1 (PAI-1) (Meng, 2014). After treatment with TGFβ a renal fibroblast monolayer is disrupted and migration is induced into nodules

in a dose dependent manner (Xu *et al.*, 2007). These nodules contained interstitial collagens and showed an increased collagen I:IV ratio- similar to that observed in a fibrotic kidney *in vivo*.

1.10.3 Rodent Models of Renal Injury

Developing an *in vivo* model of renal fibrosis and renal pathology is both essential and complex. In order to gain a better understanding of renal injury animal models have been employed to investigate various renal pathologies.

1.10.3.1 Rodent Models of Hypertensive Renal Injury

The cause of hypertension is multifactorial and inconsistent between patients, making the mechanisms that contribute to high blood pressure (BP) difficult to elucidate. Due to the complexity of the environmental and genetic interactions which are thought contribute to blood pressure control and potentially play a role in hypertension, animals models have been at the forefront of investigating mechanism and treatment.

Multiple models of hypertension both genetic and non-genetic have been developed in the mouse and the rat. These models have been developed either as a model of hypertension or as a model of multiple pathologies which commonly present in the clinic such as hypertension and diabetes. Table 2 presents a summary table of references detailing previously reported murine models of hypertension.

Model	MABP Increase	Ref
2 Kidneys 1 Clip	+20mmHg	(Wiesel *et al*. 1997)
DOCA-Salt	+20-35mmHg	(Peng *et al.* 2001)
ANG II Infusion	+45-60mmHg	(Landmesser *et al*. 2002)
High Salt Diet (8%)	+10mmHg	(Yu *et al*. 2004)
L-NAME	+5-25mmHg	(Sethi *et al.* 2006)
Combinatorial Treatment	+50mmHg	(Kirchhoff *et al.*, 2008)

Table 1 4 Table detailing the different animal models of hypertensive renal injury. 2Kidney1Clip model uses a surgical clip to reduce the diameter of the renal artery. DOCA-salt model utilises the synthetic mineralocorticoid derivative in combination with salt loading to cause hypertension. ANG II model utilises administration of angiotensin II to induce hypertension. L-NAME stands for nitro arginine methyl ester which is a nitric oxide inhibitor and is administered orally to induce hypertension. Combinatorial treatment consist of uninephrectomy, angiotensin II administration, DOCA administration and salt loading to induce hypertension in mice. (MABP – mean arterial blood pressure)

Measuring blood pressure in mice can be carried out by telemetry or tail cuff plethysmography. The gold standard for blood pressure measurement in mice is telemetry. This allows continuous monitoring of all blood pressure parameters and heart rate in a conscious, unrestrained mouse. A catheter is implanted into the carotid artery which is in turn connected to a subcutaneously placed transmitter. This allows the short and long-term variability of blood pressure and the cardiac cycle to be analysed (Monassier *et al*., 2006). Telemetry allows more subtle and continuous monitoring of blood pressure however, it is an invasive surgery and requires skilled surgeon to implant the devices.

Tail cuff plethysmography requires repetitive measurement and involves a training period for the animals to provide reliable readings. Tail-cuff plethysmography is designed to record the first appearance of the tail pulse of the mouse during the deflation cycle of the proximal occlusion cuff. The technique relies on either a standard light source or a LED light to record pulse wave signal. The advantages of tail cuff plethysmography over telemetry are the non-invasive nature of the technique and the ability to carry out the technique without specialist surgical training. Tail cuff plethysmography is sufficient to discriminate between hypertensive and normotensive animals but it cannot detect small changes in blood pressure.

C57BL6 mice are reported to be highly resistant to hypertension and hypertension induced renal injury (Hartner *et al.*, 2003), however this strain is commonly used as a background for transgenic reporter mice. Kirchhoff *et al's* model of murine hypertensive renal injury detailed a method of rendering C57BL6 mice hypertensive and inducing renal injury (Kirchhoff *et al.*, 2008). This was the basis for our murine model of hypertension.

1.10. 4 Rodent Models of Fibrosis

The models of fibrosis in the mouse include surgical injuries such as the unilateral ureteral obstruction (UUO) (Chevalier, Forbes and Thornhill, 2009) ischemia reperfusion injury (IRI) (Eddy *et al.*, 2012) and subtotal nephrectomy models (Ma and Fogo, 2003), immune-mediated (e.g. glomerulonephritis) (Tam, 1999) or administration of toxins such as adriamycin (glomerulosclerosis) (Lee and Harris, 2011) or aristolochic acid (Debelle *et al.*, 2002) or folate (tubulointerstitial fibrosis) (Long *et al.*, 2008).

The UUO model is the best characterised renal fibrosis model in the mouse (Chevalier, Forbes and Thornhill, 2009). In this model ligation of the ureter causes rapid onset of severe inflammation and interstitial fibrosis (Chevalier, Forbes and Thornhill, 2009). Only 1 ureter is ligated therefore the animal does not suffer renal failure. The surgical procedure consists of two ligatures 5mm apart in the upper 2/3 of the ureter. Interstitial fibrosis is seen as early as 3 days post-surgery with severe fibrosis 7 to 14 days after surgery. Interstitial fibrosis is shown by widening of the interstitial space and

interstitial deposition of extracellular matrix proteins, such as collagens or α- smooth muscle actin (Chevalier, Forbes and Thornhill, 2009).

The IRI model of renal fibrosis causes severe acute renal injury- acute tubular necrosis is seen followed by substantial interstitial fibrosis from day 5 onwards when the duration of ischaemia is prolonged (Eddy *et al.*, 2012). The subtotal nephrectomy model causes injury by reducing the renal mass to one-sixth of normal and this eventually promotes progressive glomerulosclerosis and tubulointerstitial fibrosis (Ma and Fogo, 2003). Nephrotic serum nephritis is a model that causes rapid glomerulosclerosis, which is accompanied by renal dysfunction and proteinuria (Tam, 1999). The injury is similar to patients with rapidly progressive glomerulonephritis(Tam, 1999). This model utilises nephrotoxic serum which in Sprague-Dawley rats causes autoimmune crescenteric glomerulonephritis in 30% of glomeruli after 3 weeks (Tam, 1999). The caveat to this model is there are few susceptible strains in mouse and rats (Tam, 1999).

Aristolochic acid model of fibrosis is a model of interstitial fibrosis after administration of aristolochic acid. Animals are administered the aristolochic acid via subcutaneous injection. A dose of 10mg/kg body weight causes modest proteinuria and elevated serum creatinine levels. Tubular atrophy and interstitial fibrosis are often seen histologically in this model (Debelle *et al.*, 2002).

Folic acid administration causes nephropathy and interstitial fibrosis. High dose administration of folic acid (250µg/g BW) intraperitoneally in mice causes folic acid crystals to form which cause tubular necrosis and patchy interstitial fibrosis by day 28-42 (Long *et al.*, 2008). Unlike the UUO model, in both the folate and aristolochic acid models progressive kidney failure is observed, which enables assessment of the effect of therapies on renal function. However the severity of the renal failure in these models can be highly variable.

Due to the fact that it was the best characterised and most rapid and reproducible injury model, the UUO model- was taken forward for our studies.

1.10.5 Rodent Models of Diabetes Mellitus (DM)

The best characterised model is the use of streptozotocin (STZ) which is a naturally occurring antibiotic. The structural analogue of STZ, N-actyl glucosamine, acts as a potent alkylating agent which results in toxicity to the β-cells in the islets, resulting in insulin deficiency and marked hyperglycaemia. This is a model of type 1 diabetes (Furman, 2015).

Genetic models of type 1 diabetes include the Akita mouse (Yoshioka *et al.*, 1997), in which a spontaneous mutation in the insulin 2 gene causes incorrect folding of the insulin protein, producing toxicity to the pancreatic beta cells, reduced beta cell mass and reduced insulin secretion. The mice develop insulin dependent diabetes, hyperglycemia, hypoinsulinemia, polydipsia and polyuria by 3-4 days after birth (Yoshioka *et al.*, 1997).

NOD mice are polygenetic model of autoimmune type 1 diabetes (Leiter 1993). These mice can be characterised by hyperglycemia, insulitis and leukocyte infiltration of pancreatic islets (Leiter, 1993). This model has a markedly decreased pancreatic insulin content (Leiter, 1993).

Models of type 2 diabetes are closely linked to models of obesity. High fat diet feeding induces a variety of systemic metabolic alterations in mice similar to the metabolic syndrome in humans such as obesity, insulin resistance, hyperglycemia and abnormal lipid profiles (Kitada, Ogura and Koya, 2016). High fat diet feeding is also reported to increase systolic blood pressure in mice (Kitada, Ogura and Koya, 2016). An alternative model is to combine STZ treatment along with high fat diet to mimic the two main pathological features of type 2 DM- insulin resistance and pancreatic β-cell dysfunction (Gilbert, 2011).

Genetic models of type 2 diabetes include the db/db mouse (Kitada, Ogura and Koya, 2016). The db/db mice have a mutation in the leptin receptor that results in abnormal splicing and a defective receptor for the adipocyte-derived hormone leptin (Kitada, Ogura and Koya, 2016). This mutation affects hypothalamic responses leading to

development of hyperphagia, obesity, hyperlipidemia, hyperinsulinemia, insulin resistance and diabetes (Kitada, Ogura and Koya, 2016).

Rat models of obesity and type 2 diabetes are also available (Kitada, Ogura and Koya, 2016). These include the Zucker diabetic rats, Wistar fatty rats, Otsuka Long-Evans Tokushima fatty rats and Goto-Kakizaki rats (Kitada, Ogura and Koya, 2016).

Hypertension is for a prerequisite for the development of advanced diabetic nephropathy in humans (Beroniade *et al*., 1987), however rodents are highly resistant to hypertension which could explain the difficulties in developing a model of diabetic nephropathy in rodents, which typically do not exhibit key pathological features of human disease, such as tubulointerstitial fibrosis, and do not develop progressive renal failure (Conway *et al.*, 2012). The Animal Models of Diabetic Complications Consortium (AMDCC) presented the necessary criteria for a murine model of DN to robustly mimic human disease (Breyer, 2004). Unfortunately no model as yet develops all of these features, and the discrepancies between the animal models and human disease may explain why many drugs that have shown promise in pre-clinical studies have not been successful in clinical trials.

Criteria
Greater than 50% decline in GFR over the lifetime of the animal
Greater than 10 fold increase in albuminuria compared to age and genotype matched controls
Pathophysiology of the kidney: Advanced mesangial matrix expansion Glomerular basement membrane thickening +/- nodular sclerosis and mesangiolysis Arteriolar hyalinosis

Table 1 5 AMDCC guidelines on criteria for a rodent model of DN (Breyer, 2004).

Previous work carried out in our lab utilised the cyp1a1mRen2 rat model of hypertension and STZ treatment to develop a rat model of diabetic nephropathy (Conway *et al.*, 2012). Due to this rat having the mouse renin 2 cDNA under the cytochrome P4501a1 promoter, hypertension is initiated by the addition of indole-3-carbinol to the diet- this gives a titratable and reversible hypertension (Conway *et al.*, 2012). The rat model exhibits transcriptomic and pathological changes typical of moderately advanced human diabetic nephropathy. In the absence of hypertension STZ treatment induced diabetes resulted in a 14-fold increase in albuminuria but only mild changes in histology and gene expression despite 28 weeks of marked hyperglycaemia (Conway *et al.*, 2012). Once hypertension was established in the model along with hyperglycaemia, albuminuria was increased by 500 fold, marked glomerular sclerosis and tubulointerstitial fibrosis was seen along with the induction

of many of the same pathways upregulated in the tubulointerstitium of humans with diabetic nephropathy.

Renal cortex lysates from the diabetic hypertensive rat were taken for microarray analysis to look for genes up and down regulated in diabetic hypertensive renal injury. 677 genes were upregulated >1.5 fold (corrected to $p<0.01$) following 28 weeks of hyperglycaemia and hypertension versus the control cohort (Conway *et al.*, 2012). Of these up-regulated genes, the expression of 85 fell back towards those observed in control animals after an additional 8-week period of tight glycaemic and blood pressure control. These were enriched for genes encoding extracellular matrix proteins, markers of myofibroblasts and pro-fibrotic growth factors. Conversely, 314 gene remained significantly elevated despite tight glycaemic and blood pressure control, and these were enriched for genes expressed in immune cells (Conway *et al.*, 2012).

1.11 SVEP1 as a choice for a novel gene involved in fibrosis, metabolism and blood pressure

From the subset of genes identified in our lab from the diabetic hypertensive rat model (Conway *et al.*, 2014) a panel of these genes were identified as having no previous links to diabetes, fibrosis or hypertension. The genes identified- akap12, emp1, lhfp, olfml2b, olfml3, pmp22, svep1 and tmem45a- were also underrepresented in the literature. Therefore, they were classed as novel genes for investigation into their role in diabetes, hypertension and renal fibrosis. Bioinformatics analysis was carried out on this panel of genes in human renal disease (chapter 4) and one of the most promising candidates was SVEP1. SVEP1 was shown to be upregulated in the diabetic hypertensive rat model during injury phase and returned to control levels when blood glucose and blood pressure were controlled (Figure 1 6).

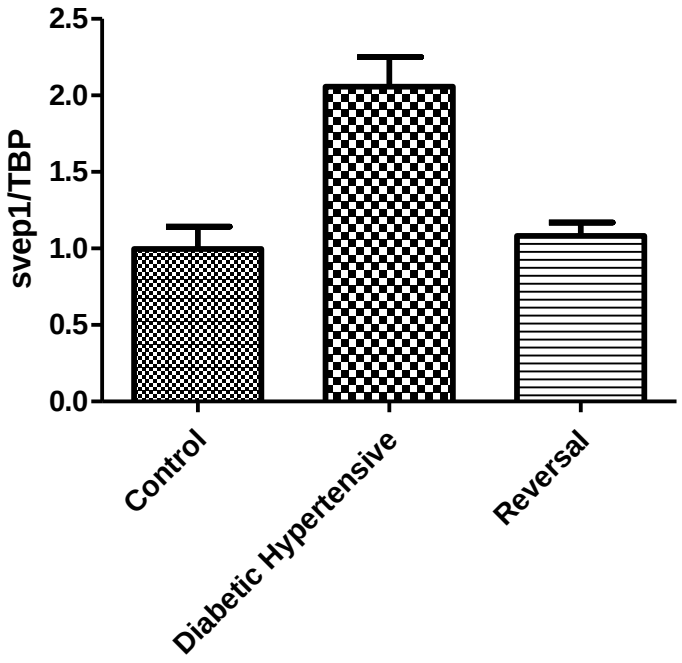

Figure 1 6 SVEP1 gene expression in the diabetic hypertensive rat model. SVEP1 was significantly upregulated during the diabetic hypertensive injury phase (p= 0.0016) and gene expression returns down to control levels after blood pressure and blood glucose are controlled. Means are ±SEM, n= 4 control, 8 diabetic hypertensive and 4 reversal cohort, one- way ANOVA.

SVEP1 was also upregulated in human renal disease (chapter 4), stained interstitially on human protein atlas using DAB staining and when identified as a ligand for alpha9beta1 integrin using immunofluorescence staining (Sato-Nishiuchi *et al.*, 2012) in mouse kidney interstitium. SVEP1 was also reported to be expressed in mesenchymal cells (Shur *et al.*, 2006) and in the mouse fibroblast cell line C3H10T1/2 cells through the murine gene atlas (Figure 1 7).

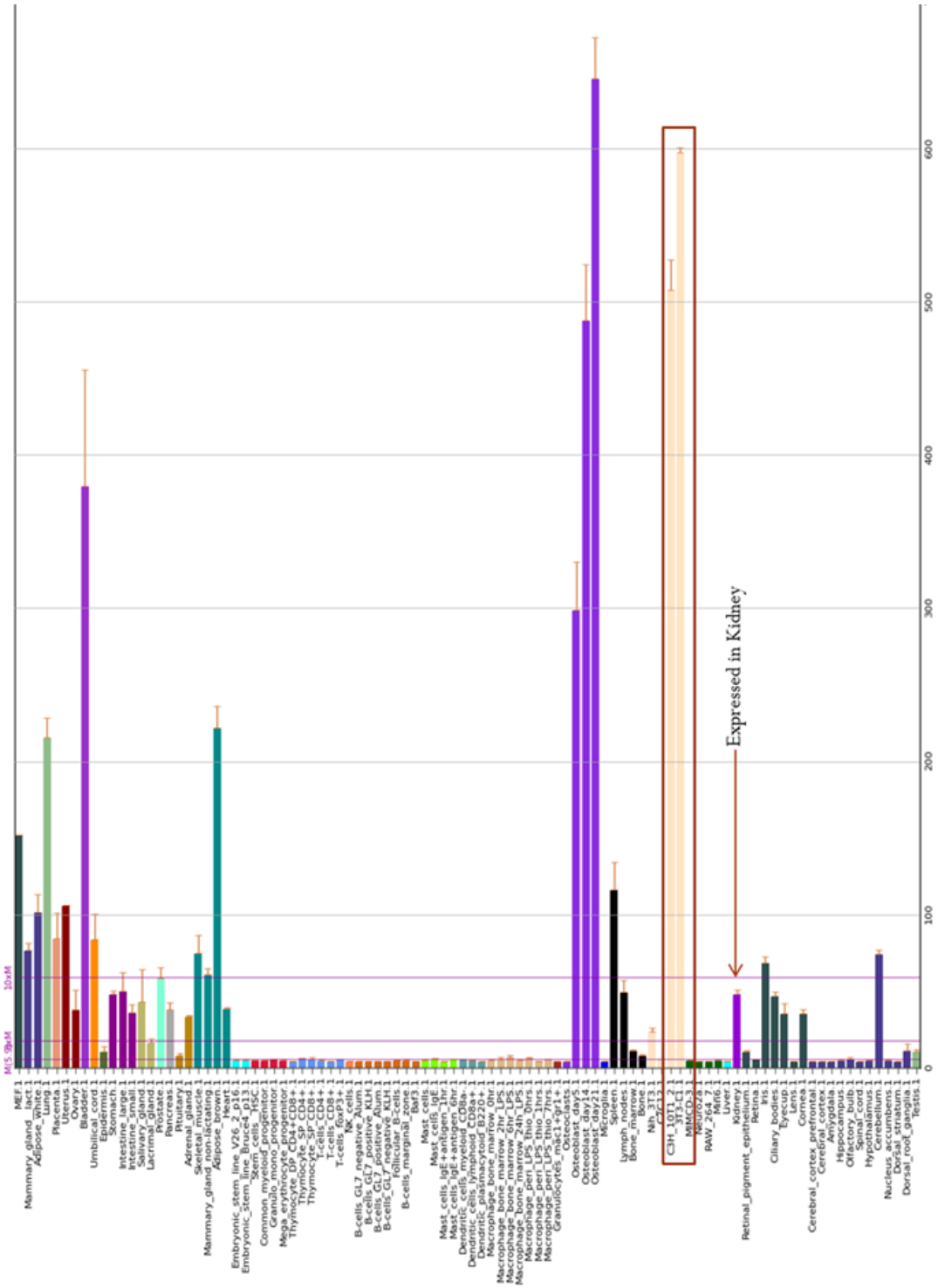

Figure 1 7 Data from murine gene atlas detailing cell type in which SVEP1 is expressed. Cell types such as mouse fibroblast cell line CH3T1/2 and primary osteoblast cells highly express SVEP1.

SVEP1 is an extracellular matrix protein which was first described in murine bone marrow stromal cells as a protein containing epidermal growth factor like domains-similar to the Notch family (Gilgès *et al.*, 2000). It was one of the 84 genes that were up-regulated in the renal cortex of Cyp1a1mRen2 rats after eight months of diabetes and hypertension and which fell towards control levels after tight glycaemic and hypertension control (Conway *et al.*, 2012). It is a protein of approximately 300kDa in weight (Morooka *et al.*, 2017) and is conserved across multiple species, from zebrafish to mouse to human (Karpanen *et al.*, 2017). The human orthologue was reported as a protein expressed on the surface of osteogenic cells (Shur *et al.*, 2006). SVEP1 is known to have an array of complement control protein domains along with a von Willebrand factor A domain, a pentraxin domain and multiple epidermal growth factor domains (Figure 1.6). SVEP1 is produced by cells of a mesenchymal lineage (Shur *et al.*, 2006).

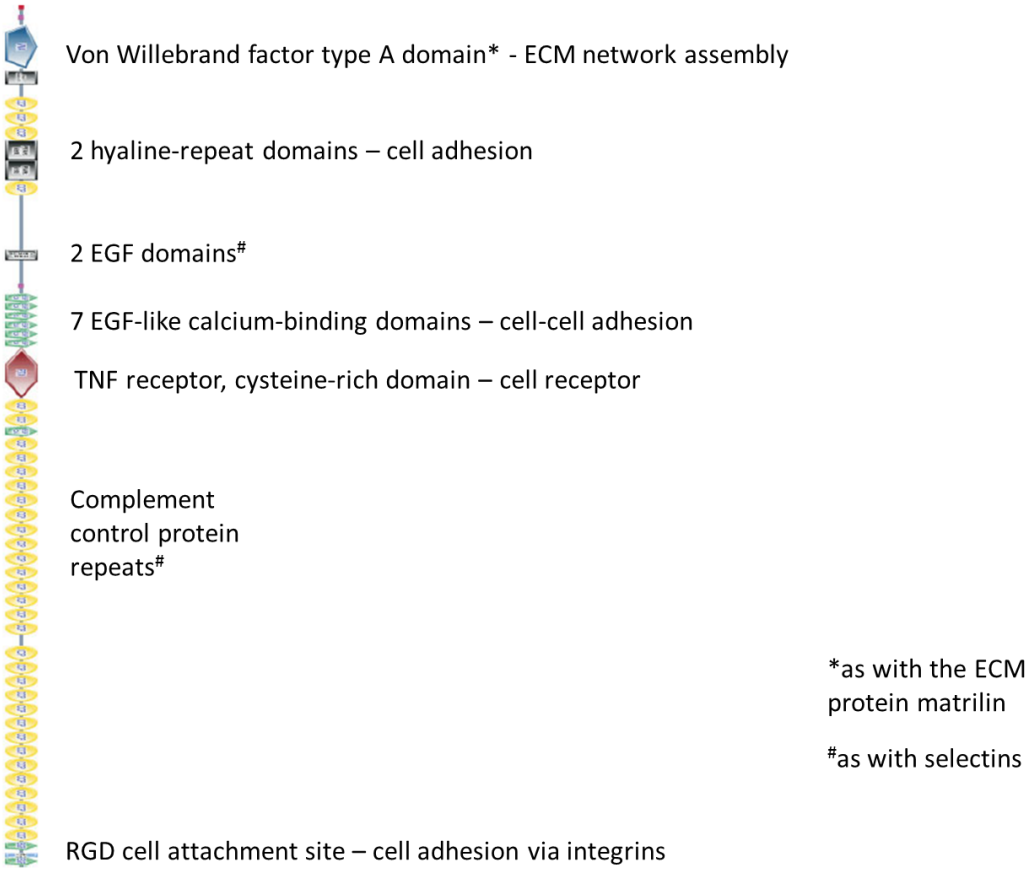

Figure 1 8 Domains present on SVEP1 protein structure (Shur et al., 2006).

SVEP1 is also known to be a high affinity ligand for integrin α9β1 integrin- a cell adhesion receptor involved in lymphangeogenesis (Sato-Nishiuchi *et al.*, 2012). The use of recombinant expression and *in vitro* cell adhesion assays showed SVEP1 was a secreted protein which mediates cell adhesion in an integrin α9β1-dependent manner (Sato-Nishiuchi *et al.*, 2012). SVEP1 was reported not to be expressed in endothelial cells (Sato-Nishiuchi *et al.*, 2012). SVEP1 is also linked to lymphatic vessel formation and remodelling. SVEP1 is deposited around lymphatic vessels but secreted from surrounding mesenchymal cells (Morooka *et al.*, 2017). SVEP1 is thought to ensure Foxc2 is upregulated in lymphatic endothelial cells- potentially through the angiopoietin-2 and tie 1/ tie 2 receptor system (Morooka *et al.*, 2017). Mice with knockout of both SVEP1 alleles show severe oedema at mid-gestation and die immediately after birth (Morooka *et al.*, 2017). In these animals a primitive lymphatic plexus develops but subsequent remodelling was impaired (Morooka *et al.*, 2017).

Zebrafish mutants of SVEP1 show a decrease in venous and lympho-venous sprouting and an increased number of intersegmental arteries along with a severe reduction in lymphatic trunk vasculature (Karpanen *et al.*, 2017). In mice with a premature stop allele in the SVEP1 gene mesenteric lymphatic structures at E18.5 failed to undergo remodelling and lack lymphatic valves (Karpanen *et al.*, 2017). Expression of SVEP1 by mesenchymal cells in intimate proximity with venous and lymphatic endothelial cells is required for sprouting and migratory events in zebrafish and for remodelling events of lymphatic intra-luminal valves in mouse embryos (Karpanen *et al.*, 2017).

SVEP1 homozygous mutant embryos have multiple defects in development. At E15.5 and E18.5 they show severe oedema and discolouration and die in the perinatal period (Dickinson *et al.*, 2016). Transverse sections of micro-CT from E18.5 embryos revealed abnormal development of the kidney pelvis, hypoplastic lungs and a thin myocardium (Dickinson *et al.*, 2016) .

The SVEP1 point mutation p.D2702G that is found in 3% of the population was linked to higher odds ratio of coronary heart disease and developing type 2 diabetes (Stitziel *et al.*, 2016). A significant association of this point mutation with blood pressure was also reported- the allele is associated with higher systolic BP (0.94mmHg higher for each copy of the allele among allele carriers) (Stitziel *et al.*, 2016). There was no

association between SVEP1 and plasma lipid traits (Stitziel *et al.*, 2016). Therefore, SVEP1 presented itself as gene with potential roles in fibrosis, hypertension and metabolism.

Hypothesis: SVEP1 plays a role in renal fibrosis, diabetes and hypertension

Aims

1. To develop a model of hypertensive kidney disease in C57BL6 mice and assess whether SVEP1 was upregulated in the hypertensive cohort.
2. To assess whether SVEP1 played a significant role in the pathophysiology of renal fibrosis.
3. To assess the role SVEP1 plays in the pathogenesis of the metabolic syndrome.
4. To assess the role SVEP1 plays in blood pressure regulation.

Chapter 2: Materials and Methods

2.1 Standard Solutions

The standard solutions used in this thesis are given in Table 2.1

Table 2 1 Table of standard solutions used throughout materials and methods

Reagents and Buffers	Recipe	Supplier
1x PBS	10 Tablets, 1L ddH_2O	OXOID (BR0014G)
4% PFA	4% paraformaldehyde in PBS	Sigma (D2650)
0.5M EDTA	EDTA in ddH_2O, 1M NaOH to adjust pH to 8.0	VWR Chemicals (192346H)
TBE buffer (10X stock)	54g Tris base, 20ml 0.5M EDTA(pH8) 27.5g boric acid, per 1L	VWR Chemicals Promega (H5135)

2.2 Animal Husbandry

2.2.1 Maintenance of SVEP1 knockdown colony

Experiments were carried out in accordance with the Animals (Scientific Procedures) Act 1986.

Mice were housed and bred in the Biological Resource Facilities at the University of Edinburgh. Genotyping was carried out by ear clipping. A 12hr diurnal cycle was maintained (7AM-7PM), with free access to water and maintained on standard mouse chow (RM1). Environmental conditions were maintained at 19-21^{o}C and 40-55% humidity. The C57BL6J mice that were used for the hypertensive model experiments were bought in from Harlan (Bicester, UK) and allowed at least a week between transportation and the start of any experiment.

B6N(Cg)-Svep1$^{tm1b(EUCOMM)Hmgu}$/J Mice

The source of animals was Jackson Laboratory, via Charles River- UK supplier (Margate, Kent, UK). B6N(Cg)-Svep1$^{tm1b(EUCOMM)Hmgu}$/J mice were hemizygous for an insertion of an L1L2_Bact_P cassette inserted upstream of the critical exons of Svep1 gene on chromosome 4. The cassette composed of an FRT site followed by LacZ sequence and loxP followed by neomycin under human beta-actin promoter, SV40 polyA, second FRT site followed by a loxP site. The critical exon(s) were thus flanked by loxP sites, and subsequent Cre-mediated excision by breeding to Sox2-Cre mice in Jackson deleted the critical sequence and neomycin selection cassette yielding a knockout LacZ reporter allele. Svep1$^{-/-}$ mice are not viable, therefore Svep1$^{+/-}$ and Svep1$^{+/+}$ (wild type) mice were obtained and bred to generate Svep1$^{+/-}$ and Svep1$^{+/+}$ littermates in a 50:50 ratio for experimental use.

Breeding of the B6N(Cg)-Svep1$^{tm1b(EUCOMM)Hmgu}$/J colony was challenging. Firstly when the mice were bought in from Jackson Laboratory it was 4 months before any pups were born from the two hemizygous breeding pairs. The first litters from the breeding pairs were 7/8 pups in the litter from both breeding pairs- this was our most successful round of breeding and generated 10 male and 5 female animals. 11 pups out of the litter were wild type and 4 were hemizygous, it was therefore necessary to place the hemizygous animals into breeding pairs to try and expand the colony. The original breeding strategy involved breeding hemizygous to hemizygous animals however litter sizes decreased (to average 4/5 pups per breeding pair) and some breeding pairs were unsuccessful therefore we began breeding two female mice to one male- all hemizygous to generate enough hemizygous male mice for our experiments. We also set up hemizygous and wild type breeding pairs to generate enough wild type animals for our experiments as the hemizygous crosses did not generate enough wild type animals. Gaining enough animals of the right genotype and age was a challenge throughout the studies utilising these animals and this has been addressed in the discussion sections of the appropriate chapters.

Only male mice were used in the studies in this thesis. This was due to the time constraints of the PhD project and the hardships of the breeding of the mice not generating enough mice to run the studies in both male and female cohorts. However,

it would be important to run cohorts of both male and female mice to provide robust data on any sex differences seen in regard to phenotype.

2.2.2 Genotyping

Genotyping was carried out from ear punches by Transnetyx (Cordova, TN, USA). The genotyping assay was designed by the assay team at Transnetyx using probes designed for genotyping the B6N(Cg)-Svep1$^{tm1b(EUCOMM)Hmgu}$/J (Table 2.2).

Protocol Primers

Primer	5' Label	Sequence 5' --> 3'	3' Label	Primer Type
18035		CAT GCA GGT CCT TTC ATC CT		Wild type Reverse
18036		TCC ATC CTT CAG ATT TGG TCA		Mutant Reverse
28393		AGC TTT TCC ACT CTA GCA AGC		Wild type Forward
oIMR7202		CGG TCG CTA CCA TTA CCA GT		Mutant Forward

Table 2 2 Table for primers used by Transnetyx to genotype the B6N(Cg)-Svep1$^{tm1b(EUCOMM)Hmgu}$/J mice.

2.3 Hypertensive Mouse Model Experiments

2.3.1 Murine Model of Hypertension Experiments

Ten week old C57BL/6J male mice (Harlan) were randomised into hypertensive and control cohorts- (n=6 in each cohort). In the hypertensive cohort (n=6) animals were anaesthetised with isoflurane and underwent uninephrectomy.

The uninephrectomy surgery was carried out by experienced animal surgeons Spike Clay and Gary Borthwick. Animals were anesthetised using isoflurane in oxygen through nose cone. The area above the left kidney on the animals flank was shaved

and ocular lubricant (Lacri-lube) was applied to prevent the animal's eyes from drying out. The mice were placed on their right flank to provide easier access to the left kidney and the shaved area was liberally bathed in iodine scrub (vetersept). An incision was made below the rib cage in the flank and through the peritoneal wall the kidney was identified by its darker red colour. An incision through the peritoneal wall was made and the kidney was popped through this incision. Blood vessels and ureter were identified to ensure a ligature encompassed all vessels and ureter. 6.0 suture or surgical clips were used to loop over the kidney to encompass all renal blood vessels and ureter. Once it was identified that all vessels and ureter were encompassed by the ligature the ligature was tightened. This was repeated so there were two ligatures around the renal vessels and ureter. Once ligatures were in place, the kidney was removed using curved scissors and the ligatures/clips were returned back inside the animal. The peritoneal wall was sutured using 7.0 suture- 1mm of muscle either side of the suture is necessary to correctly close the peritoneal wall. The skin incision was closed using surgical clips and liberally covered with iodine. Buprenorphine (vetergesic) 0.1mg/kg was administed subcutaneous along with 1ml 0.9% warmed sterile saline. Animals were placed in a heat box for 24hrs to recover (34^{o}C) and were given *ad libitum* access to vetergesic-laced jelly (0.02mg/ml buprenorphine, 45mls water and 2 cubes of jelly per animal (Hartley's, UK)). Animals were also supplied with mash (RM1 pellets soaked in drinking water for >1hr- overnight).

The control cohort (n=6) underwent a sham procedure as described a where the flank incision was made and the kidney raised to the surface, however instead of clipping the kidney, it was returned into the animal.

At day 0 hypertensive mice were implanted subcutaneously with a 75mg DOCA pellet and an ANGII osmotic mini pump (Alzet 2006; Alzet) which dispensed 200ng/kg/min of ANGII in 0.9% sodium chloride for 4 weeks. Control animals were administered a blank pellet and mini pump which dispensed 0.9% sodium chloride. Animals were allowed 2 days recovery from the implantation surgery, then the treatment cohort was administered 3% sodium diet (SDS) and the control cohort was fed RM1 chow (0.25% sodium).

2.3.2 Angiotensin II administration via osmotic mini pump

Angiotensin II (Sigma-Aldrich) was dissolved in 0.9% sodium chloride to achieve a dose of 200ng/kg/min over 4 weeks, according to the mean flow rate of the osmotic mini-pump and weight of the mouse. Mini-pumps were weighed before and after filling to check that correct volume had been inserted. Control mini-pumps contained 0.9% sodium chloride. Mini-pumps were incubated over night before implantation in sterile phosphate buffered saline (PBS) at 37^{o}C.

2.3.3 Mini-pump implantation

Mini-pumps were implanted under isoflurane anaesthesia delivered by nose cone. Fur at the nape of the neck was shaved and the site prepared by cleaning with antiseptic wipe and iodine (vetersept). A small incision was made and a subcutaneous pocket made by blunt dissection at the nape of the neck. Once the mini-pump was implanted the wound was closed using surgical clips and opioid analgesic was injected (buprenophrine 50µg/kg as Vetergesic) subcutaneously. Mice were recovered in a heat box (34^{o}C) until mobility was regained (<30mins) and then transferred to a clean cage. *Ad libitum* access to vetergesic-laced jelly and mash were given (method of preparation described above).

2.3.4 Measurement of clinical parameters

Systolic blood pressure was measured twice weekly using tail cuff plethysmography. Animals were also weighed at this time.

For tail cuff plethysmography mice were preconditioned for four days and systolic blood pressure was measured on the fifth day. Preconditioning and measuring was performed at the same time each day for consistency. Mice were placed in a heat box prior to taking systolic blood pressure measurement. Restraint was placed on a surgical heat mat to keep mouse warm while readings being taken to ensure best results. Animals were removed from heat box (34^{o}C) after <10mins and placed in restraint and tail cuff applied approximately 1cm from the base of the tail. The cuff was then inflated to approximately 60mmHg and adjusted until a clear sinusoidal wave could be seen

and mouse was quiet and still. Four inflation and deflation cycles were carried out and systolic BP was measured when there was the largest sinusoidal deflections.

Urine collections were obtained by placing mice in metabolic cages for 24 hours once every 2 weeks. Urinary albumin was measured by the immunoturbidimetric method (Microalbumin Kit, Olympus Diagnostics Ltd, Watford, UK) on a Cobas Fara centrifugal analyser (Roche Diagnostics Ltd, UK) by Forbes Howie (Centre for Reproductive Health, University of Edinburgh). On day 28 the animals were culled. Blood was drawn by cardiac puncture. Kidney, heart and spleen were removed. Both kidneys (where applicable) and hearts were weighed. Kidneys were halved and fixed in methcarn fixative, while the other half was snap frozen using liquid nitrogen for RNA analysis.

2.4 Unilateral Ureteric Obstruction (UUO) experiment

8 week old male Svep1 hemizygous mice and littermate controls (n=8 for each genotype) underwent UUO surgery (Hesketh *et al.*, 2014). Surgeries were carried out by experienced animal surgeon Gary Borthwick. Animals were anesthetised under isoflurane anaesthesia with oxygen through a nose cone. Ocular lubricant (Lacri-lube) was applied to rodent's eyes to prevent them drying out. The mouse was placed in supine position and limbs fixed to surgical heat mat using low-tack adhesive tape. Analgesia was adiminstered subcutaneously (0.06mg/kg buprenorphine (vetergesic)). The area under the rib cage shaved and bathed in iodine scrub (vetersept). A midline laparotomy was carried out to gain access to peritoneal cavity, the mouse was surgically draped and a colibri retractor placed into the incision. To expose the left ureter sterilised cotton buds were used to displace the intestines and these were covered with moistened drapes. The left ureter was exposed and lifted to be ligated with 6.0 silk sutures between the bladder and renal pelvis. To isolate the bladder from the ureter the ureter is then divided with two ligatures. The intestines were then replaces carefully and the peritoneum closed with 5.0 silk sutures and the skin closed with surgical skin clips. The wound was then liberally covered in iodine to prevent post-operative infection and 1ml of warmed 0.9% saline administered subcutaneous. Animals were

placed in a heat box (34ºC) for 24hrs and given *ad libitum* access to vetergesic-laced jelly and mash as previous described.

Both Svep1$^{+/-}$ and control mice underwent UUO to causes rapid onset of severe interstitial fibrosis. At the 7 day time point animals were culled and tissues removed and fixed in both zinc and PFA fixatives for immunohistochemical analysis or snap frozen in liquid nitrogen for RNA analysis.

2.5 Metabolic Experiment

2.5.1 GTT

8 week old male Svep1$^{+/-}$ (n=4) and Svep1$^{+/+}$ (n=4) littermates were obtained from the in-house colony. A glucose tolerance test (GTT) was then carried out on the mice after a 6 hour fast. 25% D-glucose (Sigma-Aldrich) was made up in 50mls MilliQ water and left to dissolve for 1hr. A tail vein incision was made and basal glucose levels were recorded using OneTouch Ultra Glucometer with disposable test strips (LifeScan, UK). Blood samples were collected using Microvette CB 300 tubes (Sarstedt, Germany) and stored on ice. A glucose bolus (2mg per gram body weight) was administered by gavage at time 0. Blood glucose and a blood sample were then collected at time points 15mins, 30mins, 60mins and 120mins. The blood samples were centrifuged at 4ºC, 3000rpm for 10mins to separate plasma from packed red cells. The plasma supernatant was obtained and stored at -80ºC for insulin analysis by ELISA (CrystalChem, Zaandam, Netherlands).

2.5.2 Insulin ELISA

Manufacturers instructions were followed (CrystalChem, 90080). Briefly, the wide range assay was used. The anti-insulin antibody-coated microplate was fixed to the frame and 95µl of sample diluent per well was added. 5µl of the sample or working mouse insulin standard was added per well. The microplate was incubated for 2 hours at 4ºC. Each well was then washed 5 times with wash buffer and 100µl of anti-insulin antibody-enzyme conjugate per well was added. The microplate was incubated for 30mins at room temperature and then washed 7 times with wash buffer. 100µl of enzyme substrate solution was then applied to each well and incubated for 40mins at

room temperature avoiding exposure to light. The enzyme reaction was stopped by adding 100µl of enzyme reaction stop solution per well and the absorbance was measured using a plate reader within 30 minutes- A_{450} and A_{630} values were measured and A_{630} values were subtracted from A_{450} values. Insulin concentrations were calculated using the standard curve. The standard curve was prepared by pipetting 150µl of sample diluent and 50µl of mouse insulin stock solution (25.6ng/ml) into a microtube labelled 6.4ng/ml and mixed. 50µl of sample diluent was then added to 6 microtubes and labelled 0.1,0.2, 0.4, 0.8, 1.6, and 3.2ng/ml. 50µl of 6.4ng/ml standard was added to the 3.2ng/ml tube and mixed. From the 3.2ng/ml tube a serial dilution was carried down to the bottom standard- 0.1- taking 50µl each time.

2.5.3 TSE Phenomaster System- indirect gas calorimetry

Mice were singly housed in phenomaster cages (TSE, Bad Homburg, Germany) and acclimatised to the cages for 72hrs and measurements taken for 24 hours. TSE phenomaster cages utilised indirect calorimetry to calculate the respiratory exchange ratio (RER) of each mouse. The phenomaster system is able to measure VCO_2 expelled and VO_2 consumed by the mice to calculate the RERusing the equation:

$$\text{RER}= \frac{vco2}{vo2}$$

RER is an indication of what fuel is being metabolised. An RER value of 1 is indicative of carbohydrate metabolism, 0.8 a balance between fat and carbohydrate and 0.7 predominantly fat metabolism.

The phenomaster cages calculate food and drink intake as food hoppers and water bottles are monitored on weight sensors. Animal body weights can be monitored by a body weight sensor in the form of a glass tube attached to a weight sensor. The TSE system is equipped with ActiMot2 technology which measures locomotor activity using an infrared light system. A metal frame surrounds the cage with evenly spread infrared light beams emitted on the X and Y axis. Beam interuptions caused by animal movement are sensed and registered at high spatial and temporal resolution.

Mice were returned after indirect calorimetry measurements to the animal holding rooms and placed on a HFD (58kcal% fat with sucrose Surwit Diet (D12331) 58.0kcal% fat, 25.5kcal% carbohydrate and 16.4kcal% protein, Research Diets, New Jersey, USA) for 6 weeks. The animals were placed back in the phenomaster cages for 72 hours reacclimatisation followed by a second batch of readings taken over 24hrs. Animals were kept on a HFD for a further 6 weeks and then a final GTT reading was taken and animals were culled and tissues removed for real time PCR analysis.

Mice body composition analysis was carried out using the minispec LF50 TD-NMR system (Bruker, Coventry, UK). Time domain nuclear magnetic resonance imaging acquires and analyses TD-NMR signals from all protons in the entire sample (live unrestrained mouse) and provides precise measurements of lean tissue, fat and free body fluid. The system works on similar principles to MRI imaging in that high tissue contrast exists between fat and muscle based on relative relaxation times of protons in the magnetic field.

2.6 BP measurement by Radiotelemetry

Radiotelemetry is the gold standard for measuring blood pressure in mice. It allows remote, real-time analysis of BP, HR and activity in conscious, unrestrained mice. The surgeries were carried out by Dr Jess Ivy and methodology was obtained from the thesis of Dr Jess Ivy.

Radio telemetry devices (PA-C10, Data Science International, Hertogenbosch, The Netherlands) were coupled with their receiver pads and assigned to a mouse. The offset of each device was quality controlled (range of -2 to +2 mmHg). The details of the mouse, devices and offset is able to be recorded using DSI software.

Surgery to insert radio telemetry devices was carried out by Dr Jessica Ivy. Surgery was carried out using aseptic technique (Hoogstraten-Miller et al). Devices were implanted under general anaesthesia using isoflurane in oxygen delivered through a nose cone.Buprenorphine (Vetergesic ®) at a dose of 0.1mg/kg along with 1ml 0.9% sterile saline was given subcutaneously after induction of anaesthesia. Ocular lubricant (Lacri-lube ®) was applied to the rodent's eyes to prevent them drying out. The mouse was then positioned in dorsal recumbancy and the ventral neck shaved and bathed in

iodine scrub (Vetersept ®). A ventral cervical skin incision was made and a subcutaneous pocket made down the left flank. Blunt dissection was utilised to isolate the carotid artery and separate it from the vagus nerve gently. A tight double-knotted ligature was applied to the anterior end of the carotid artery and loose ends secured with a large haemoclip to produce light tension on the artery. A loose ligature was applied to the carotid and the posterior ends were occluded with micro-haemoclamp. A bent 23 gauge blue (BD Microlance, FST) needle was used to puncture the artery and to hold it open. The device catheter (Data Science International) was gently fed into the carotid artery using vessel cannulation forceps and secured by tightening the loose ligature around it. A radio was used to check for interference with the device caused by gripping the catheter; once posterior occlusion was open a pulsing sound can be heard over the radio if the catheter is patent.

The micro-haemoclamp was removed from the posterior end of the artery and the catheter was fed up until resistance is felt. Both the anterior and initial securing ligatures were double knotted and tissue glue (3M™VetBond™) was applied to the knots. The body of the device was then placed into the subcutaneous pockets previously made and the wound closed with 3-5 silk sutures (size0.5, non-absorbable, Vicryl). Tissue glue was used to seal the wound and oxygen was fed through the nose cone for 3-5 mins till the mouse was conscious. The mouse was allowed to recover in the heat box (34^{o}C) until mobility is regained (<30mins). *ad libitum* access to vetergesic-laced jelly (0.02mg/ml buprenorphine in 45ml water, 2 cubes jelly per animal (Hartley's, UK)) and mash (RM1 pellets soaked for >1hour to overnight in drinking water) was given.

Data were collected during a 1min period every 30mins at an acquisition rate of 1kHz. Baseline measurements were obtained for 3 weeks before high salt diet was initiated. Animals were then placed on the diet for 1 week and reading taken on a high salt diet. Animals were culled after high salt diet measurements were taken. How the data were presented is outlined in each specific figure in chapter 6. Briefly, data were recorded over 5 consecutive days on both normal chow and high salt diet. In some analyses, 6 hour running means were calculated for each mouse over the 5 day time points. In other analyses, the raw telemetry data rather than the 6 hour running means are given.

2.7 Histological Analysis

2.7.1 Tissue Preparation

Kidneys were removed from the mouse, decapsulated and halved. The tissue was placed directly in methcarn (60% methanol, 30% chloroform and 10% glacial acetic acid), Paraformaldhyde (PFA) or zinc fixative (552658, BD Bioscience, Oxford, UK). (5mls), rotating overnight at room temperature. Fixed tissue was then placed in 70% EtOH for storage of minimally 1 week before embedding.

2.7.2 Sectioning

Kidneys were embedded in paraffin and sectioned using a microtome to 4μm thick sections and mounted on electrostatic slides and incubated at 37^{o}C overnight and then stored at room temperature before staining.

2.7.3 Immunohistochemistry Staining

Staining of kidney sections with Haematoxylin and Eosin to assess tissue morphology

Sections were deparaffinised and rehydrated using a sequence of xylene and decreasing concentrations of EtOH (100%, 95%, 80%, 70%) then washed under running tap water. Sections were stained with haematoxylin for 5mins, washed under running tap water and placed in alkaline tap water for 1min followed by acidic alcohol for 5 secs. Sections were then washed in tap water and placed in 70% EtOH for 1min followed by alcoholic Eosin Y for 30secs to stain the cytoplasm. Sections were then washed again under tap water and dehydrated in increasing concentrations of EtOH and finally xylene. Sections were mounted in DPX mounting medium (VWR), coverslipped and left to dry overnight. Image analysis was carried out using a Zeiss Akioskop microscope (Zeiss; Germany) and images captured using KS300 3.0 imaging software (Zeiss).

2.7.4 Staining of kidney sections with Picrosirius Red (PSR) as a pan-collagen marker for fibrosis

Sections were deparaffinised and rehydrated as described in section 2.7.3. Sections were stained in PSR/Fast Green stain (made by mixing equal volumes of 0.1% Direct

Red 80 and Fast Green and diluting 1 in 9 with aqueous picric acid solution- Sigma Aldrich) for 2 hours at room temperature in the dark. Sections were then rinsed in running tap water and dehydrated in increasing concentrations of EtOH followed finally by immersion in xylene. Slides were coverslipped using DPX as previously described.

Images were taken at x100 magnification using a Zeiss Akioskop as describe in section 2.4.3. Images were also acquired using the Zeiss Axioscan as described in section 2.7.6.

2.7.5 Staining of Kidney sections with Periodic Acid Schiff (PAS) as a marker of glomerulosclerosis

Sections were deparaffinised and rehydrated as described in section 2.7.3. Sections were placed in 1% periodic acid for 20mins then washed in tap water for 20mins. Sections were then placed in Schiff Buffer for 20mins and then washed again in tap water. Slides were then counter stained in haematoxylin for 30secs, rinsed in tap water and placed in Scott's tap water solution till sections turned blue. Sections were finally rinsed in tap water and dehydrated and mounted using DPX.

2.7.6 Immunohistochemistry for collagen III, α-SMA, PDGFRβ and KIM1- UUO fibrosis phenotype staining

Kidney sections were deparaffinised and rehydrated as described in section 2.7.3. Endogenous peroxidase activity was quenched with 2% hydrogen peroxide (made up by adding 18mls 30% H_2O_2 with 252mls dH_2O- Sigma SZBD3300V). Slides were then rinsed with running tap water. Slides were loaded onto a Shandon Sequenza coverplate on a Shandon Sequenza rack (ThermoFisher, Loughborough, UK) with a tight seal established. Endogenous staining was avoided by blocking with avidin/biotin (Vector) and the sections washed with 1x PBS between avidin and biotin blocking steps. Sections were blocked using serum-free protein block (DAKO) for 10 minutes. This protein block was not washed off when primary antibody was added. 125µl of primary antibody (See table 2.3 for antibody concentrations and suppliers) diluted in antibody diluent (DAKO) was added to each section. Primary antibody incubation was

overnight at 4^{o}C with the sequenza lid on to prevent evaporation. Sections were washed in PBS twice and secondary species-specific biotinylated secondary antibody was added at a concentration of 1:300 for 30mins at room temperature. Sections were washed in PBS twice and avidin-biotin-peroxidase complex (ABC Kit, Vector) was added for a 30min incubation at room temperature. Sections were washed twice in PBS before developing with diaminobenzidine kit (DAB) (DAKO). DAB was made up by adding a drop to each ml substrate buffer required for the number of slides to be stained- 125µl was added to each slide. DAB was incubated for 5mins or until sections appeared brown. Sections were counterstained in haematoxylin for 30secs and then rinsed until clear. Sections were dipped in Scott's tap water until sections turned blue and rinsed finally in running tap water. Slides were then dehydrated in increasing concentrations of EtOH and finally immersed in xylene. Slides were mounted using DPX and allowed to dry overnight.

Sections used in the hypertensive mouse model experiments were examined using a Zeiss Axioscope (Zeiss, Germany) as previously described. Quantification was carried out using Adobe Photoshop CS6 software. 15-20 images were taken from randomly chosen regions of the kidney section and the amount of DAB staining quantified. Firstly a colour range that defined positive staining was established and saved for batch analysis. This allowed every image from each different mouse to be quantified using the same colour range. Using the histogram tool the number of pixels stained was obtained and this was used to calculate the pixels stained as a percentage of the total pixels of the image.

Sections stained for collagen III, α-SMA and PSR in Svep1$^{+/-}$ and wild-type animals were examined using the Zeiss Axio Scan.Z1. This enabled the whole section to be scanned for analysis. Images were taken at random throughout the whole section. 15 images were taken per section at 400x magnification using the Zeiss image processing software. Staining was quantified using the Image J IHC profiler macro.

Antibody (Company)	Primary Concentration	Species Specificity	Species Raised	Secondary Antibody (Company)	Secondary Concentration
Collagen III (Southern Biotech,1330-01)	1:300	Human, Mouse, Rat, Chicken, Hamster, Chinchilla, Porcine, Equine, Rabbit, Bovine, Feline, Rhesus, Canine, Guinea Pig and Tree shrew	Goat	Anti-goat biotinylated (Vector)	1:300
PDGFRβ (Abcam, ab32570)	1:800	Human, Mouse and Rat	Rabbit	Anti-goat biotinylated (Vector)	1:300
α-SMA (Abcam, ab5694)	1:500	Mouse, Rat, Chicken, Guinea pig, Cow, Dog, Human and Pig	Rabbit	Anti-rabbit biotinylated (DAKO)	1:500
KIM1 (Abcam, ab47635)	1:800	Mouse and Human	Rabbit	Anti-rabbit biotinylated (DAKO)	1:500

Table 2.3. Primary and Secondary antibodies and staining conditions used.

2.8 Estimating the abundance of mRNA transcripts by rt-PCR

2.8.1 Tissue RNA extraction

RNA from kidney tissue was extracted using the RNeasy plus mini kit (Qiagen, 74134). Half of a frozen kidney was allowed to rest of a bed of dry ice to allow around 30mg of cortex tissue to be removed using a scapel, while keeping the remaining tissue frozen. Cortex fragments were then added to a 2ml eppendorf and the rest of the kidney returned to -80^{o}C storage. To the kidney cortex 600µl RLT buffer was added with a steel bead (5mm, 69989, Qigen, Manchester, UK). Samples were placed in a magnetic mixer mill (Retsch, MM301) and shaken for 90secs at a frequency of 30/s to homogenise the tissue. The magnetic bead was then removed and the lysed tissue centrifuged for 3mins to reduce frothing. 150µl RLT buffer and 300µl 70% ethanol (VWR chemicals, 20821.330) was added and the samples were then loaded onto spin column and the manufacturer's instructions were followed. Using this method 5-25µg RNA was routinely extracted in 30µl of RNase-free water.

Extraction of RNA from adipose tissue utilised Qizol (Qigen, Manchester, UK). Adipose tissue was homogenized in 750µl Qizol and then incubated on the bench at room temp for 5mins. 140µl of chloroform was then added and the tubes shaken vigorously for 15 seconds. The tubes were then incubated for 3mins at room temperature and centrifuged at 12,000xg for 15mins at 4^{o}C. The upper aqueous phase was then removed to a fresh tube containing 70% ethanol and then samples were loaded onto spin columns for the RNeasy mini kit as described above.

2.8.2 Cell RNA extraction

350µl RLT buffer was added to cells grown and treated in 6 well plate. Cells had media removed and washed 3 time with PBS prior to being incubated with RLT buffer. RLT buffer was washed across the well 3 times to detach and collect all cells. Sample in RLT buffer was then removed to a 1.5ml eppendorf and vortexed for 30s to homogenize sample. Homogenized lysate was then transferred to a gDNA Eliminator spin column and manufacturer's instructions followed (RNeasy Plus Mini Kit 74134, Qiagen). Using this method 5-25µg RNA was routinely extracted in 30µl RNase-free water.

2.8.3 Quantification and quality control of RNA-Agarose Gel Electrophoresis and Nanodrop

2µl of RNA sample was taken forward to quantify the concentration using the Nanodrop 1000 spectrophotometer- this gives the concentration in ng/ml based on absorbance at 260nm. RNA concentrations were between 200-1000ng/µl. Purity was also assessed using the A260/280 and A260/230 ratios given by the nanodrop analyser.

The integrity of the RNA was assessed by agarose gel electrophoresis. Briefly, a 1.2% agarose gel (SeaKem LE agarose, Lonza) was prepared using 0.5xTBE (45mM Tris Base, 45mM Boric acid, 0.625M EDTA) and Gel Red DNA stain (5µl/100ml, Biotium) was added. Samples were prepared for loading on the gel by adding 2µl RNA to 8µl nuclease free water and 2µl 6xLoading Dye (Promega, G1881). Samples were electrophoresed at 100V for approximately 1hr. RNA was visualised by exposure to ultraviolet light using a UVI pro system (UVItec) with an Olympus C-4000 digital camera attached (Figure 2.1).

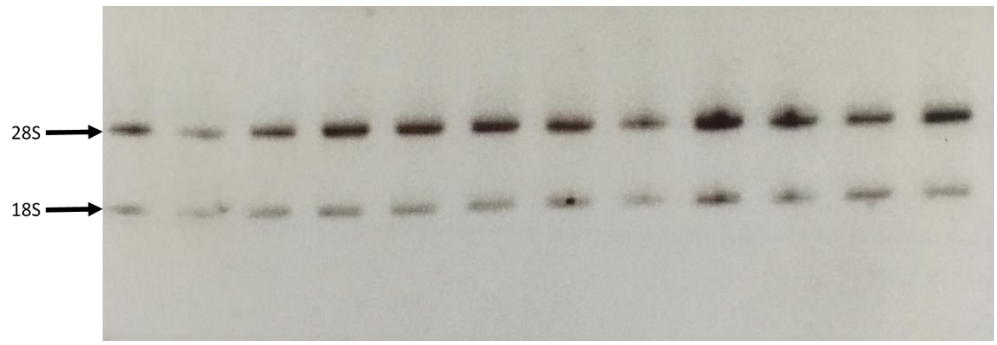

Figure 2 1 **Representative example of agarose gel electrophoresis of RNA samples.** 500ng of each RNA sample was resolved on a 1.2% agarose in 0.5%TBE buffer and visualised using Gel Red DNA stain. Image shows RNA preparations which are not degraded.

2.8.4 Reverse Transcription

cDNA synthesis was carried out using the QuantiTect Reverse Transcription Kit (Qiagen, 205311) according to the manufacturer's instructions. Briefly, 1µg RNA was reverse transcribed. 2µl of gDNA wipeout was added to 1µg RNA diluted in RNase free water for 2mins at 42^{o}C then transferred to ice to eliminate any genomic DNA. A reverse transcription master mix was prepared of 1µl Quantiscript reverse transcriptase, 4µl Quantiscript RT buffer 5x, 1µL RT primer mix and finally the 2 µl template RNA. The reverse transcription reaction was performed in a ThermoCycler (Applied Biosystems, Veriti 96-well) with incubation at 25^{o}C for 10mins, 37^{o}C for 120mins and 85^{o}C for 5mins. The cDNA was then stored at -20^{o}C.

2.8.5 Quantitative Polymerase Chain Reaction (qPCR)

qPCR was carried out using a 1:40 dilution of sample cDNA. Diluted sample was aliquoted to allow amplification of all genes of interest. Neat cDNA was also used to create a standard curve in a series of 1:8, 1:16, 1:32, 1:64, 1:128, 1:256, 1:512 and a blank H_2O control. Samples were performed in triplicate. A master mix of 8µl in each well was made up of 5µl perfecta QPCR fast mix II (Quanta-Biosciences, 95118-012), 2.75µl nuclease free H_2O and 0.25µl of mouse specific Taqman gene expression assay. The primer and probe assays employed are given in table 2.4. 2µl cDNA was added to each well. The rtPCR reaction was carried out on a Roche Lightcycler 480 at 95^{o}C for 15mins, followed by 95^{o}C for 10s, 60^{o}C for 30s, 72^{o}C for 1s, repeated for 50 cycles, ending with 40^{o}C for 30secs. The absolute quantification was determined sing the standard curve.

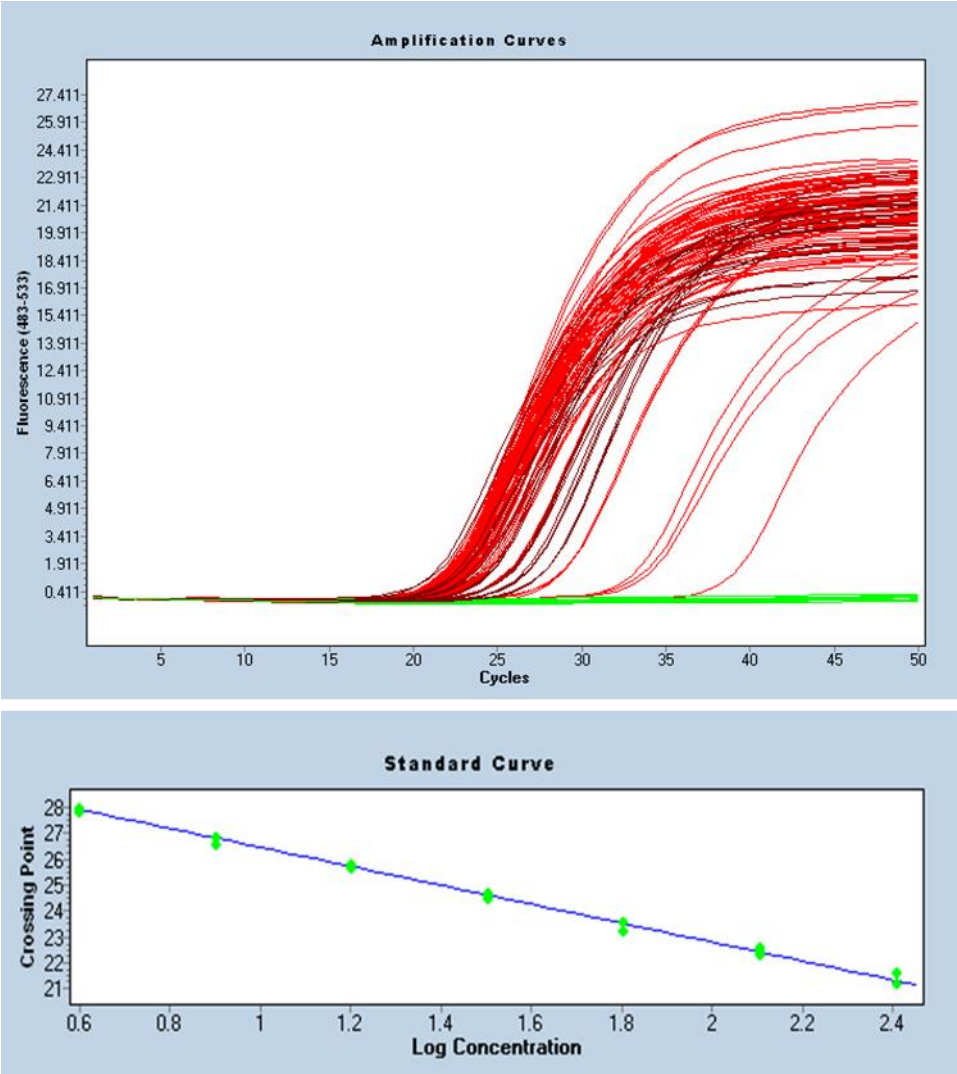

Figure 2 2 Example of a fluorescence intensity plot and standard curve for a rtPCR assay (cyclophillin).
A= Plot of fluorescence intensity versus cycle number for kidney samples and 7 point serial dilutions of pooled cDNA template and no template negative control (green) performed in triplicate.
B= Standard curve constructed from Cp values obtained from A.

Probe Name	Probe Number
COL1A1 (Collagen 1)	Mm00801666_g1
COL3A1 (Collagen III)	Mm01254476_m1
PDGFRβ (PDGFRβ)	Mm00435546_m1
Havcr1 (KIM1)	Mm00506686_m1
TBP (tbp)	Mm00446971_m1
Cyclophillin (Ppia)	Mm02342430_m1
HPRT1 (hprt)	Mm03024075_m1
SVEP1 (Svep1)	Mm01346904_m1
COL4A1 (Collagen IV)	Mm01210125_m1
Acta2 (α-SMA)	Mm01204962_gH
Fibronectin (Fn1)	Mm01256744_m1

Table 2.4. Probes for RTPCR analysis of gene expression. All assays were Taqman Gene expression Assays, ThermoFisher Scientific.

2.9 Cell Culture Techniques

2.9.1 Maintenance of Cells

Standard cell culture consumables employed in the studies are presented in table 2.5.

Reagent	Catalogue Number	Company
DMEM, high glucose and glutaMAX supplement	61965059	Life Technologies, Thermo Fisher Scientific
Fetal Calf Serum (FCS)	10500064	Life Technologies, Thermo Fisher Scientific
Trypsin-EDTA (0.05%) Phenol Red	25300054	Life Technologies, Thermo Fisher Scientific
Penicillin and Streptomycin (10,000U/ml)	15140122	Gibco, Life Technologies, Thermo Fisher Scientific
Mouse recombinant TGFβ	7666-MB-005	R and D Systems Europe
Costar 6 well plates	3516	Scientific Lab Supplies
Corning 25cm^2 flasks	430639	Scientific Lab Supplies
Corning 75cm^{2}flasks	354638	Scientific Lab Supplies

Table 2.5. Table of generic cell culture reagents.

C3H 10 T1/2 fibroblasts, clone 8 (ATCC- CCL-226™) were maintained at 37^{o}C in 5% CO_2, 95% air in a HeraCell (Heraeus) incubator in Corning cell culture flasks (75cm^2) until 60-70% confluency was achieved (fibroblasts die at 90% confluency). Media and cell culture reagents were heated to 37^{o}C in a water bath before use.

2.9.2 Passaging of cells

Fibroblasts were passaged by aspirating off the media and washing in 5mls PBS. 1ml trypsin per 75cm^2 was used to detach cells and the flask was left at 37^{o}C in the incubator for 2mins to produce a single cell suspension. 5ml prewarmed medium was then added to the flask to deactivate the trypsin and cells pelleted by centrifuging at 300g for 3mins. Cells were then resuspended in 10mls of DMEM and 2mls taken to a fresh flask to continue culture up to passage 15.

2.9.3 Cryopreservation of Cells

Cells were prepared for cryopreservation by passaging as described in 2.9.2 and resuspended in freshly-made, filtered freezing medium (90% FCS 10% DMSO). The cell suspension was then transferred into cryovials (CryroPure, Starstedt, 73.377) and placed immediately into the -80^{o}C freezer wrapped in tissue to slow down the freezing process and stored in liquid nitrogen.

2.9.4 Cell Counting

Cells were counted using a Hemocytometer (Neubauer, Hawksley). After passaging as described in 2.9.2 cells were resuspended in 5mls of prewarmed media and 50µl pipetted onto the haemocytometer. Four boxes of the haemocytometer were counted and averaged.

2.9.5 TGFβ treatment of CH3 10 T1/2 fibroblasts

Cells were cultured as described in 2.9.1, 2.9.2 and 2.9.4 into 25cm^3 flasks. Cells were seeded at 0.7x10^6 and allowed to grow to 80% confluence (cells die at 100% confluence). Cells were serum starved for 24hrs before TGFβ was administered at 5ng/ml in cell culture media. Experimental time course was 48hrs as described in figure 2 3, fresh TGFβ was administered daily. Cells were washed and removed from the flasks in RLT buffer for RNA analysis.

Figure 2 3 Experimental time course TGFβ experiment in CH3 10 T1/2 fibroblasts.

2.10 Nephroseq patient information and data analysis

Bioinformatic analysis was carried out on freely available data sets from www.nephroseq.org. Normal human tissue was made available from the Higgins normal tissue pane (Higgins *et al.*, 2004). This was used to look at SVEP1 expression in different tissues (Figure 5 15). In this study gene expression was analysed in dissected renal lobes from 5 adult human kidneys. Samples were obtained from the non-tumorous portion of nephrectomy specimens removed for renal neoplasia. RNA was isolated from the inner and outer cortex, inner and outer medulla and glomeruli were isolated by sieving. Samples underwent gene expression analysis utilising Gene Pix 4000. Glomeruli from 4 individuals and glomeruli-deplete inner and outer cortex from 5 individuals were used in the analysis of location of Svep1 gene expression in chapter 4.

Samples from the CKD data on Nephroseq set were made available from Ju et al 2015 (Ju *et al.*, 2015). 32 living donor transplant biopsies obtained at time of transplantation were used as controls. CKD biopsies were obtained from the European renal cDNA bank consortium (ERCB) (Yasuda *et al.*, 2006). Glomeruli were microdissected under a dissection microscope and RNA was prepared from the glomerular and residual tubulointerstitial compartments and analysed using an Affymetrix Human Genome U133 Plus 2.0 Array

Samples from the diabetic nephropathy cohort were made available from Woronieka *et al* (Woroniecka *et al.*, 2011). 44 human kidney samples were obtained from living allograft donors, surgical nephrectomies and surplus portions of diagnostic kidney biopsies. Tissues were manually microdissected into glomerular and tubular compartments and RNAextracted and analysed on an Affymetrix Human Genome U133 Plus 2.0 Array. Patient demographics are reported (Woroniecka *et al.*, 2011).

Raw microarray data was presented as log2 on Nephroseq and this was converted to fold change prior to presentation of the data in chapter 4. Means were then calculated and presented in the figures- the specific statistical analysis employed is highlighted in the figure legends.

2.11 Data analysis and statistics

All data are presented and analysed using GraphPad Prism software version 5.0. Data are presented as mean ±SEM. The number of biological replicates (n number) is given in each experimental group in the figure legend corresponding to the data along with the statistical tests used. Two-way ANOVAs and T-tests are predominantly used in this work. Two-way ANOVA was used when analysing the effect of two independent variables (e.g. genotype and diet) on a parameter and to determine whether there is an interaction between the variables. The interaction effect tests the null hypothesis that any differences within the first independent variable are the same for each group within the second independent variable. For each test p values are provided for each independent variable along with the "interaction". Repeated two-way ANOVA was employed where readings from the same animals were available across multiple time-points. Throughout the thesis, the level of significance required to reject the null hypothesis was set at 5%.

Chapter 3: A Mouse Model of Hypertensive Renal Injury

3.1 Introduction

To examine the role of Svep1 in the pathogenesis of hypertensive renal fibrosis *in vivo*, a murine model of hypertensive renal injury was required. As many transgenic mice, such as the Svep1 knockout mouse, are available on a C57BL6 background, we wished to develop a model of hypertension in this strain. However, C57BL6 mice are highly resistant to hypertensive renal injury. After examining a range of models described in the literature (Chapter 1, table 3), the model of Kirchhoff *et al* was used as a basis for the development of the model of hypertensive renal injury. This model employs combinatorial insults including uninephrectomy, infusion of angiotensin II, administration of DOCA and a high salt diet. This model was used due to the significant renal injury seen which is consistent with hypertension, many alternative models had a reduced ability to cause renal fibrosis. The model showed elevations in albuminuria and renal fibrosis- both hallmarks of hypertensive renal injury therefore, it was taken forward in this body of work. A pilot investigation was carried out including infusion of angiotensin II, administration of DOCA and a high salt diet but without uninephrectomy. This resulted in an increase in blood pressure but no renal injury/scarring and no increase in albuminuria. Therefore, the uninephrectomy was deemed a necessary component of the hypertensive model.

3.1.1 Aims

1. To develop and characterise a model of hypertensive renal injury in the C57BL6 murine strain.
2. To determine whether SVEP1 is upregulated in a mouse model of hypertension.

3.2 Results

3.2.1 Model experimental time-line

In this study the hypertensive cohort underwent uninephrectomy and then received the combinatorial insults including ANGII (200ng/kg/min), DOCA (75mg) and 3% Sodium chow (high salt diet) (Figure 3.1).

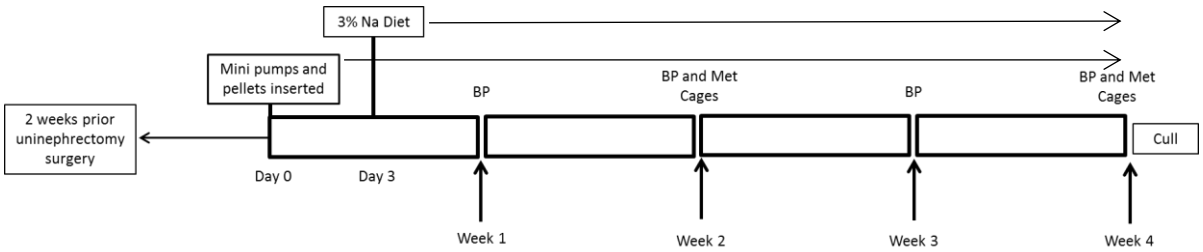

Figure 3.1Time course of the murine model of hypertensive renal injury. Animals were uninephrectomised 2 weeks before the commencement of the study. Angiotensin II minipumps and DOCA pellets were implanted subcutaneously before the animals were placed on a 3% high salt diet. The experimental duration was 4 weeks. Blood pressure was monitored weekly and urine collected via metabolic cage every 2 weeks.

3.2.2 Hypertensive animals exhibited an increase in blood pressure, proteinuria and kidney weight

The combinatorial treatment produced an increase in systolic blood pressure (BP) to 140mmHg compared to 112mmHg in the control group at week 4 of the study (figure 3.2). Urine collected from these animals was used to quantify the albumin: creatinine ratio which is an important clinical readout of renal injury. A 200 fold increase in urinary albumin: creatinine ratio was noted in the hypertensive cohort compared with control animals by week 4 of the study (figure 3 3).

When normalised for body weight, there was a significant an increase in heart weight ($p=0.0175$) and left kidney weight ($p=0.0001$) in the hypertensive cohort compared with controls (Figure 3 6). Body weight was not significantly different between the two groups (Figure 3 5).

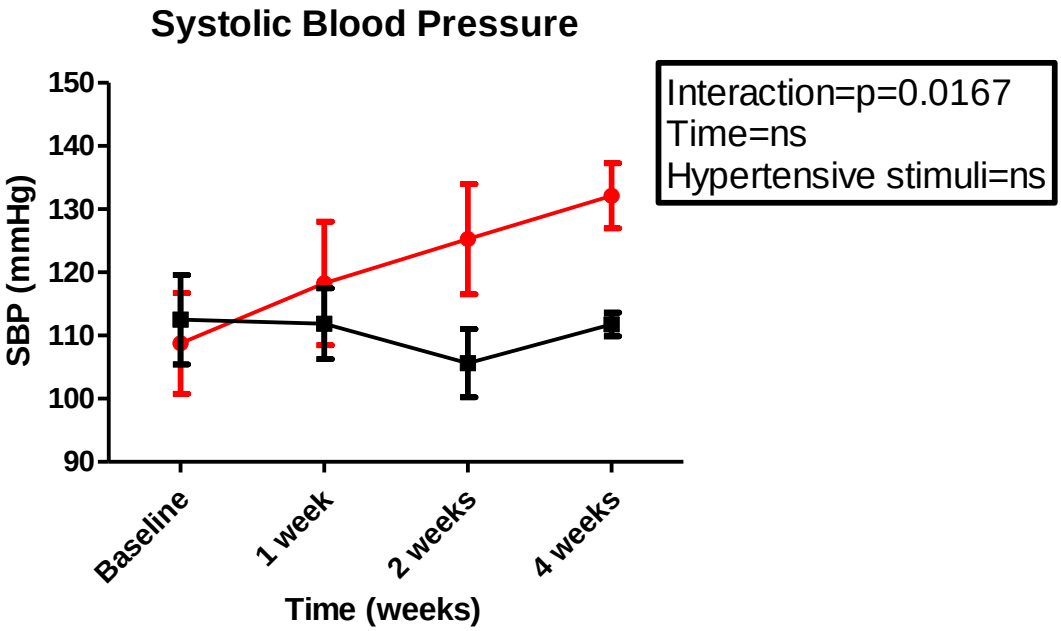

Figure 3 2 Mean systolic BP in hypertensive mice vs control mice.
SBP is increased in the hypertensive cohort (n=4, red) in comparison to control animals (n=5, black). Means±SEM, n=4-5, repeated measures 2 way-ANOVA.

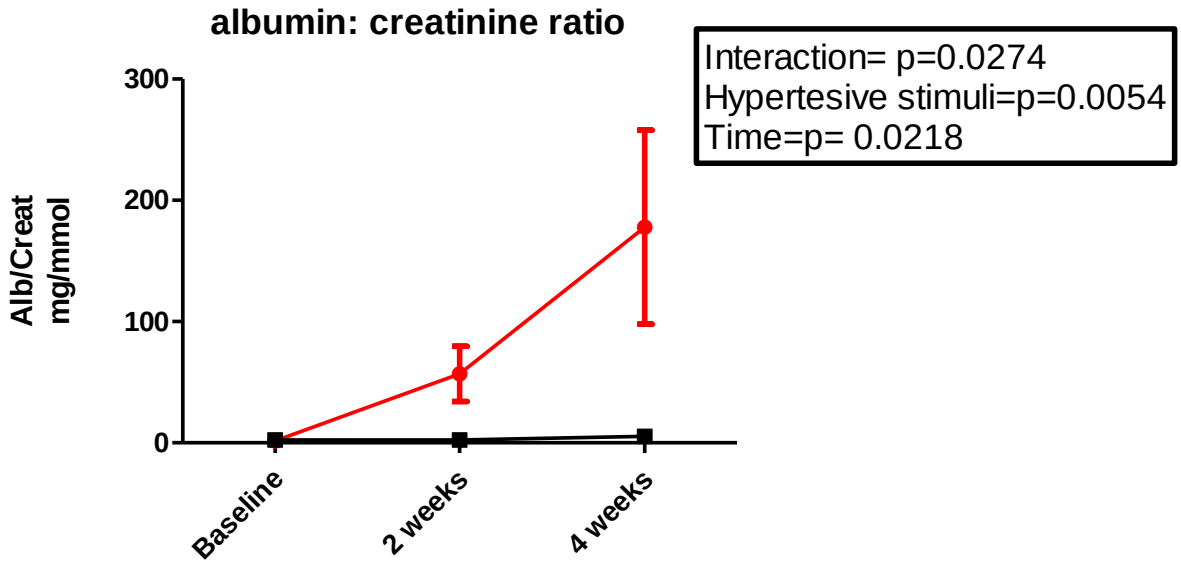

Figure 3.3 Urinary Albumin Creatinine ratio in hypertensive mice compared to control. Albuminuira is increased in hypertensive mice (red) compared to control mice (black) (p=0.0054). Means ±SEM, n=4, 2 way-ANOVA.

During the development of the hypertensive mouse model a number of animals died. Two consecutive rounds of the hypertensive model experiment saw 5 animals of 12 die (Table 3 1). Hypertensive animals were found to have suffered from what was discovered to be cardiac tamponade. Sham animals had to culled due to mini pump protrusion and one animal was culled due to deterioration in condition- cause of death was never clarified but on post-mortem there was some blood clotting in the pleural cavity. There was also one sham mouse found dead and no cause of death was evident on post-mortem. The deaths resulted in lower n numbers than expected in some of the experimental groups.

	Sham	Hypertensive
Study 1	1	0
Study 2	2	2

Table 3 1 Table detailing the death rates of animals before experiment completion during the hypertensive model.

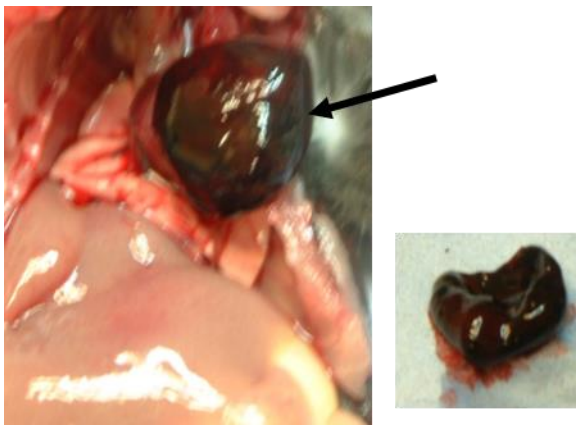

Figure 3 4 Schematic of cardiac tamponade in one of the hypertensive model animals. Evidence of cardiac tamponade was revealed after animals were become unwell and being found dead. The large clot enveloping the heart is arrowed and panel shows once clot was removed from heart.

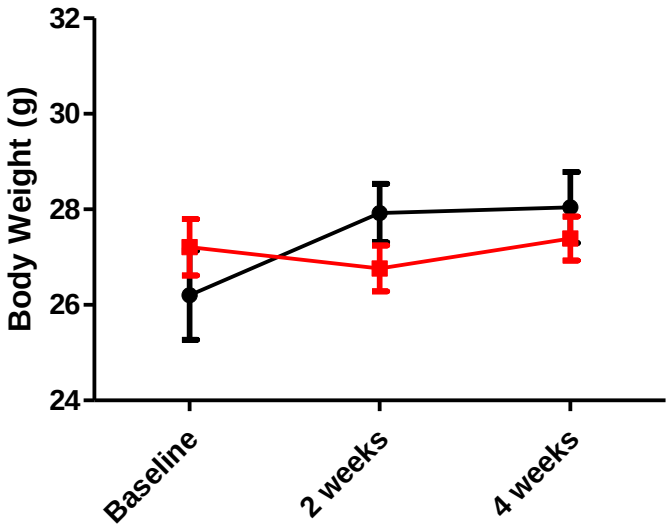

Figure 3 5 Body weights of hypertensive and control cohort over the 4 week experimental period. No significant difference was noted between hypertensive (red) cohort and control (black) cohort. Means±SEM, N=4/5, repeated measures 2-way ANOVA.

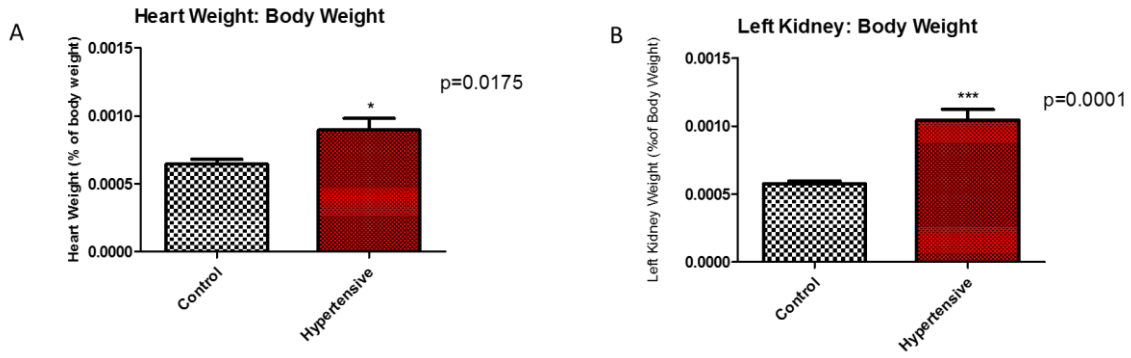

Figure 3 6 Heart weight normalised to a % of body weight and left kidney weight normalised to % of body weight in hypertensive mice (red) compared to control mice (white).
A= Heart weight normalised to % body weight is significantly increased in hypertensive cohort compared to control (p=0.0175).
B= left kidney weight normalised to % body weight was significantly increased in hypertensive mice compared to control mice (p=0.0001).
Means ±SEM, n=4-5, unpaired t-test.

3.2.3 Histological analysis shows patchy renal fibrosis in hypertensive animals

Histological analysis was carried out in both the control and hypertensive cohorts. Firstly, the kidney was stained with Hemotoxylin and Eosin (H and E) and Picrosirius Red (PSR, a pan-collagen marker) (Figure 3 7), to examine the morphology and extent of fibrosis in the renal tissue. It was observed that areas of fibrosis, predominantly in the tubulointerstitial compartment of the cortex, had developed in the hypertensive group. The H and E sections gave no indication of glomerulosclerosis. An infiltration of cells to the tubulointerstital compartment of the cortex (arrowed A) highlighted by the H and E staining was hypothesized to be inflammatory cells such as macrophages.

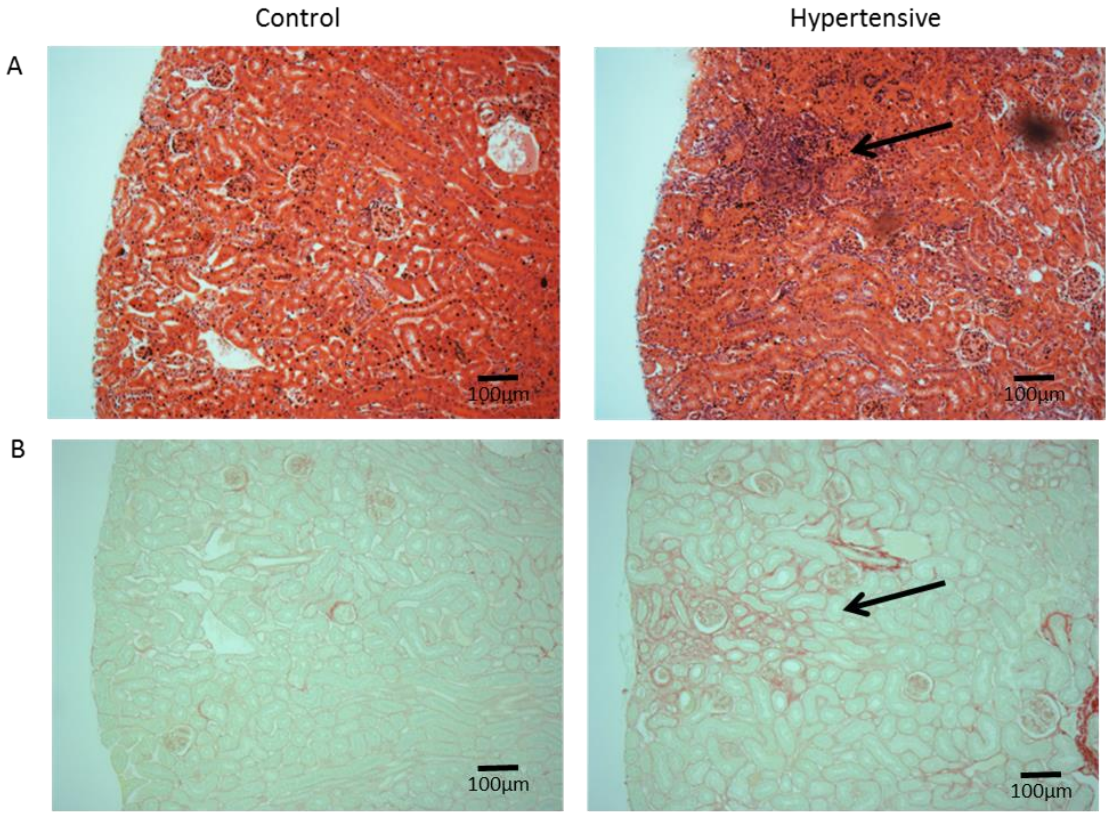

Figure 3 7 Representative images of H and E staining (A) and Picrosirius Red staining (B) on serial sections of the renal cortex from control and hypertensive animals.
A= H and E stained tissue showed an infiltration of cells in hypertensive cohort which was absent in the control cohort.
B=Picosirus Red staining demonstrated areas of fibrosis specifically in the cortex of hypertensive mice The fibrotic areas (arrowed) are found in close proximity to the cellular infiltrate in A.

3.2.4 Periodic Acid Schiff staining showed evidence of mild glomerulosclerosis in hypertensive cohorts

Perodic Acid Schiff (PAS) staining was carried out specifically to investigate glomerular fibrosis (Figure 3 8). Quantification of PAS staining using Adobe Photoshop showed a trend towards an increase in staining in the hypertensive cohort compared to control, however this was not statistically significant (Fig 3 9).

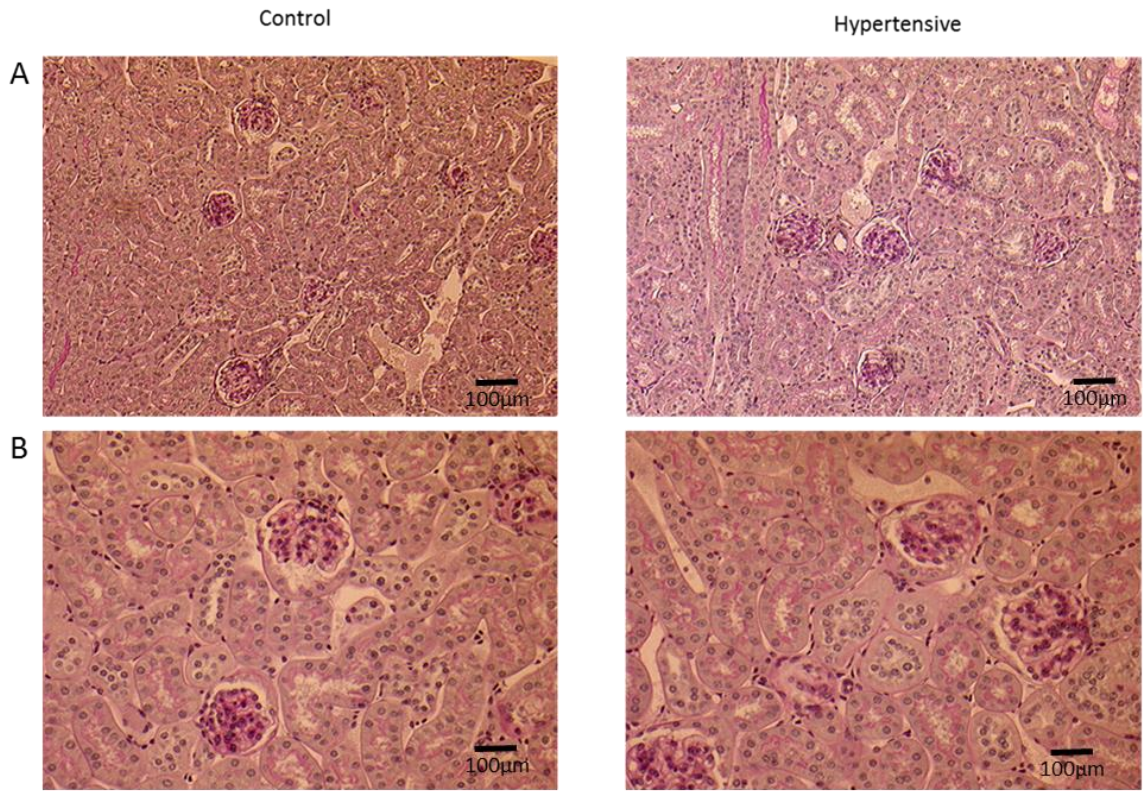

Figure 3 8 Representative images of PAS staining in the renal cortex of hypertensive and control animals at (A) x100 or (B) x200 magnification.
No overt glomerular scarring was noted in either the control or hypertensive groups.

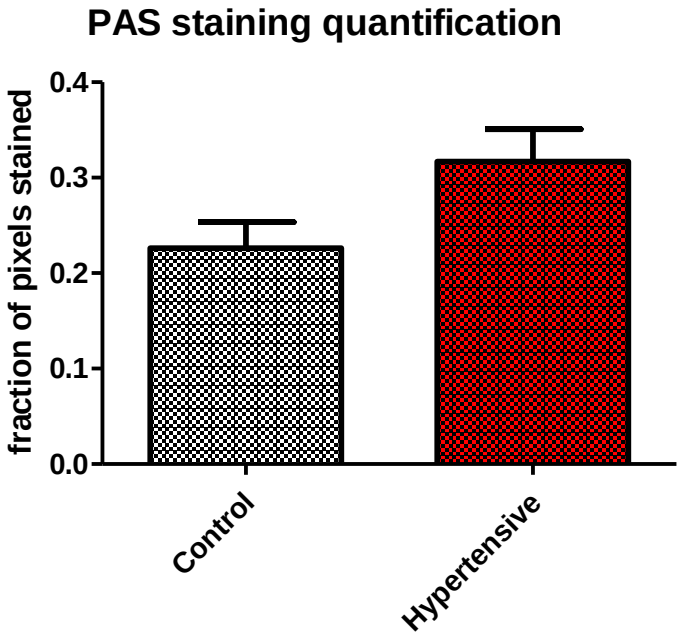

Figure 3 9 Quantification of PAS staining in the glomerulus of both control and hypertensive animals.
PAS staining was quantified using Adobe Photoshop and demonstrated a non-significant trend towards an increase in staining in the hypertensive cohort.
Means±SEM, n=4/5, unpaired t-test (ns, p=0.1574).

3.2.5 Tubulointerstitial fibrosis was observed in the renal cortex of hypertensive animals

To further characterise the nature of the extent of fibrosis and injury in the hypertensive animals immunohistochemistry (IHC) was performed for PDGFRβ, Collagen III, α-SMA and KIM1.

Collagen is a key component to the extracellular matrix (ECM). When the collagen III staining was quantified, there proved to be a significant increase (p=0.0050) in staining in the hypertensive cohort when compared to control, with areas of intense staining noted, as was observed with picrosirius red staining (Figure 3 10).

Alpha- Smooth Muscle Actin (α-SMA) staining was carried out to quantify myofibroblast numbers in the renal cortices of hypertensive and control animals and to determine if there was early glomerular staining. Early glomerular staining of α-SMA indicates mesangial cell activation towards a myofibroblast phenotype. In the control animals the α-SMA staining was restricted to the smooth muscle wall of blood vessels, while in the hypertension cohort α-SMA staining was also observed focally in

peri-tubular regions (Figure 3 11A+B). Quantification of α-SMA staining showed a trend towards an increase in the hypertensive cohort however, this was not significant (Figure 3. 11 C, P=0.0896). Little evidence of glomerular staining was noted.

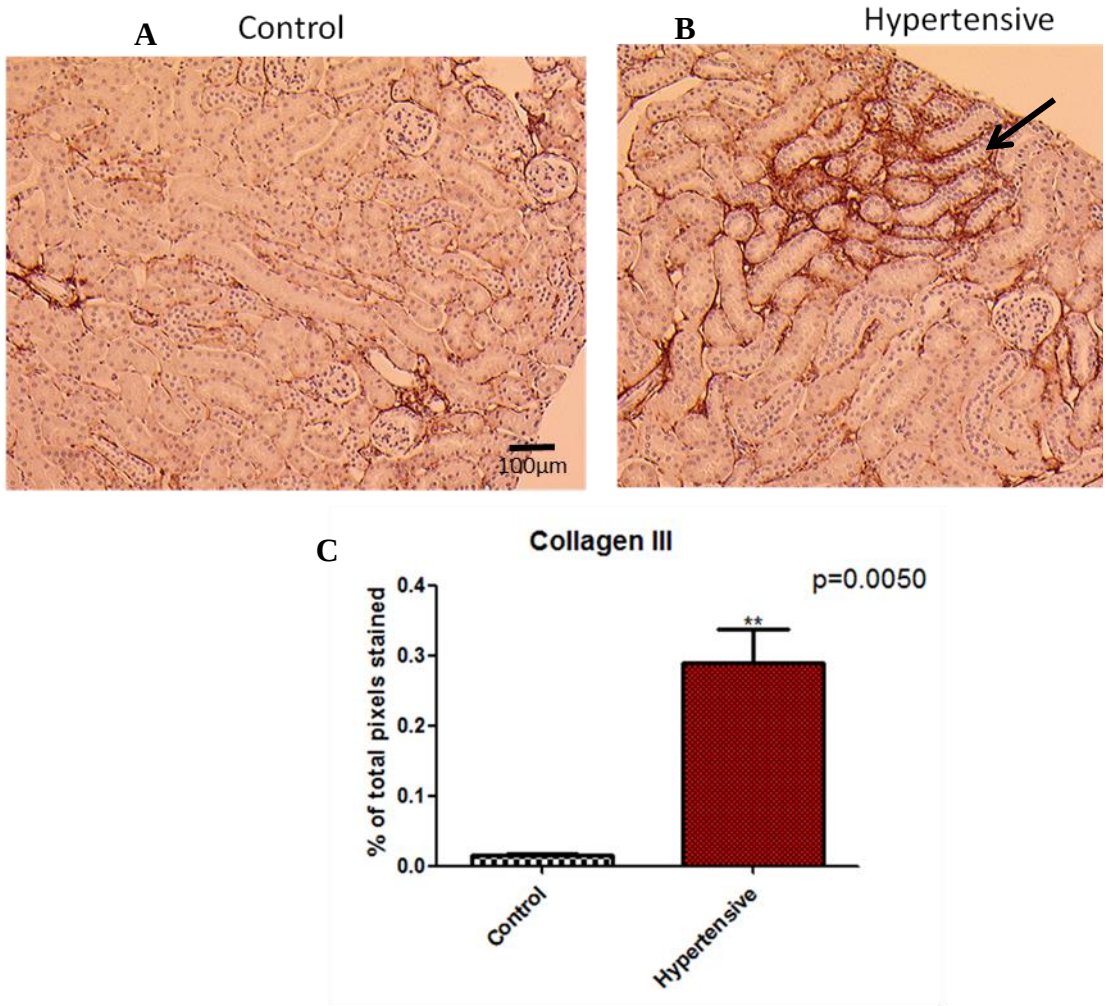

Figure 3 10 Representative images and quantification of Collagen III staining in hypertensive mice compared to control cohort.
Representative immunohistochemistry images of collagen III staining on methacarn-fixed paraffin embedded sections from control (A) and hypertensive (B) mice. There is focal peri-tubular brown (DAB) staining in the cortex of the kidney of hypertensive animals. C: The percentage of total pixels stained with DAB in hypertensive mice compared to control mice. There is a significant increase in the percentage of pixels stained with DAB in hypertensive mice compared to control cohort (p=0.0050). Means ±SEM, n=4-5 in each group, unpaired t- test.

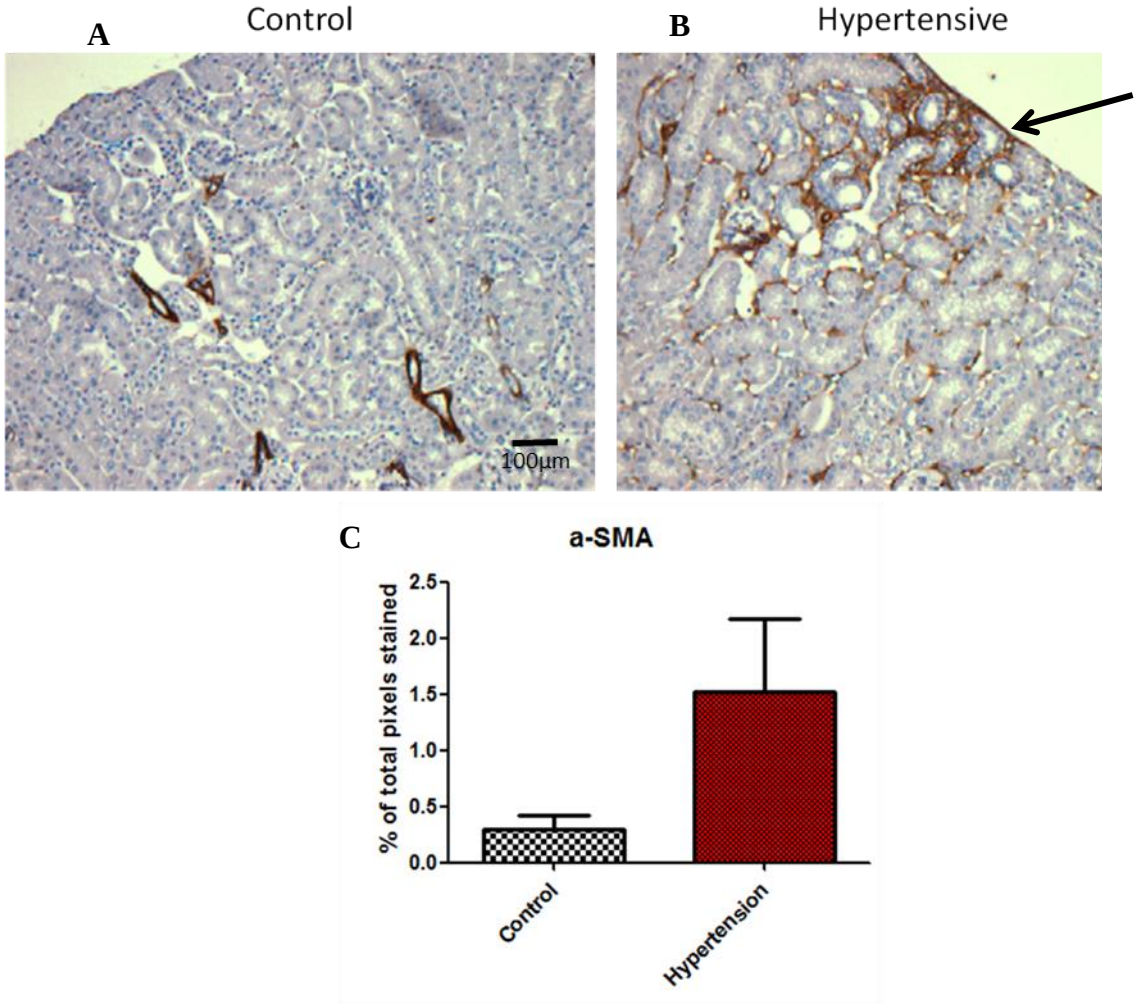

Figure 3 11 Representative images and quantification of α-SMA staining in hypertensive cohort compared to control.

Representative immunohistochemistry images of methacarn fixed paraffin embedded sections stained for α-SMA. Brown DAB staining in hypertensive animals (B) showed patchy peri-tubular staining in the cortex region of the kidney which was absent in control animals (A). C: Percentage of pixels stained with DAB was calculated using Adobe Photoshop. There is a trend towards an increase in the percentage of pixels stained with α-SMA in hypertensive cohort compared to control however, this is not significant. Means ±SEM, n=4-5, unpaired t-test.

3.2.6 Pericyte involvement in renal fibrosis in murine model of hypertensive renal injury

Platelet derived growth factor receptor beta (PDGFRβ) was used as both a pericyte marker and to determine if there was an increase in myofibroblasts in this model. In the literature it has been reported that during injury pericytes can differentiate into myofibroblasts which are the main ECM producing cells in fibrosis (Humphreys et al. 2010).

Sections stained for PDGFRβ showed an increase in staining in the cortex region of the sections- similar to the collagen III staining (Figure 3 12). On quantifying PDGFRβ staining it was shown to be significantly increased ($p=0.0056$) in the hypertensive cohort in comparison to control animals (Figure 3 12C).

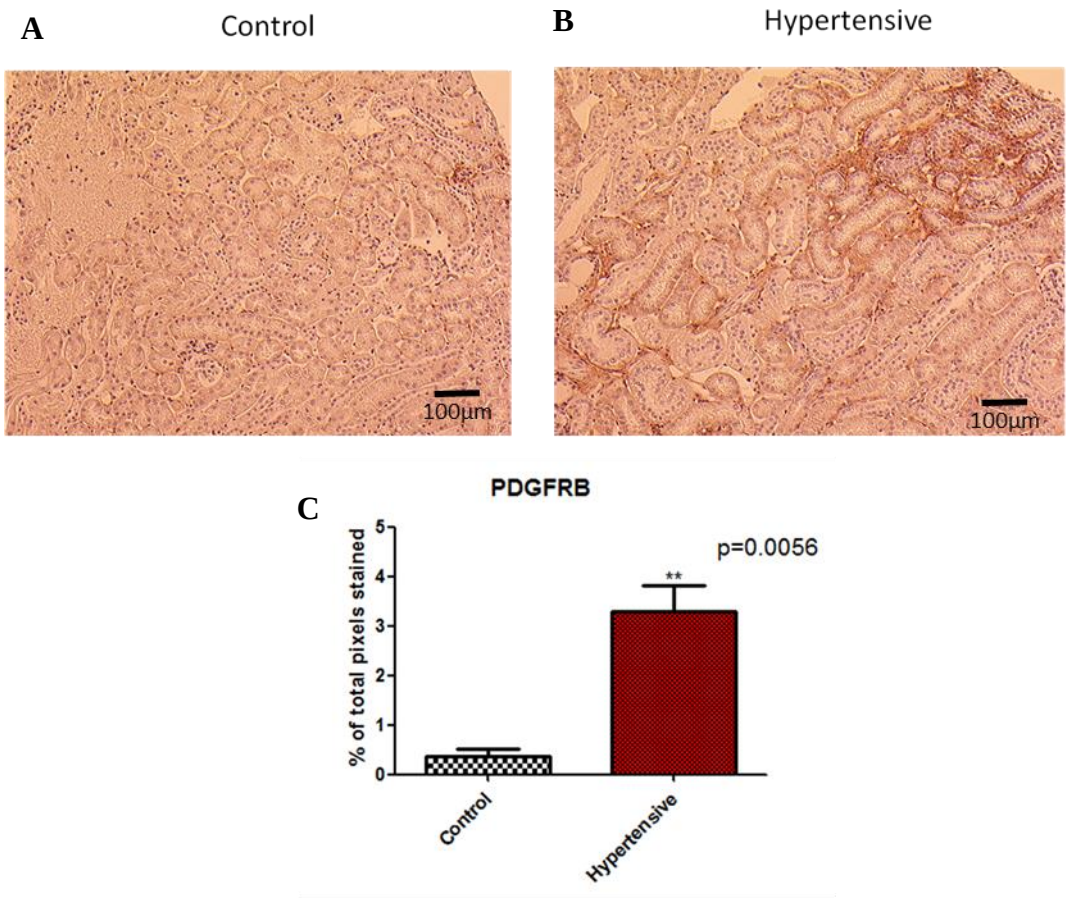

Figure 3 12 Representative images and quantification of PDGFRβ staining in the cortex of hypertensive mice compared with controls.
Representative immunohistochemistry images of methcarn fixed paraffin embedded sections show brown DAB staining denoting PDGFRβ localised to patches in renal cortex-similar to pattern seen in collagen III staining in the hypertensive mice (B). This staining is absent in control cohort (A). Staining was patchy around the cortex of the kidney in hypertensive animals. C: Percentage of pixels stained with DAB shows a significant increase in the hypertensive cohort compared to control (p=0.0056). Unpaired student's t-test. Means ±SEM, n=4-5, unpaired t-test.

3.2.7 Hypertensive animals show evidence of proximal tubule damage

Sections were also stained for Kidney Injury Molecule 1 (KIM1) - which is known to be markedly up-regulated in the injured kidney, specifically in the proximal tubular. Regions of very intense staining were observed in the treatment cohort which were absent in the control cohort (Figure 3 13). This was quantified by counting the number of positive tubular cross-sections, which tended to be more frequent as in the hypertensive group, although this was not statistically significant (Figure 3 13C).

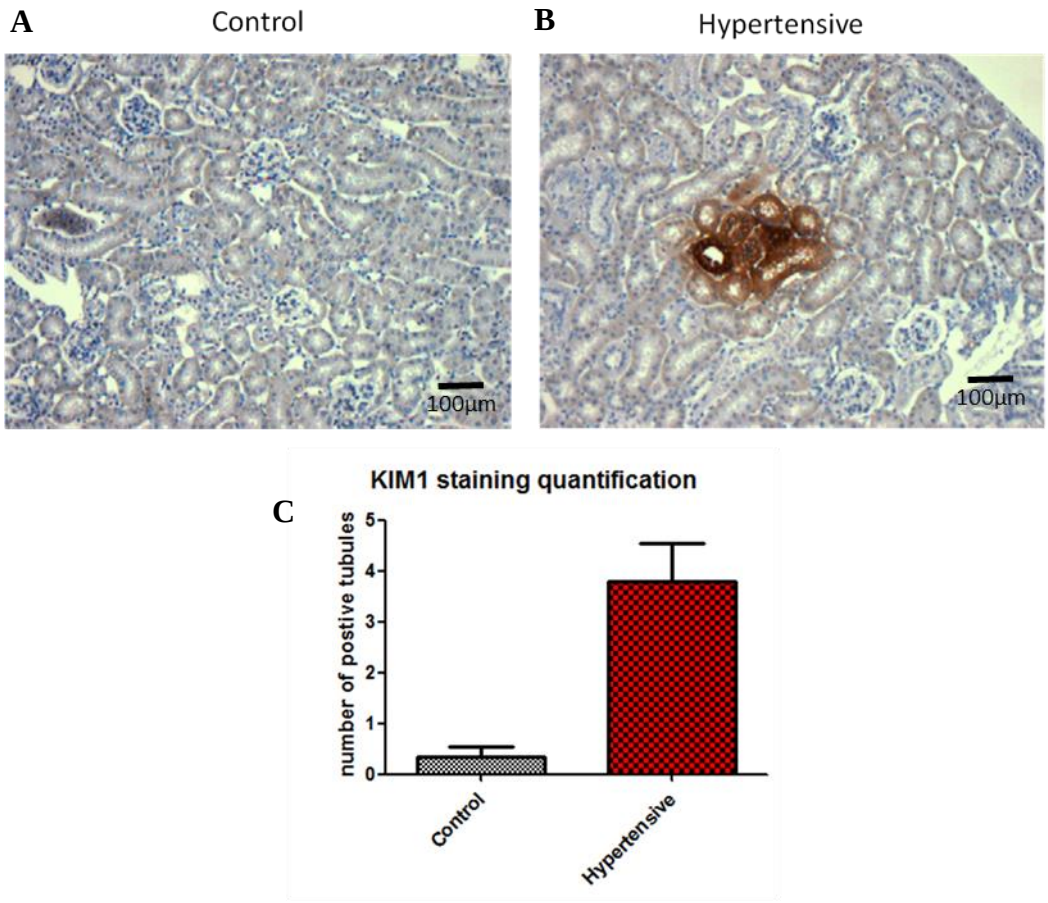

Figure 3 13 Representative images and quantification of KIM1staining in hypertensive and control mice.

Representative immunohistochemistry images of methcarn fixed paraffin embedded sections show strong detection of KIM1 staining in hypertensive (B) but not control mice (B). C: The number of positive stained tubules stained in x400 field with KIM1 shows a trend towards an increase in the hypertensive cohort compared to control but this is not significant. Means ±SEM, n=4-5, unpaired t-test.

3.2.8 There was an increase in mRNA expression of key fibrotic genes in hypertensive animals compared with controls

To further phenotype the developing model of hypertensive renal injury RT-PCR was carried out on RNA extracted from the renal cortices of mice from the hypertensive and control cohorts. The genes analysed were COL3A1 (Collagen III), COL1A1 (Collagen I), HAVCR1 (KIM1), PDGFRβ and TBP was used as the house keeping gene. While there was no difference in expression of PDGFRβ gene, there was a significant increase in collagen I (p= 0.0215) and collagen III (p=0.001) along with KIM1 (p=0.0225) in the hypertensive cohort compared with controls (Figure 3 14).

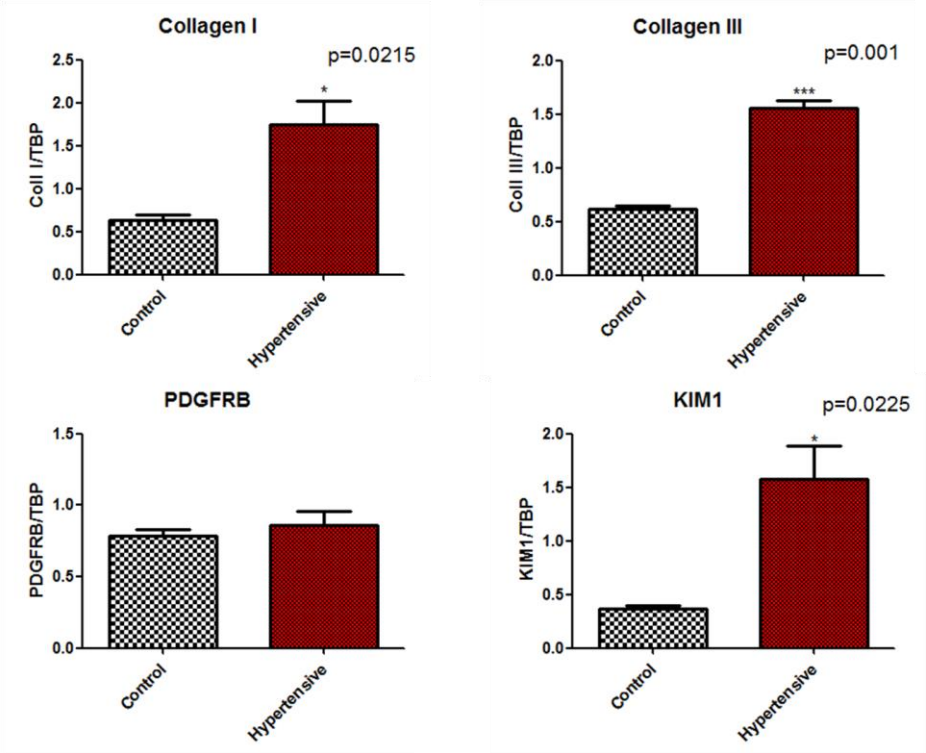

Figure 3 14 Expression of mRNA encoding fibrotic genes in the hypertensive cohort compared to controls.
rtPCR measurement of kidney mRNA levels relative to house-keeper gene mRNA levels was conducted on tissue removed from the cortex of the kidney. Genes examined were collagen I, collagen III, kidney injury molecule 1 (KIM1) and the pericyte marker PDGFRβ. A significant increase was noted in collagen I (p=0.0215), collagen III (p=0.001) and KIM1 (p=0.0225) when compared to control cohort. No difference was seen in PDGFRβ expression between the cohorts. Means ±SEM, n=4-5 (unpaired student's t-test).

3.2.9 Fibrotic genes elevated in murine models of fibrotic renal injury

Having established that many genes known to be implicated in fibrosis were up-regulated in the hypertensive mouse model, a key goal was to assess whether this was also the case for fibrosis-associated genes that had been identified in a microarray that was carried out on kidney samples from a rat model of diabetes and hypertension (Hesketh *et al.*, 2014). A subset of eight of the putative fibrosis genes were taken forward for replication in the murine model of hypertension. Almost all of these genes showed a trend for up-regulation in the renal cortex of hypertensive mice compared to control mice, however only Svep1 p=0.0050) and Tmem45a (transmembrane protein 45-alpha) (p=0.0071) were significantly up-regulated (Figure 3 15).

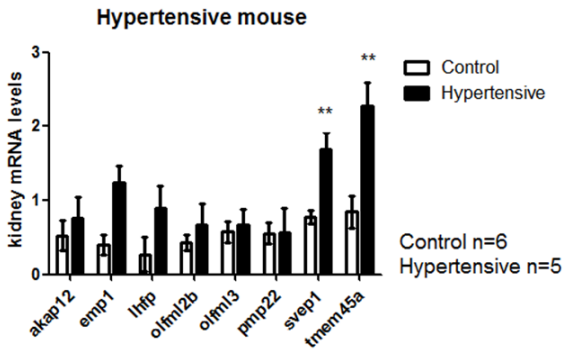

Figure 3 15 Novel genes from microarray of diabetic and hypertensive rat model in the murine model of hypertension.
There is a trend for genes to be upregulated in the hypertensive mouse model with SVEP1 (p=0.0050) and TMEM45α (p=0.0071) significantly upregulated.
Means±SEM, n=5/6, unpaired t-test.

3.3 Discussion

The combination of uninephrectomy, ANGII, DOCA and high salt diet results in hypertension, marked albuminuria, patchy renal fibrosis and an increase in the renal cortical expression of genes known to be implicated in the development of fibrosis. A model of hypertensive renal injury in the mouse was produced but due to side effects of the high dose ANG II infusion animals also exhibited aortic dissection. Due to the adverse nature of the model further study using the model as a basis for hypertensive renal injury was not pursued.

3.3.1 Uninephrectomy in combination with administration of ANG II, DOCA and high salt diet causes hypertensive renal injury and aortic dissection in the C57BL6 mouse

The patchy nature of the fibrosis in this model could be attributed to the relative resistance of the C57BL6 mouse to hypertension. It has previously been reported that 129/Sv mice are more susceptible to DOCA induced hypertension than the C57BL6 mouse (Hartner 2003). 129/Sv mice exhibited a mean arterial BP of 154.5±1.4 after DOCA treatment compared to C57BL6 animals with a MABP of 102.3±11.9 after DOCA treatment. The mice in the current study were mild-moderately hypertensive; the systolic blood pressure was measured at 140mmHg compared to malignant hypertension measuring above 200mmHg. This increase in blood pressure is enough to cause patchy fibrosis but not marked fibrosis as seen other murine models of fibrosis such as unilateral ureteric obstruction (UUO). In the UUO model many of the novel genes identified from microarray to be upregulated in the diabetic hypertensive rat model were also seen to be significantly upregulated in UUO, more so than in the hypertensive mouse model (figure 4 6). One hypothesis could be that due to the large fibrotic phenotype exhibited in mice after UUO, the genes which are upregulated in diabetic hypertensive injury are more highly expressed due to the increase in fibrosis in the UUO model.

In characterising the hypertensive murine model increases in blood pressure alone was not enough to drive renal injury. A pilot investigation was carried out without using uninephrectomy to determine if fibrosis was evident after ANG II, DOCA and high salt diet. Blood pressure increased but there was no evidence of fibrotic scarring in the

kidney. Therefore, uninephrectomy was needed to cause renal fibrosis in this model. Increases in profibrotic markers in both immunohistochemistry and rtPCR were established in this model. Increases in α-SMA staining in this model could represent myofibroblast infiltration into scarred areas from potentially differentiated pericytes. It could be hypothesized that pericytes may be transdifferentiating into myofibroblasts due to induced hypertensive injury and are therefore laying down ECM proteins producing fibrotic scarring. KIM1 has also been used as a marker for kidney injury in this chapter. The staining of KIM1 appears patchy. KIM1 is described as a marker of early kidney injury (Han *et al.*, 2002), the patchy nature of the staining in this chapter therefore suggests that the sparse staining could be due to the KIM1 antibody only staining active injury rather than established fibrotic scarring.

Due to the limited number of animals surviving to the end of the study there was difficulty in determining robust differences in results. For example, while there appeared to be an increase in α-SMA and KIM1 staining in the renal cortex of the hypertensive animals, this did not reach statistical significance due to the high standard error of the mean in both groups.

An increase in PDGFRβ IHC staining in the treatment group when compared with the control group was noted, however no significant difference in PDGFRβ gene expression between the groups was seen. Given the patchy nature of the fibrosis in this model, this could be due to the region of tissue chosen for RNA preparation not corresponding to the areas of fibrosis stained in the immunohistochemistry. Alternatively, it could be due to lack of statistical power, given the limited number of animals that survived to tissue harvest.

The development of fibrosis in this model is most likely due to ANG II. ANG II is both a vasoconstrictor and stimulates the release of aldosterone- this works to increase blood volume and blood pressure due to salt and water retention (Leong, Ng and Jaarin, 2015). ANG II primarily causes hypertension through the AT_1 (type 1 angiotensin receptor) receptor in the kidney (Crowley *et al.*, 2006). AT_1 receptors are absolutely required for development of ANG II dependent hypertension and cardiac hypertrophy (Crowley *et al.*, 2006). Once the AT_1 receptors have been eliminated from the kidney the residual repertoire of systemic, extra- renal AT_1 receptors is not sufficient to induce

hypertension/cardiac hypertrophy (Crowley *et al.*, 2006). ANG II mediated hypertension in rats was reported to show an increase in vascular superoxide production via membrane NADH/NADPH oxidase activation- this contributed to alterations in vascular tone. These rats exhibited impaired relaxations to acetylcholine- when Losartan was administered relaxations were normalized (Rajagopalan *et al.*, 2002). Due to its prevalence in causing hypertension numerous investigations into the cellular level and the mechanism behind ANG II actions have been reported (Rajagopalan *et al.*, 2002). ANG II is known to directly cause cell growth, regulate gene expression of bioactive substances such as vasoactive hormones, growth factors, ECM components and cytokines (Rajagopalan *et al.*, 2002). ANG II is also known to activate multiple intracellular signalling cascades in cardiovascular and renal cells suggesting that it is a major player in hypertension pathophysiology (Kim and Iwao, 2000).

These findings support that a model of hypertensive renal injury has been developed however, a more extensive injury would be desirable, where the injury is more homogenous throughout the kidney and between animals. This could be achieved by lengthening the experimental period however due to the deaths of animals to aortic dissection and cardiac tamponade this will not be possible.

3.3.2 Differences between hypertensive renal injury model and published model (Kirchhoff et al)

The current model of hypertensive renal disease was developed based on the findings of Kirchoff et al; however certain parameters were altered. This model was utilised due to the renal fibrosis exhibited by the model. The model gave a robust interesitial fibrosis with increased albumin:creatinine readings both of which are representative in the pathology of human hypertension.

The ANG II concentration in the model was lowered in this model as previous research indicated that a dose of 200ng/kg/min would be sufficient to increase blood pressure to a moderately hypertensive phenotype. Kawada *et al* (Kawada *et al.*, 2002) describes an increase in systolic blood pressure of 45%, while Harada (Harada *et al.*, 1998) *et al* describe blood pressures of 135mmHg when administered 200ng/kg/min

ANG II. To induce hypertension Kirchhoff *et al* employed 1% sodium in the drinking water whereas we employed a 3% sodium diet in our model. Due to the decrease in ANG II infusion concentration it was hypothesized that an increased sodium administration in the diet would reproduce similar levels of blood pressure to the Kirchhoff *et al* paper. The 3% sodium diet does not produce a taste aversion which is reported in high sodium administration in the water (Vollmer *et al.*, 2006). The recommended daily allowance of sodium in humans is 2.3g or 6g sodium chloride per day. On average humans consume 2000g of food per day making this approximately 1% of the overall diet. In mice the normal RM1 chow contains 0.25% sodium therefore the 3% sodium diet represents a large increase in sodium intake- 12 fold increase in sodium to a normal RM1 chow.

3.3.3 *Uninephrectomy in combination with administration of ANG II, DOCA and high salt diet causes increased mortality due to aortic dissection in the C57BL6 mouse*

While the combinatory injury stimuli resulted in measurable renal injury, it was noted that more animals in the hypertensive cohort were dying. On post mortem analysis the cause of death was found to be cardiac tamponade. No mortality results were presented in the paper by Kirchoff et al, however personal correspondence with the senior author revealed that they encountered up to 50% mortality from aortic dissection. Had this information been available at the time of deciding on a model of hypertension, an alternative model would have been employed. Other models such as reducing the ANG II dose to a lower 100ng/kg/min could have been employed to avoid aortic dissection. Alternatively finding a model which did not utilise ANG II, such as the DOCA and high salt diet along with uninephrectomy could have been trialled to determine if ANG II was necessary to the development of hypertension and subsequent renal fibrosis in this model. This illustrates the necessity to include all adverse effects in publications as recommended by the ARRIVE guidelines (Kilkenny *et al.*, 2010). Which of the combinatorial injuries was responsible for the aortic dissection is uncertain, but it is notable that high doses of ANG II have been employed to produce a model of aortic dissection in mice (Saraff et al 2003). Given that the mortality rate observed was greater than that permitted on the project licence, an amendment to the project licence was needed to enable continued use of the model. An amendment was

submitted in which the dose of angiotensin was further reduced, however the amendment was not granted for 8 months, therefore a decision was taken to move away from the model given the time constraints of the PhD project.

A power calculation utilising Lehr's formula (Equation 1) was carried to determine how many animals would be required for the hypertensive mouse model to be adequately powered. The parameters were set at 80% power and 5% significance to detect a 20% change in fibrotic response in collagen III staining. 36 mice in each group, as calculated from Lehr's formula, would be adequate to determine a 20% difference at 80% power 5% significance. This high n number in each group is largely due to the variability in fibrotic response between animals. As previously discussed the fibrosis in these animals was patchy and therefore variability between animals was large. This variability and the high death rate in the animals from cardiac tamponade coupled with the lengthy amendment to project licence prevented optimisation of the model and further work being pursued.

$$sample\ size\ needed\ per\ group = 16 \div (D)^2$$

$$D = \frac{d}{\sigma}$$

$$d = difference\ in\ means\ you\ want\ to\ find$$

$$\sigma = standard\ deviation$$

Equation 1 Lehr's Formula

3.3.5 Conclusions

A model of hypertensive renal injury was established but the injury is patchy and therefore variable between animals. Due to amendment to project licence the further development and phenotyping of the model had to cease. Further work on this model such as refining ANG II dose to prevent aortic dissection and increasing experimental length towards a more uniform fibrosis was planned to have an adequately powered

model however, in attempting to get the model licenced on the project licence an amendment was required. This took 18 months to be returned therefore further refinement of the model was out of the timescale of this PhD.

Chapter 4: The role of SVEP1 in the pathogenesis of renal fibrosis

4.1 Introduction

Fibrosis can be described as excessive accumulation of ECM which results in tissue destruction and compromised organ function (Eddy, 2000). Renal fibrosis is a defining feature of chronic kidney disease (CKD), regardless of the underlying disease aetiology (Efstratiadis *et al.*, 2009). Renal injury due to diseases such as diabetes or hypertension triggers a series of downstream pathways that destroy the normal parenchyma and lead to progressive fibrosis (Sun *et al.*, 2016). Tubulointerstitial fibrosis is the best histological predictor of adverse clinical outcomes even in kidney diseases where the primary injury is considered to be in the glomerulus (Mariani *et al.*, 2018). Hence, inhibiting the development of fibrosis is a longstanding therapeutic goal.

In the kidney, myofibroblasts are thought to be the predominant cell type responsible for increased production and deposition of extracellular matrix (ECM) proteins (Duffield, 2014). Myofibroblasts are α-SMA positive and are mainly located in the renal interstitium and to a lesser extent the glomeruli (Sun *et al.*, 2016). The origin of these interstitial myofibroblasts is controversial (Sun *et al.*, 2016), with varying studies suggesting that they arise from circulating fibrocytes (Abe *et al.*, 2001), via endothelial or epithelial to mesenchymal transition (Kalluri and Neilson, 2003) or from activation of pericytes . Recent studies suggest that pericytes are the major precursor of scar-producing myofibroblasts during kidney fibrosis (Gomez et al 2016). Like myofibroblasts, pericytes are derived from the mesenchymal lineage and in addition they are crucial for vascular homeostasis (Sun *et al.*, 2016). Pericytes are reported to produce renin (Stefanska *et al.*, 2016), which is important in regulating the extracellular volume to control blood pressure. Pericytes are stromal cells in close contact with the interstitial capillary endothelial cells and may function to regulate capillary permeability (Sun *et al.*, 2016). However, the lack of specific pericyte markers renders it difficult to determine the exact contribution of pericytes to fibrogenesis. For example, LeBleu *et al* have suggested that the contribution of pericytes to the myofibroblast pool is negligible (Lebleu *et al.*, 2013). They used

lineage tracing to demonstrate that only a small percentage of α-SMA positive myofibroblasts also expressed NG2 and PDGFRβ which are recognised pericyte markers. When the NG2 and PDGFRβ positive cells were depleted in the unilateral ureteric obstruction (UUO) model of renal fibrosis the severity of the fibrosis was not diminished, therefore LeBlue *et al* concluded that pericytes do not contribute to the myofibroblast pool significantly (Lebleu *et al.*, 2013) . Hence, the study of fibrosis is challenging as the cell type which is most responsible for causing the pathophysiology still unclear.

To investigate molecules that may be implicated in the progression and regression of fibrosis in chronic kidney disease, our lab previously developed a rat model of reversible diabetes and hypertension (Conway *et al.*, 2012). This model utilised the cyp1a1mRen2 rat, which has the mouse renin II cDNA integrated into the genome under the cyp1a1 promoter. The administration of indole-3-carbinol in the diet induces expression of mouse renin and the rats develop reversible and titratable hypertension. To render the rats diabetic, the pancreas toxin, streptozotocin, was administered. The rats were maintained hyperglycaemic and hypertensive over a 28 week time course, at the end of which the animals were culled and renal cortex was collected for histology and microarray purposes. Microarray was carried out to identify novel genes which were associated with diabetic/hypertensive injury and could potentially provide mechanistic insight or be targetable for therapy.

One of the genes identified from the microarray conducted on kidney tissue from the diabetic hypertensive rat model was sushi, von Willebrand factor type A, EGF and pentraxin domain containing 1 (*Svep1*). Under diabetic and hypertensive conditions an increase in expression of *Svep1* was noted, which reverted towards control levels after tight glycaemic and blood pressure control (Conway *et al.*, 2012). Furthermore, renal Svep1 expression correlated with that of other genes known to be implicated in fibrosis such as multiple collagen isoforms and PDGFRβ, a marker of pericytes/fibroblasts. Svep1 gene expression was also found to be elevated in the kidney in the murine model of hypertension (chapter 3). These finding led to a hypothesis that SVEP1 plays a role in the pathophysiology of renal fibrosis.

SVEP1 was first described in cultured bone marrow stromal cells (Shur *et al.*, 2006), and immunogold electron microscopy has demonstrated that it is located on the cell surface, consistent with a role in cell adhesion (Socher et al 2003). More recently it has been found to be a secreted extracellular matrix (ECM) protein (Morooka *et al.*, 2012). Svep1 is expressed in the tubulointerstitium of the kidney and is a ligand for α9β1 integrin (Sato-Nishiuchi *et al.*, 2012). This is of interest as ligand binding of α9β1 integrin has been linked to the activation of myofibroblasts (Ma *et al.*, 2016). These findings support the hypothesis that Svep1 may be implicated in fibrosis.

To assess the role of SVEP1 in renal fibrosis it was necessary to utilise *in silico*, *in vitro* and *in vivo* techniques. Firstly, a bioinformatics approach using publically available datasets (www.nephroseq.org) was employed to assess Svep1 gene expression in human kidney from patients with diabetes and chronic kidney disease and healthy transplant donors. Secondly, a mouse fibroblast cell line was used to determine the response of SVEP1 to a fibrotic stimulus. Finally, *in vivo* studies using the SVEP1 hemizygous mouse (B6N(Cg)-Svep1$^{tm1b(EUCOMM)Hmgu}$/J) in a robust model of renal fibrosis- unilateral ureteric obstruction (UUO)- were conducted to assess whether reduced SVEP1 expression altered the severity of renal fibrosis.

4.2 Chapter Aims

1. To assess whether Svep1 gene was differentially expressed in kidney tissue from patients with kidney disease compared with healthy controls
2. To investigate SVEP1 expression *in vitro* in a fibroblast cell line in response to fibrotic stimuli.
3. To determine the effect of a reduction of SVEP1 on renal fibrosis in a murine model of unilateral ureteric obstruction.

4.3 Results

4.3.1 Renal Svep1 gene expression is increased in human kidney disease

Microarray data derived from human kidney tissue available on the nephroseq database (www.nephroseq.org) was used to determine the expression of Svep1 in kidneys from healthy controls and patients with chronic kidney disease. In normal human kidney SVEP1 is significantly expressed 35% more in the renal tubulointersitium than the glomeruli (Figure 4 1).

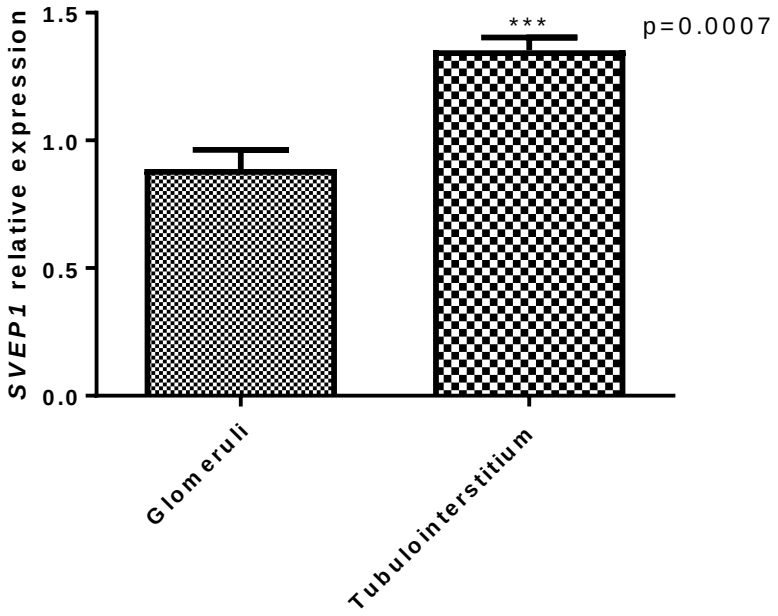

Figure 4 1 SVEP1 expression in glomeruli vs tubulointerstitium in normal human kidney. SVEP1 expression is significantly higher in the renal tubulointerstitium when compared to the glomeruli. Data are derived from the Higgins normal tissue panel from the Nephroseq database (Higgins et al. 2004). Values ± SEM, n= 20 in each group, unpaired t-test.

SVEP1 gene expression was significantly increased in the tubulointerstitium in patients with chronic kidney disease (CKD) versus healthy living donor biopsy samples (Figure 4 2 A). SVEP1 was also significantly higher expressed in the glomeruli in patients with diabetic nephropathy (Figure 4 2 B) when compared to healthy living donors.

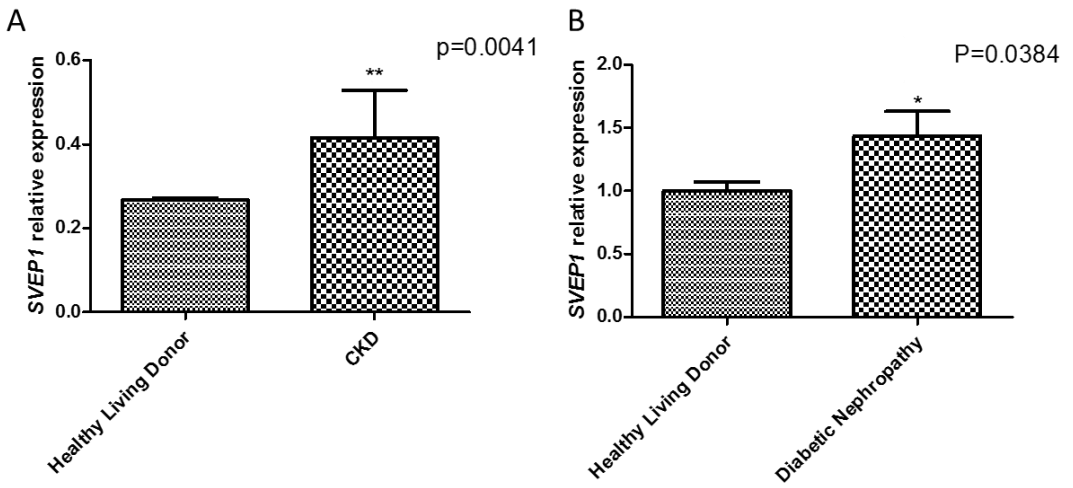

Figure 4 2 SVEP1 expression in healthy living donors vs (A) patients with chronic kidney disease (CKD)in the tubulointertitium and (B) patients with diabetic nephropathy in glomeruli.
A= SVEP1 expression in kidney biopsy from healthy living donors and patients with CKD. SVEP1 was significantly increased in CKD (p=0.0041).
B= SVEP1 expression in diabetic nephropathy patients vs healthy living donor kidney biopsy. SVEP1 expression was significantly increased (p=0.0384) in biopsies from patients with DN compared to healthy living donors.
Data are derived from the Ju CKD (Ju et al. 2015) (healthy living donor n=31, CKD, n=6) and the Woroniecka Diabetic nephropathy (Woroniecka et al. 2011) (healthy living donor n=13, diabetic nephropathy, n=9) datasets available from the Nephroseq database (www.nephroseq.org). Data are means ±SEM, unpaired t-test.

Glomerular SVEP1 gene expression was negatively correlated with glomerular filtration rate (GFR) - this is often used in the clinic as a readout of kidney function - suggesting that higher renal expression of SVEP1 was associated with lower renal function (Figure 4 3 A). Similarly, glomerular expression of col1a1, which encodes the extracellular matrix protein collagen I, was also negatively correlated with eGFR (Figure 4 3 B). Expression of the Col1a1 and SVEP1 genes were positively correlated, suggesting that col1a1 and SVEP1 expression may be similarly regulated (Figure 4 3 C).

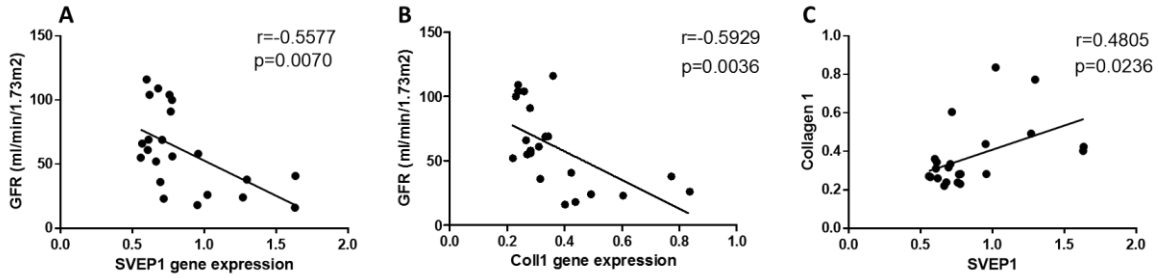

Figure 4 3 Correlation of SVEP1 with glomerular filtration rate (GFR) and collagen 1 in patients with diabetic nephropathy.
A= GFR was negatively correlated with glomerular gene expression of (A) Svep1 (r=-0.5577) and (B) Col1a1, a well-established marker of renal fibrosis, (r=-0.5929)
C= SVEP1 and col1a1 gene expression demonstrated positive correlation(r=0.4805) in patients with CKD. Data are derived from the Woroniecka Diabetic Nephropathy dataset, healthy living donor n=13, diabetic nephropathy n= 9)(Woroniecka et al. 2011) R and p values calculated using linear regression tool on GraphPad Prism 5.

4.3.2 Svep1 gene expression did not increase with administration of TGFβ in a fibroblast cell line

To assess the regulation of Svep1 in response to pro-fibrotic stimuli a mouse fibroblast C3H10T1/2 cell line was treated with TGFβ, a classical pro-fibrotic growth factor. Administration of TGFβ resulted in increased gene expression of acta2, which encodes α-smooth muscle actin (α-SMA), a marker of myofibroblast activation and col1a1, which encodes collagen I, an extracellular matrix protein found in scar tissue (Figure 4 4 A+B).

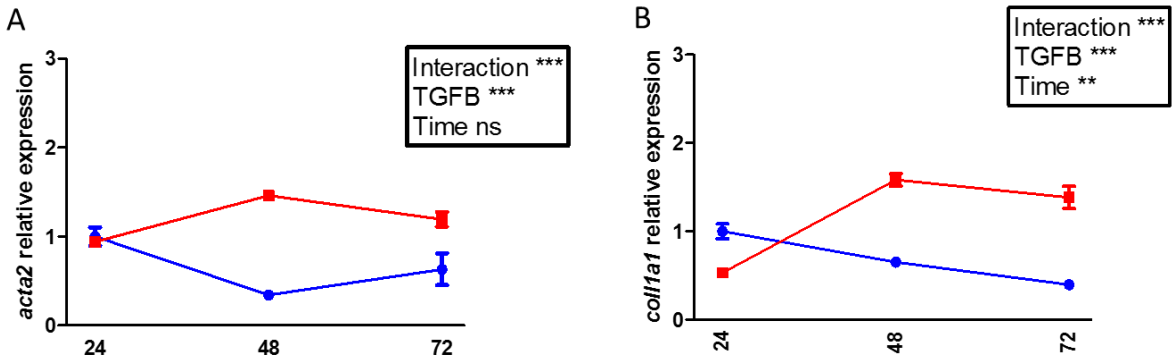

Figure 4 4 Expression of (A) α-SMA and (B) col1a1 genes in the C3H10 T1/2 fibroblast cell line in response to administration of TGFβ over 72hrs.
In C3H10 T1/2 cells treated with TGFβ (red line) daily there was increased expression of the (A) acta2 and (B) col1a1 genes at 24hrs, 48hrs and 72hrs, compared with non-treated cells (blue line). Data are means ± SEM, n=3, repeated measures 2 way-ANOVA where ***p<0.0001, ** p 0.0016, ns >0.05.

In this model SVEP1 gene expression, quantified by rtPCR, showed no statistical difference on administration of TGFβ compared to control cells which had no TGFβ administration (Figure 4 5).

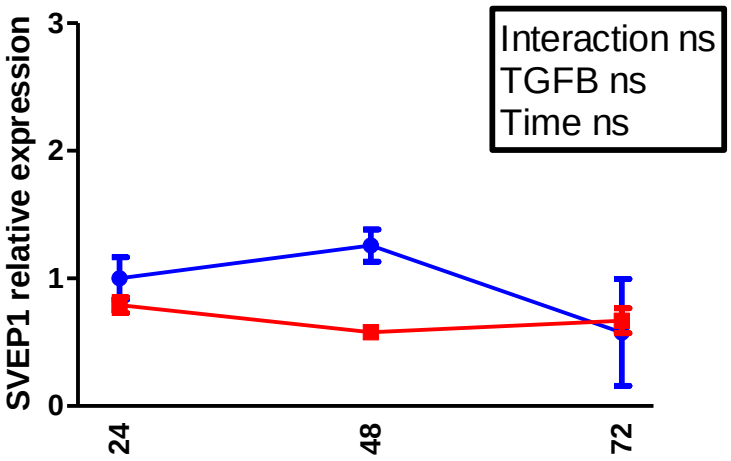

Figure 4 5 SVEP1gene expression in C3H10 T1/2 cells (control= blue) after 24hrs, 48hrs and 72hrs treatment with TGFβ (red).
Administration with TGFβ shows a trend towards reduced expression of SVEP1 compared with non-treated C3H10 T1/2 fibroblasts.
Means ± SEM, n=3, repeated measures 2 way- ANOVA, ns p>0.05.

4.3.3 Svep1 gene expression is up-regulated in the kidney in a model of fibrosis – unilateral ureteric obstruction

The human gene expression data determined that increased Svep1 expression was associated with renal disease, reduced renal function and correlated with expression of known markers of fibrosis. To determine whether Svep1 was causal in the fibrotic process, it was necessary to manipulate the Svep1 gene in a model of renal fibrosis. While the renal expression of the Svep1 gene was increased in the model of hypertensive kidney disease (Chapter 3), the high rate of mortality in this model precluded further study. Hence, an alternative model of fibrosis, unilateral ureteric obstruction (UUO) was considered. To determine whether renal Svep1 gene expression was increased in this model, the same panel of fibrotic genes that were up-regulated in the diabetic and hypertensive rats (Conway et al) and tested in the hypertensive mouse model including Svep1 (Chapter 3) was assessed using archived tissue from mice that had undergone UUO or sham surgery. Many of the genes seen to increase expression in the diabetic hypertensive rat model and hypertensive mouse model were seen to be significantly upregulated in the UUO model (Figure 4 6).

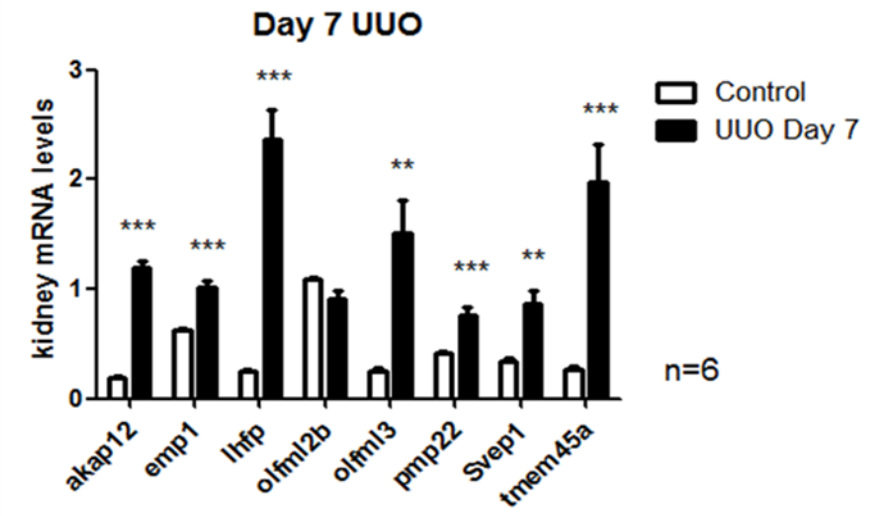

Figure 4 6 Renal cortical expression of genes that were linked to fibrosis in the diabetic and hypertensive rat model was assessed in mice that had undergone UUO and in sham controls.
7 days following UUO, akap12 (P=<0.0001), emp1 (P=0.0002), lhfp (P=<0.0001) olfml3 (P=0.0021), pmp22 (0.0009), svep1 (P=0.0029) and tmem45a (P=0.0006) are all significantly upregulated. Data are means±SEM, n=5/6, unpaired t-test.

Hence the UUO model was taken forward for investigation into the potential role of the Svep1 gene in renal fibrosis.

4.3.4 Svep1+/- mice did not exhibit an altered fibrotic response following UUO

Svep1-/- mice are not viable as they develop severe oedema during embryogenesis (Dickinson et al. 2016) potentially due to deficiency in lymphatic development (Karpanen et al. 2017). Hence Svep1+/- were imported from Jackson laboratories and used to assess the role of SVEP1 in renal fibrosis using the UUO model. UUO was performed by an experienced animal surgeon (Gary Borthwick) and 7 days later, RNA was extracted from the renal cortex of the obstructed and contralateral kidney and rtPCR was performed. Svep1 expression was reduced in Svep1$^{+/-}$ animals in both the obstructed and contralateral control kidneys, as expected from the animals having only 1 allele of SVEP1(Figure 4 7). Unexpectedly, SVEP1 expression was not significantly different between the obstructed and contralateral kidneys in either genotype (Figure 4 7).

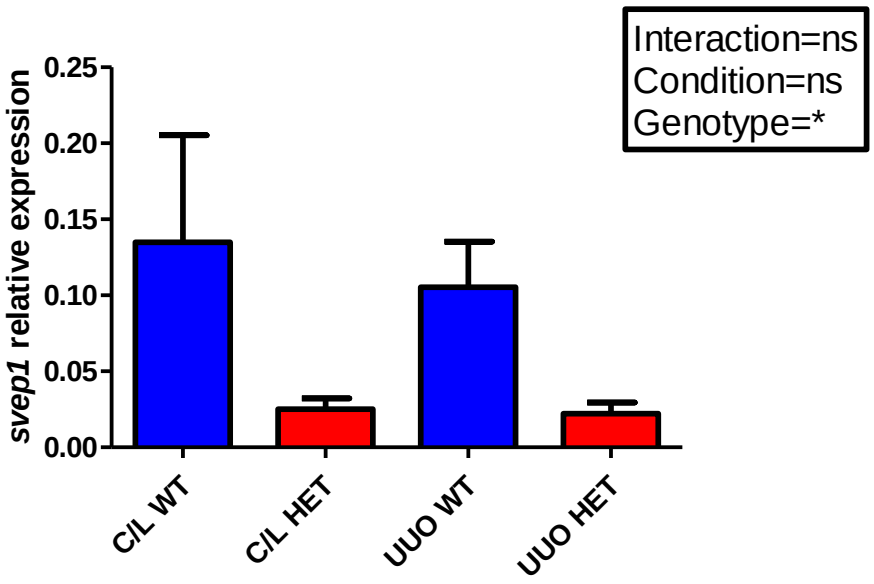

Figure 4 7 SVEP1 expression in wildtype (WT) versus SVEP1 hemizygous animals (HET). SVEP1 expression is reduced in animals which are hemizygous both in the contralateral and obstructed kidney. Gene expression is normalized to average expression of HPRT and cyclophilin. Data are mean ±SEM, n=8, 2 way ANOVA, * = p=0.0274.

All fibrotic markers were upregulated in the obstructed kidney compared to the contralateral kidney in both genotypes (Figure 4 8). There was no difference in the expression of Col1 (encodes collagen 1) and Col1a3 (encodes collagen 3) between genotypes in the contralateral (Figure 4 8 A+B) or obstructed kidneys. While Fn (encodes fibronectin) and Acta2 (encodes α-SMA) expression were comparable between the genotypes in the contralateral kidney, in the obstructed kidney there was a trend towards lower expression of both genes in the hemizygous animals but this was not significant (Figure 4 8 C+D).

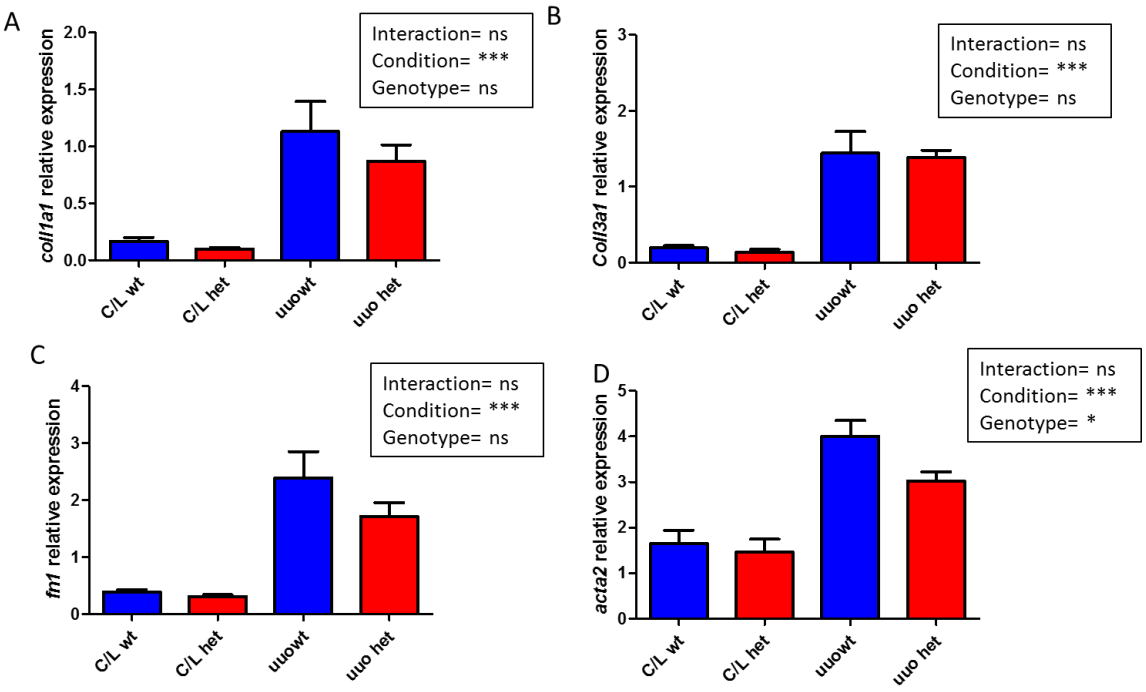

Figure 4 8Fibrotic gene expression in contralateral (C/L) vs UUO kidneys in SVEP1$^{+/-}$ (het) and wildtype animals (wt).
(A)= Col1a1, (B) Col3a1, (C) Fn1 and (D) Acta2 expression was increased in UUO kidney (p=<0.0001) compared with the contralateral kidney but only Acta2 showed a significant decrease after UUO in SVEP1$^{+/-}$ animals (p=0.0339). Fibronectin shows a trend towards a decrease after UUO in SVEP1$^{+/-}$ mice but this was not statistically significant. Data are means ±SEM, n=8, 2way-ANOVA.

Immunohistochemistry was carried out for fibrosis markers- collagen III, α-SMA and the pan collagen marker picrosirius red (PSR) staining. Images were quantified to determine if SVEP1$^{+/-}$ animals showed a different fibrotic response to wildtype animals in response to UUO.

α-SMA staining in the contralateral kidney is restricted to the smooth muscle wall of blood vessels and this can be seen in both genotypes (Figure 4 9 A+C). Interstitial α-SMA staining was observed in the renal cortex of obstructed (Figure 9 B+D), but not contralateral kidneys (Figure 9 A+C).

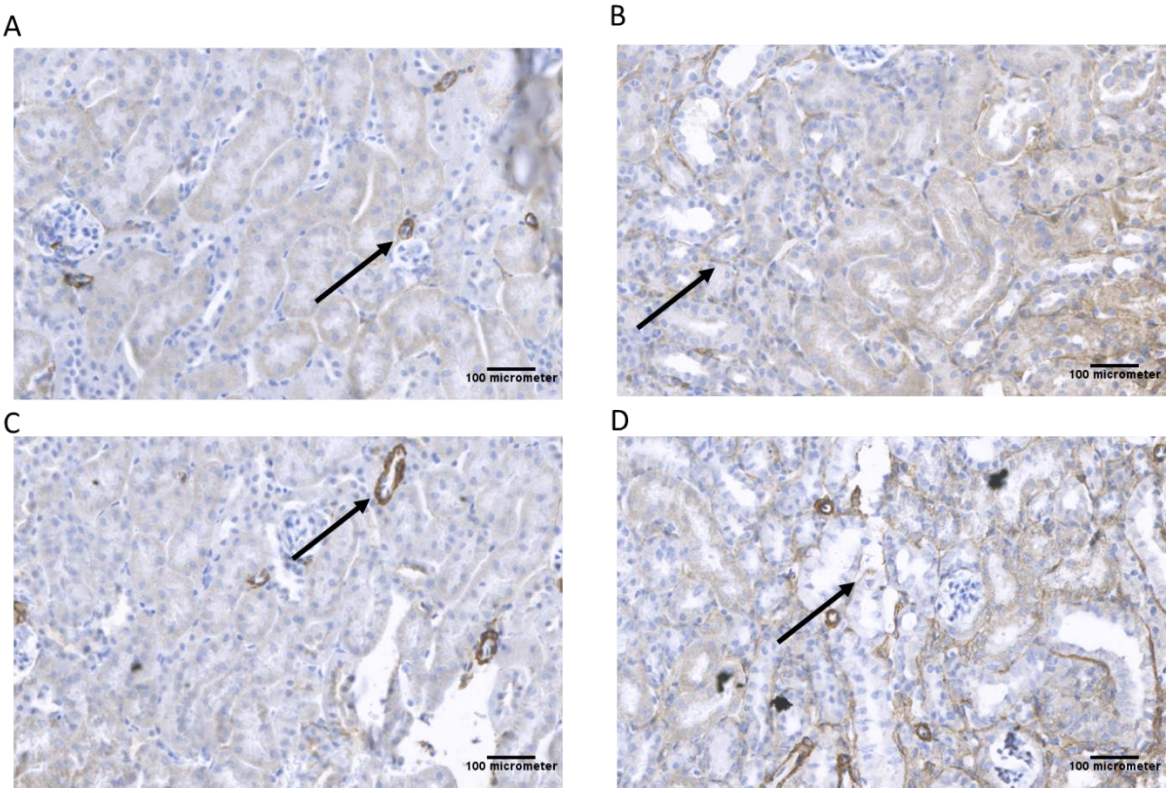

Figure 4 9 Representative images of immunohistochemistry staining for α-SMA in contralateral and UUO kidney sections.
A= IHC staining for α-SMA in contralateral kidney (x200) in wildtype animals. Staining only evident in blood vessels (arrowed).
B= IHC staining for α-SMA in UUO kidney (x200) in wildtype animals. Greater evidence of interstitial staining (arrowed).
C= IHC staining for α-SMA in contralateral kidney (x200) in hemizygous animals, blood vessel staining (arrowed).
D=IHC staining for α-SMA in UUO kidney (x200) in hemizygous animals, interstitial staining evident (arrowed).

Quantification of the α-SMA staining demonstrates that expression of α-SMA is similar between genotypes. After UUO animals show a significant increase in staining compared to the wildtype animals (Figure 4 10).

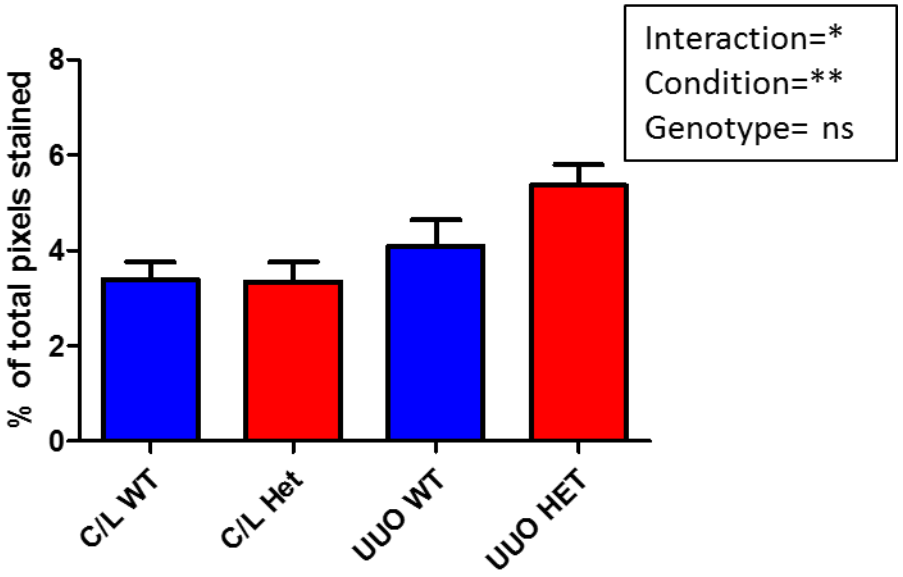

Figure 4 10 Quantification of α-SMA IHC comparing wildtype (WT) animals to hemizygous animals (Het).
α-SMA staining was significantly greater following UUO, however no significant difference was seen between genotypes in either the contralateral kidney or the kidney after UUO.
Data are means ± SEM, n=8, 2 way ANOVA *=p=0.044, **=p=0.0037.

Animals showed an increase in collagen III staining interstitially in the obstructed kidney (Figure 4 11 B+D) compared with the contralateral control (Figure 4 11 A+C).

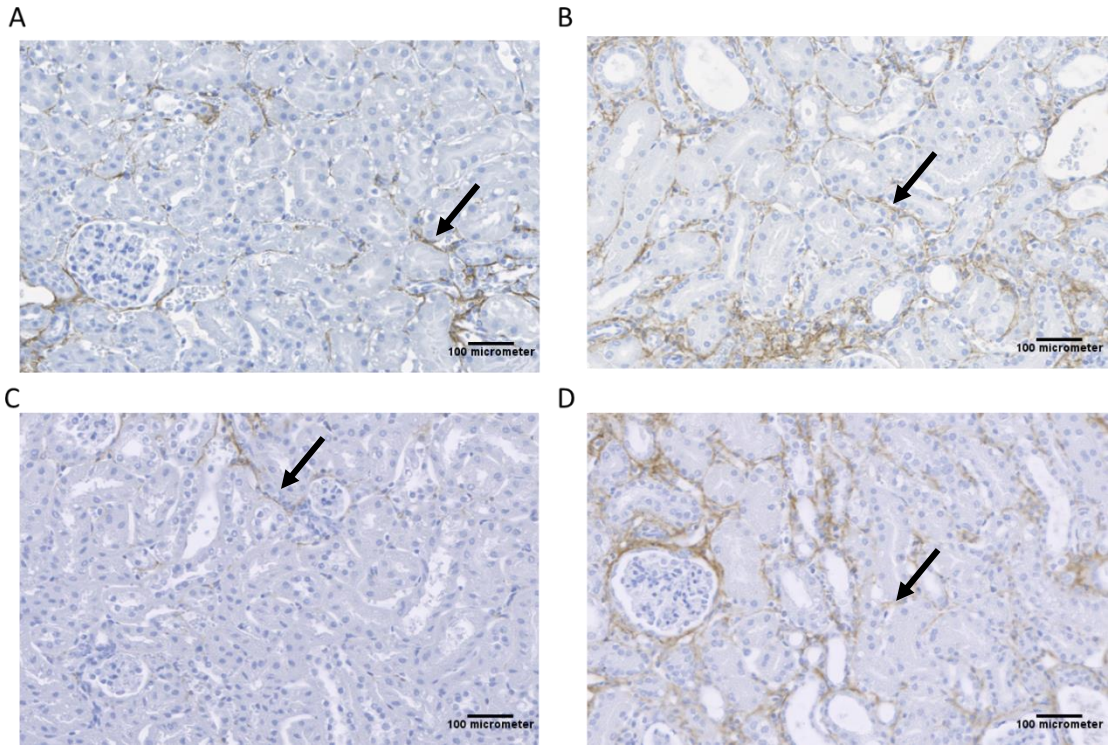

Figure 4 11 Representative images of immunohistochemistry staining for collagen III in contralateral and UUO kidney sections.
A= IHC staining for collagen III in contralateral kidney (x200) in wildtype animals.
B= IHC staining for collagen III in UUO kidney (x200) in wildtype animals. Greater evidence of interstitial staining (arrowed).
C= IHC staining for collagen III in contralateral kidney (x200) in hemizygous animals.
D=IHC staining for collagen III in UUO kidney (x200) in hemizygous animals, interstitial staining evident (arrowed).

On quantification of the collagen III staining there was a significant increase in staining between UUO and contralateral kidney but no statistically significant differences between genotypes (Figure 4 12).

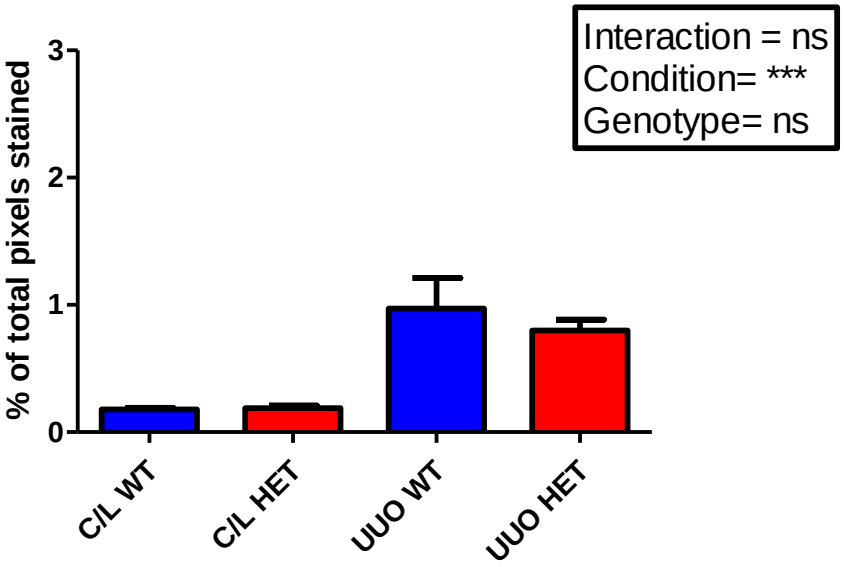

Figure 4 12 Quantification of collagen III staining between wildtype (WT) animals and hemizygous animals (HET). There was a significant increase in collagen III staining after UUO, however no differences in collagen III staining was observed between genotypes.
Means ±SEM, n=8, 2 way ANOVA, ***=p=<0.0001.

Sections of UUO and contralateral kidney from both SVEP1$^{+/-}$ and wildtype mice were stained for the pan collagen marker picrosirius red (PSR). PSR highlights collagen deposition and therefore, fibrosis in red. Evident increases can be noted by eye in the UUO kidney compared with contralateral kidney in both SVEP1$^{+/-}$ animals and wildtype animals. The red collagen staining has been identified with an arrow to show the interstitial fibrosis (Figure 4 13 B+D).

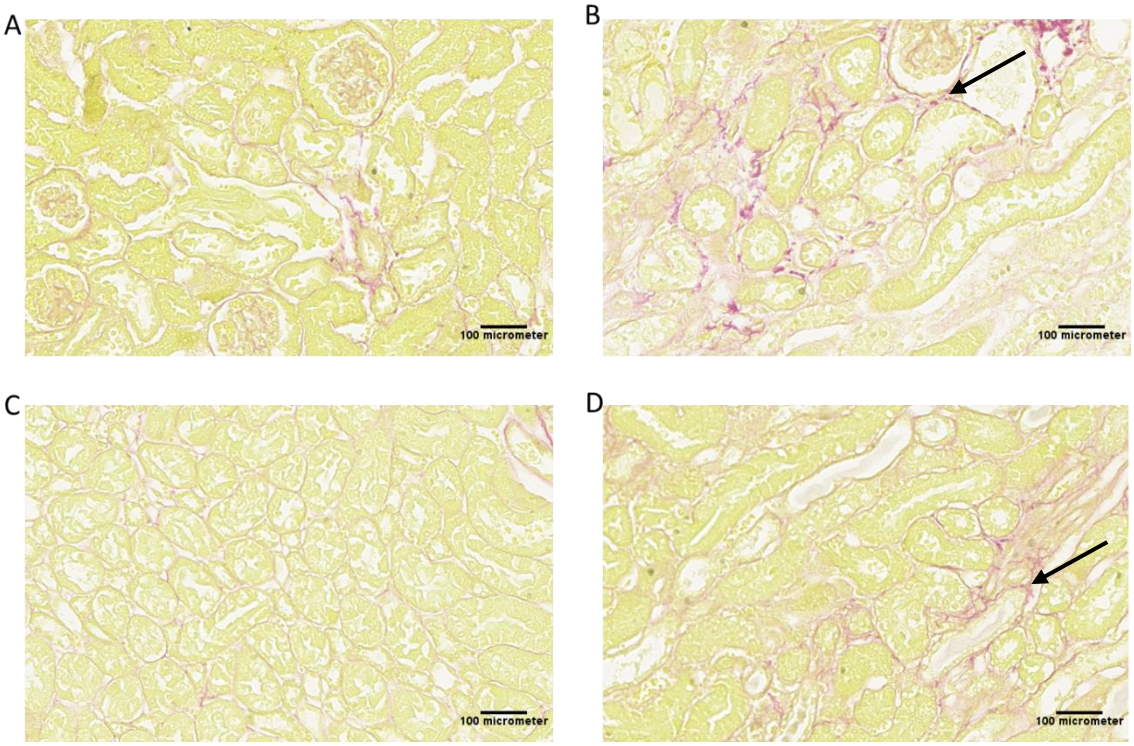

Figure 4 13 Representative images of Picosirus Red (PSR), a pan collagen marker.
A= PSR staining of contralateral kidney (x200) from wildtype animal.
B= PSR staining of UUO kidney (x200) from wild type animal, large areas of red staining denoting fibrosis in UUO kidney (arrowed).
C= PSR staining of contralateral kidney (x200) from hemizygous animal.
D=PSR staining of UUO kidney (x200) from hemizygous animal, showing increased red staining denoting fibrosis (arrowed).

On quantifying the PSR staining no differences were noted between genotypes. A significant increase in staining was noted between UUO and contralateral sections (Figure 4 14).

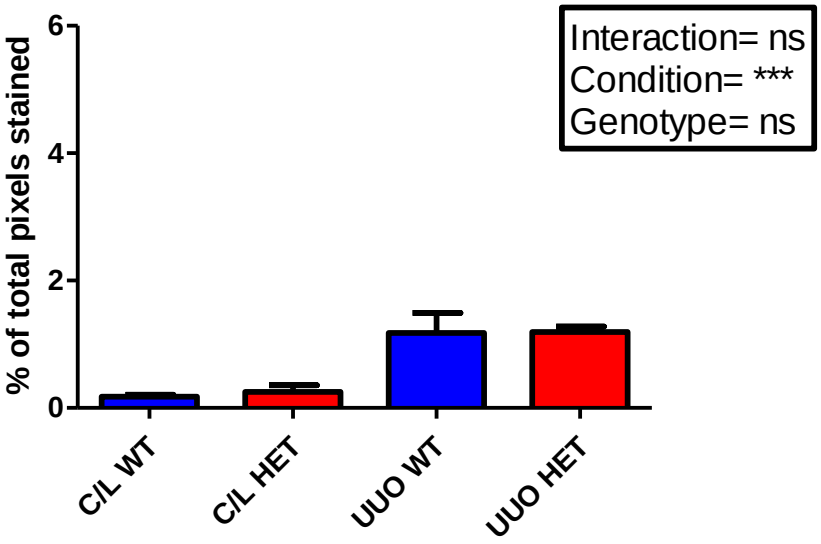

Figure 4 14 Quantification of PSR staining between wildtype (WT) animals and hemizygous animals (HET). There was a significant increase in PSR staining after UUO, however no difference in PSR staining was seen between genotypes.
Means ±SEM, n=8, 2 way ANOVA, ***=p=<0.0001.

4.4 Discussion

Svep1 expression was increased in the renal cortex in other animal models of fibrosis- namely the murine model of hypertension (Chapter 3) and the diabetic hypertensive rat model (Conway *et al.*, 2012, 2014). In the current chapter, analysis of publically available gene expression data from biopsy samples from the renal cortex of patients with kidney disease and controls indicated that Svep1 expression increased in human fibrotic kidney disease. Furthermore, the expression of Svep1 correlated with that of known pro-fibrotic genes, such as col1a1. This led to the hypothesis that Svep1 may be implicated in the pathogenesis of renal fibrosis. In this chapter the role of SVEP1 in renal fibrosis was assessed using both *in vitro* and *in vivo* models.

4.4.1 In vitro studies

The key findings from the *in vitro* studies were although other profibrotic genes such as acta2 (encodes α-SMA) and col1a1 (encodes collagen I) showed increased expression after the prototypical profibrotic stimulus TGF-β, SVEP1 expression showed a trend towards a decrease in expression, however, this was not significant. This model was performed in a pericyte/fibroblast cell line that has previously been used to model transition to a myofibroblast phenotype (Fabian et al. 2012). This cell line was chosen as it was hypothesised that Svep1 may be expressed in fibroblasts, given its association with other extracellular matrix genes.

It may be that the fibroblast line was not the best option to study Svep1 *in vitro* as it may be expressed more highly in other renal cell types. Attempts have been made to determine SVEP1 cellular location using immunofluorescence staining on tissue from wildtype and $SVEP1^{+/-}$ animals but difficulties in getting an antibody working prevented cellular localisation being determined. $SVEP1^{+/-}$ animals have a lacZ reporter which could be utilised to determine in what cell type animals express SVEP1. Immunofluorescence for β-galactosidase has also been attempted but with a negative result. X-gal staining has not been attempted due to the lack of specificity of this stain in the kidney.

Without knowledge of SVEP1 cellular localisation it is difficult to hypothesize what potential role it could be playing in both a metabolic phenotype and a fibrosis pathology.

4.4.2 In vivo studies

The *in vivo* fibrosis studies utilised the SVEP1$^{+/-}$ hemizygous mouse to determine if a reduction in SVEP1 would affect fibrosis pathophysiology. In these studies SVEP1$^{+/-}$ mice showed no difference both in fibrotic gene expression and immunohistochemistry for fibrotic markers compared to wildtype mice. Therefore, it appears that SVEP1 does not play a major role in the pathophysiology of renal fibrosis contrary to the hypothesis of this chapter.

SVEP1 expression was seen to be increased in both the hypertensive mouse model and diabetic hypertensive rat model (chapter 3). The role of SVEP1 in mediating renal fibrosis in hypertension and diabetic nephropathy could have been analysed by using one of the above models. However, in the hypertensive mouse model renal fibrosis is heterogeneous and patchy and therefore would be difficult to determine any effect by genotype. Furthermore, the high mortality rate in this model precluded further use. The diabetic hypertensive rat model was not used due to the length of the study being 28 weeks to see injury and due to the time constraints of the PhD this was not deemed appropriate. Furthermore, no rat models of genetic Svep1 depletion were available, while the Svep1+/- mouse was available from Jackson laboratories.

The *in vivo* model of fibrosis employed - UUO- is widely recognised as a standard model of renal fibrosis in mice. Fibrosis can be induced rapidly (<1 week) and the surgery is not technically challenging. Preliminary studies using archived tissue determined that Svep1 gene expression was increased in the renal cortex 7 days following UUO. Unexpectedly in the study performed in this chapter, there was no increase in Svep1 expression in the UUO compared with the contralateral kidney, indeed there was a trend downwards. The reasons for this discrepancy were not clear. It may be a chance finding, or it may relate to the fact that contralateral kidney is not the best choice of control as it may undergo changes induced by obstructing the opposite kidney. Kidneys from animals that have undergone sham surgery would have

been a better choice of control, but this was not possible due to the limited number of Svep1$^{+/-}$ animals available in the colony.

The conclusion of the current study is that Svep1 does not play a major role in the pathogenesis of renal fibrosis. SVEP1 has been reported as an ECM protein (Morooka *et al.*, 2017) and therefore could be produced alongside other ECM proteins, and be a bystander in the pathogenesis of renal fibrosis. However, some limitations of the study preclude definitive rejection of a role for Svep1 in fibrosis.

An approximately 50% reduction in Svep1 expression was observed in the Svep1$^{+/-}$ mice, as would be expected from loss of one allele. It may be that this degree of reduction in Svep1 was insufficient to alter the fibrotic outcome. SVEP1 expression in the current UUO model showed a trend towards a decrease after UUO. The fact that Svep1 is down-regulated during UUO may explain why no differences were seen with further Svep1 depletion in the SVEP1$^{+/-}$ mice compared with wildtype mice. Hence, overexpressing SVEP1 might be of interest to determine if that alters the pathophysiology of renal fibrosis

A power calculation utilising Lehr's formula (Equation 1) was carried to determine if the *in vivo* experiments were adequately powered to disprove the null hypothesis. The parameters were set at 80% power and 5% significance to detect a 20% change in α-SMA gene expression. 21 mice in each group would be required to detect a 20% difference at 80% power 5% significance.

$$sample\ size\ needed\ per\ group = 16 \div (D)^2$$

$$D = \frac{d}{\sigma}$$

$$d = difference\ in\ means\ you\ want\ to\ find$$

$$\sigma = standard\ deviation$$

Equation 2 Lehr's Formula

The results from Lehr's formula suggest that the study is underpowered to state SVEP1 does not play a more minor role in the pathogenesis of renal fibrosis and therefore the null hypothesis for this body of work cannot be automatically assumed.

4.4.3 Stimulus and models used to produce fibrosis

Cell models of fibrosis have predominantly been developed in renal cell lines and there is a precedent for study of fibrosis *in vitro* in the liver field (Iredale, 2007). However, cell lines cannot model the complex interplay of the *in vivo* microenvironment (Jenkinson *et al.*, 2012). Cell lines offer a detailed study of cell behaviour and effect of specific mediators but not the cell-cell interactions which occur *in vivo*. TGFβ administration is the most used fibrosis initiator in renal cell lines. Mesangial cells and renal fibroblasts grown in an 8-well plate showed disruption of cell monolayer and induced cell migration into nodules in a dose, time and smad 3 dependent manner when treated with TGFβ (Xu *et al.*, 2007). SVEP1 expression tends to decrease on administration of TGFβ however, α-SMA expression and collagen I expression are both significantly increased suggesting that a fibrotic phenotype has been established in the C3H10 T1/2 cell line in our hands. Alternative stimuli- ANG II and PDGF-BB were also trialled in the CH3T1/2 cells however, the fibrotic phenotype was not seen.

An alternative *ex vivo* model to investigate fibrosis is the precision cut kidney slices - both murine and human kidney slices have been reported in the literature. This model gives the cellular heterogeneity and organ architecture that is missing in *in vitro* work. Stribos *et al* report viability of human kidney slices by utilising ATP content and LDH leakage and show slices to be viable to 96hrs. However, there is a decrease in viability particularly at the 72hr and 96hr time point. On administration of TGFβ fibrotic markers such as fibronectin and collagen 1 increase. This work is corroborated in Poosti *et al* showing that mouse kidney slices were viable up to 72hrs (utilising ATP as a marker) (Poosti *et al.*, 2015).On TGFβ1 administration fibrotic markers-α-SMA, fibronectin and collagen 1- expression was increased. In our lab we conducted some work on precision cut kidney slices but found it impossible to maintain the viability of the slices for the 72 hour period that would be required to study fibrotic mechanisms, and therefore this work was preliminary and not included in the thesis.

Animal models of renal fibrosis are reviewed in chapter one however, the use of UUO as a model for fibrosis will be discussed here. UUO was chosen as a model of renal fibrosis due to it being the most commonly used model of renal fibrosis in the literature (Peng *et al,*. 2015). UUO may be used to initiate fibrosis in order to study pro-fibrotic mechanisms but it may also be used to evaluate antifibrotic treatment. It causes a rapid onset of interstitial fibrosis (within 7 days) compared to the hypertensive mouse model in chapter 3, which requires 6 weeks. The UUO surgery is relatively straightforward and hence induces a robust interstitial fibrosis (Peng *et al,*. 2015)which is similar in every mouse when the work is conducted by a rodent surgeon.

Other models of renal fibrosis in rodents do exist such as the 5/6 nephrectomy- first described by Platt in 1952. In this model 2/3 of the left kidney are excised followed by a right nephrectomy. This causes compensative renal hypertrophy, glomerular necrosis, capillary wall collapse, progressive mesangial distension, tubular cell atrophy and fibrosis (Peng *et al,*. 2015). Another well reported model is the ischemia-reperfusion model which particularly focuses on tubule damage as they are highly sensitive to ischemia and hypoxia (Peng *et al,*. 2015). This model causes detachment of the brush border of tubular epithelial cells, epithelial cell degeneration, necrosis, detachment and apoptosis of tubular epithelial cells. This is the classic model for acute tubular injury and regeneration, but may also cause interstitial fibrosis if the ischaemia is prolonged.

4.4.4 Future Directions

The *in vitro* findings of a trend towards a decrease in SVEP1 expression in a fibroblast cell line following administration of TGF-β are interesting however extra work is required to solidify these findings. Further repetitions of the TGF-β assay are required to see whether the trend for a decrease in Svep1 gene expression is genuine. The TGFβ stimulus was used as the fibrotic stimulus in this body of work as it is a well-recognised fibrotic stimulus for *in vitro* work. Other stimuli such as ANG II and PDGF-BB could be added to the fibroblasts. Further studies could be attempted to look at SVEP1 expression in response to ANG II which is more aligned to a hypertension phenotype. However, recreating hypertensive (or diabetic) model *in vitro* presents many issues as to the similarity of an *in vitro* system to the *in vivo* environment.

The most pressing future direction would be to establish in which cell type SVEP1 is expressed. This could be critical to the hypothesis that SVEP1 is a marker of a fibroblast and that the reason no difference was seen between $SVEP1^{+/-}$ mice and wildtype mice was due to the fact SVEP1 is just an ECM protein, a bystander in the fibrotic process. Further studies have begun to isolate $PDGFR\beta^{+}$ cells from a $PDGFR\beta^{+}$ reporter mouse to determine if the pericyte/fibroblast population expresses SVEP1. This could be significant in understanding which cells express SVEP1 and to try to determine where in the cell SVEP1 resides. Such information may also enable Svep1 to be genetically depleted in specific cell types. While $Svep1^{-/-}$ mice are not viable, it may be possible to knock out both Svep1 alleles in specific cell types and produce viable mice. Such mice may be more useful than $Svep1^{+/-}$ mice in assessing the role of Svep1 in fibrosis.

Further analysis of SVEP1's role in the pathophysiology of renal fibrosis *in vivo* could be furthered by repeating in other animal models of fibrosis. The UUO is a very robust model of fibrosis and may overwhelm any protective effect of Svep1 depletion. However, as outlined above, other models of renal fibrosis such as the hypertensive model described in chapter 3 or fibrosis induced by toxins such as folate or aristolochic acid are not without their limitations also.

4.4.5 Chapter Conclusion

SVEP1 is upregulated in human chronic kidney disease and correlates with known fibrotic markers in human kidney injury. However, *in vitro*, in the fibroblast cell line, C3H10 T1/2 cells show a decrease in expression of SVEP1 after administration of TGFβ. No differences in fibrosis pathophysiology were seen when $SVEP1^{+/-}$ mice underwent UUO compared to wildtype littermates this could suggest that SVEP1 does not play a major role in fibrosis development and progression however, the study was underpowered to say definitively that SVEP1 does not play a role in renal fibrosis.

Chapter 5: SVEP1's role in Metabolism

5.1 Introduction

The previous chapter focused on the role of Svep1 in the development of renal fibrosis. While this work was being performed, a paper by Stitziel *et al* was published detailing the association between a single D2702G point mutation in Svep1 and coronary artery disease, type 2 diabetes and an increase in blood pressure in humans (Stitziel *et al.*, 2016).

Stitziel *et al* reported that there was a 14% higher risk of development of coronary artery disease in those who inherited the low-frequency missense variant of SVEP1 D2702G (Stitziel *et al.*, 2016). This variant is found in approximately 3% of Caucasians and results in the substitution of aspartate for glycine. It was also associated with higher systolic blood pressure- 0.94mmHg higher for each copy of the 2702G allele. The 2702G variant was reported to be associated with a 14% increased risk of type 2 diabetes, however plasma lipid levels were not significantly different between those who had the 2702G variant and 2702D homozygotes. The authors speculated that the increased blood pressure and risk of type 2 diabetes could be responsible for the increase in coronary heart disease associated with the 2702G allele. However, little is known about the function of the Svep1 protein and the authors of the paper did not speculate on the mechanism by which the 2702G variant confers higher risk of type 2 diabetes or increases blood pressure.

Therefore, it was essential to investigate the mechanisms by which SVEP1 regulated metabolic risk and the current chapter will describe studies performed in B6N(Cg)-Svep1$^{tm1b(EUCOMM)Hmgu}$/J mice to address this question.

Chapter Hypothesis:

SVEP1$^{+/-}$ mice would show a more insulin resistant phenotype to wildtype littermates.

5.2 Chapter Aims

1. To determine if SVEP1$^{+/-}$ mice have altered body weight and/or body composition (such as lean or fat mass).
2. To determine if SVEP1$^{+/-}$ mice have altered blood glucose and/or insulin sensitivity.

5.3 Experimental Plan

The experimental plan is described in Figure 5 1 below. At the start of the experiment the Svep1$^{+/-}$ mice and their wildtype littermates were weighed and body composition, including lean and fat mass, was assessed using time domain nuclear magnetic resonance scanning (TDNMR).

Animals were trained to use water bottles which are specific for the Phenomaster system and were then placed in the Phenomaster system cages and allowed to acclimatise before readings being taken for 24hrs. The TSE Phenomaster indirect calorimetry cages were used to investigate fundamental metabolic parameters such as respiratory exchange ratio (RER), vCO_2 exhalation, vO_2 inhalation, activity and calorie utilisation to give an insight into potential metabolic differences between Svep1$^{+/-}$ mice and wildtype littermates.

Due to the D2702G point mutation in humans being linked to type 2 diabetes, determining blood glucose and insulin sensitivity was also important. An oral glucose tolerance test (GTT) was performed at baseline and we utilised a glucometer to measure blood glucose and an ELISA to measure plasma insulin before and after the administration of glucose by gavage. From these results we could produce a HOMA-IR which is indicative of insulin resistance from basal measurements of plasma insulin and glucose.

Once the baseline metabolic assessment was performed, animal were commenced on a high fat diet. Over a 6 week timeline, animals had body weights monitored. At the end of the 6 weeks animals were placed back in the Phenomaster system and allowed to re-acclimatise and then readings taken for 24hrs. GTT and body weights were then conducted. At this time point it was determined from the GTT result that no overt diabetic phenotype was being displayed and therefore animals were kept on the HFD

for a further 6 weeks. At the 12 week time point a final GTT was conducted and animals were culled and organs harvested for analysis.

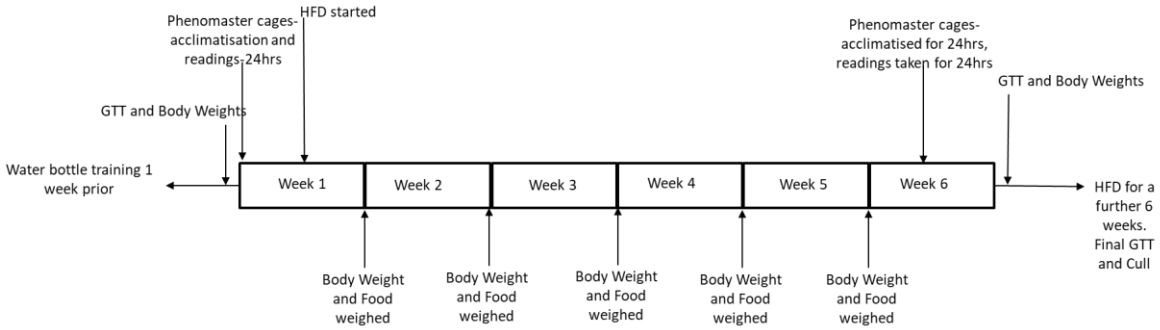

Figure 5 1Schematic representation of the metabolic study using the phenomaster system. Animals had an oral GTT at time 0.. Mice were placed in the phenomaster cages for 48hrs and readings taken in the second 24hr period. Animals were removed and placed back in the home cage and a high fat diet (HFD) was administered. Body weight and food was monitored weekly until the 6 week time point and animals were placed back in the phenomaster cages for a further 48hrs before the 6 week GTT was carried out. Mice were kept on a HFD for a further 6 weeks and a final GTT conducted at the 12 week time point.

5.4 Results

The body mass of Svep1$^{+/-}$ mice and wild-type littermates was similar at baseline (Fig 5.2A). On a high fat diet the weight gain was similar between the two genotypes (Figure 5.2 B).

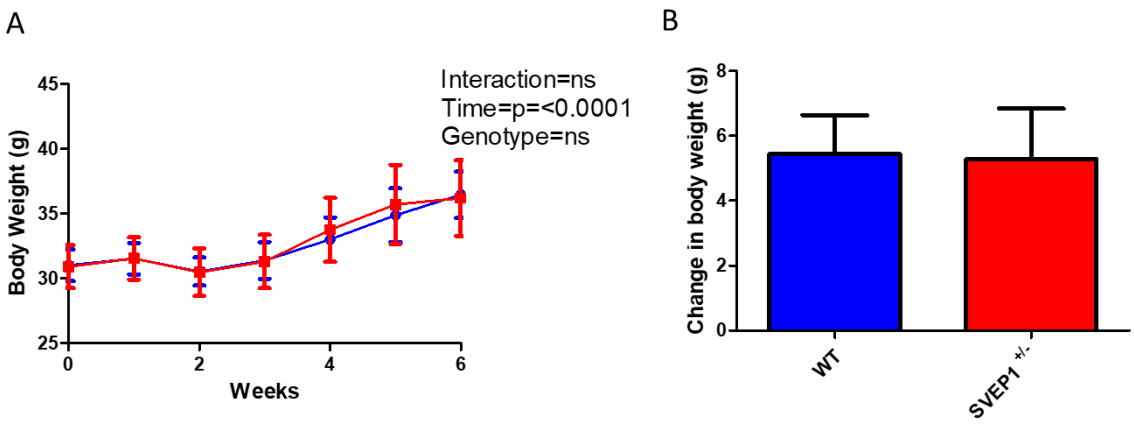

Figure 5 2 Body weights of wild type (blue) and hemizygous mice (red) at baseline and during 6 weeks of HFD.
A= No difference in body weight was seen between genotypes at baseline or during 6 weeks of HFD. Animals gained weight on HFD, this was significant (p=<0.0001).
Means ±SEM, N=4, repeated measures 2 way-ANOVA.
B= change in body weights from baseline and after 6 weeks HFD. No significant difference was noted between genotypes. Means ±SEM, N=4, unpaired t-test.

The lean and fat mass of the experimental cohort was measured before and after high fat diet using Time Domain Nuclear Magnetic Resonance (TDNMR). Lean mass tended to be lower after 6 weeks of high fat diet, but this was not statistically significant, while fat mass increased with HFD (Fig 5.3). There was no significant difference between the genotypes in either lean or fat mass on normal chow or after high fat diet.

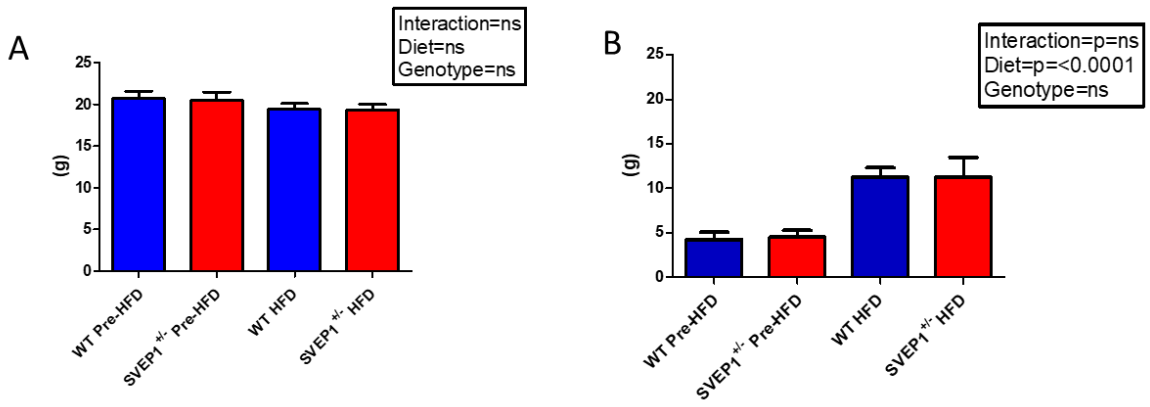

Figure 5 3 Lean and Fat mass measured by Time Domain Nuclear Magnetic Resonance (TDNMR). A= lean mass on control (RM1chow) and after high fat diet (HFD) in both wild type (blue) and hemizygous (red) animals. Lean mass tended to be lower after high fat diet, though this was not statistically different (p=0.18). No difference was detected between genotypes.
B= fat mass of wild type and hemizygous mice on control (RM1 chow) and after HFD feeding. Fat mass increased after HFD feeding, but there was no significant difference between genotypes.
Means ±SEM, N=4, 2 way-ANOVA.

After 12 weeks on a high fat diet animals were culled and subcutaneous, gonadal and mesenteric fat pads were weighed. In addition, another cohort of Svep1$^{+/-}$ and WT mice on normal chow were culled and their fat depots were weighed. SVEP1$^{+/-}$ mice showed a significant decrease in subcutaneous fat pad weight compared to WT mice (p=0.0030) (Figure 5 4 A). There was a trend towards the gonadal and mesenteric fat pads being lighter in Svep1$^{+/-}$ mice than wildtype littermates (Fig 5.4B+C).

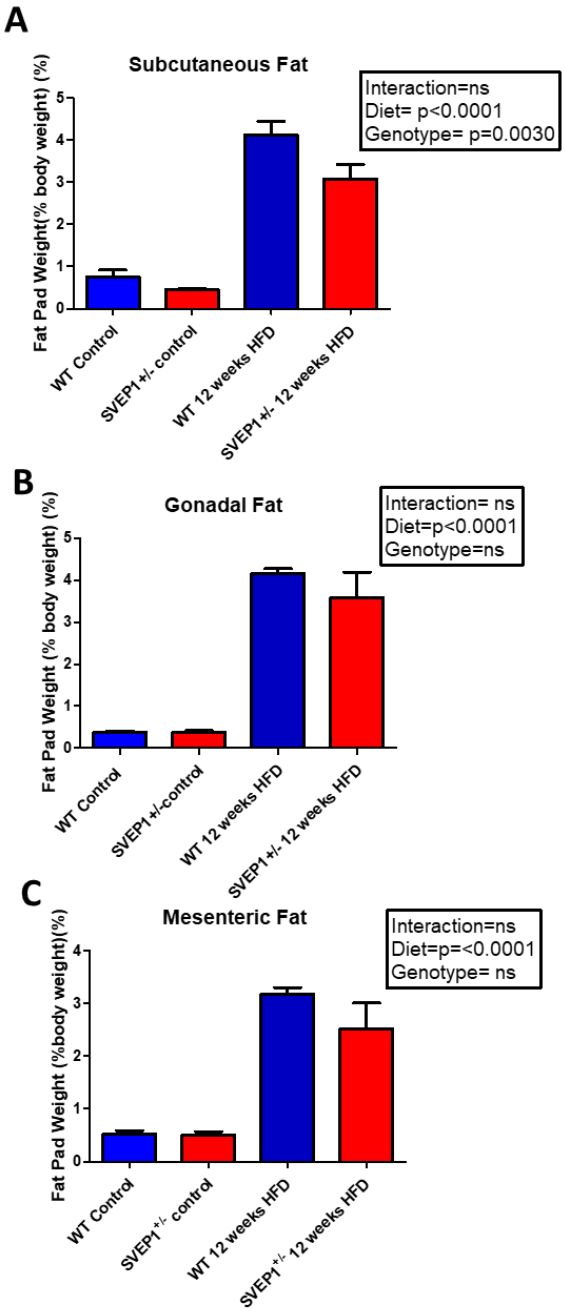

Figure 5 4Fat depot weights normalised to body weight on normal chow and after HFD.
A= subcutaneous fat pad weight normalised to body weight in control and hemizygous animals on control (RM1) chow and post 6 week HFD. Subcutaenous fat pad was significantly heavier (p=<0.0001) after HFD and there was a significant reduction (p=0.0030) in fat pad weight between genotypes.
B= gonadal fat pad weight normalised to body weight in control and hemizygous mice on control (RM1) chow and post 6 week HFD. No statistical difference was noted between the genotypes but gonadal fat significantly increased (p=<0.0001) on HFD feeding.
C= mesenteric fat pad weight normalised to body weight in control and hemizygous animals on control (RM1) chow and post 6 weeks HFD. No statistical difference between genotypes however, mesenteric fat mass significantly increased (p=<0.0001) with 6 weeks HFD. Means ±SEM, n=4-8, 2-way ANOVA.

The Phenomaster system records the weight of food consumed by the animals in 24hrs to determine if any metabolic differences are due to either genotype consuming more/less food. No statistical difference was seen between genotypes while animals were on a chow diet (Fig 5.5). There was a trend towards a decrease in consumption of HFD during the light and dark phase in Svep1+/- mice compared to wildtype however, this was not statistically significant.

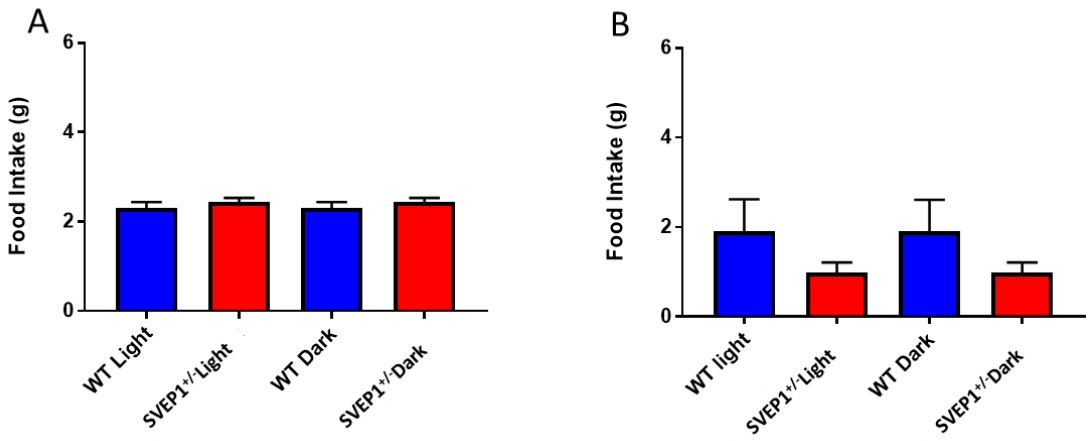

Figure 5 5Food intake in 24hrs in hemizygous and wildtype animals on control diet (RM1 chow) and after 6 weeks of high fat diet (HFD).
A= Food intake in wildtype and hemizygous animals on chow diet, no differences were seen between the two genotypes.
B= Food intake in wildtype and hemizygous animals on HFD, hemizygous animals show a trend to consuming less food in the light and dark phase than wildtype animals- this was not statistically significant.
Means ±SEM, N=4, unpaired t-test.

Calorie utilisation (H4) normalised to the lean mass of the animal can be calculated using the Phenomaster system. There was an increase in H4 when animals were placed on a high fat diet, however no statistical difference in calorie utilisation was seen between the genotypes before or after HFD (Fig 5.6A). No statistical differences between the genotypes were noted when calorie utilisation was broken down into light and dark phases on either normal chow or high fat diet (Fig 5.6B+C). However, in both genotypes on both diets more calories were utilised in the dark phase when mice are active due to their nocturnal circadian rhythm.

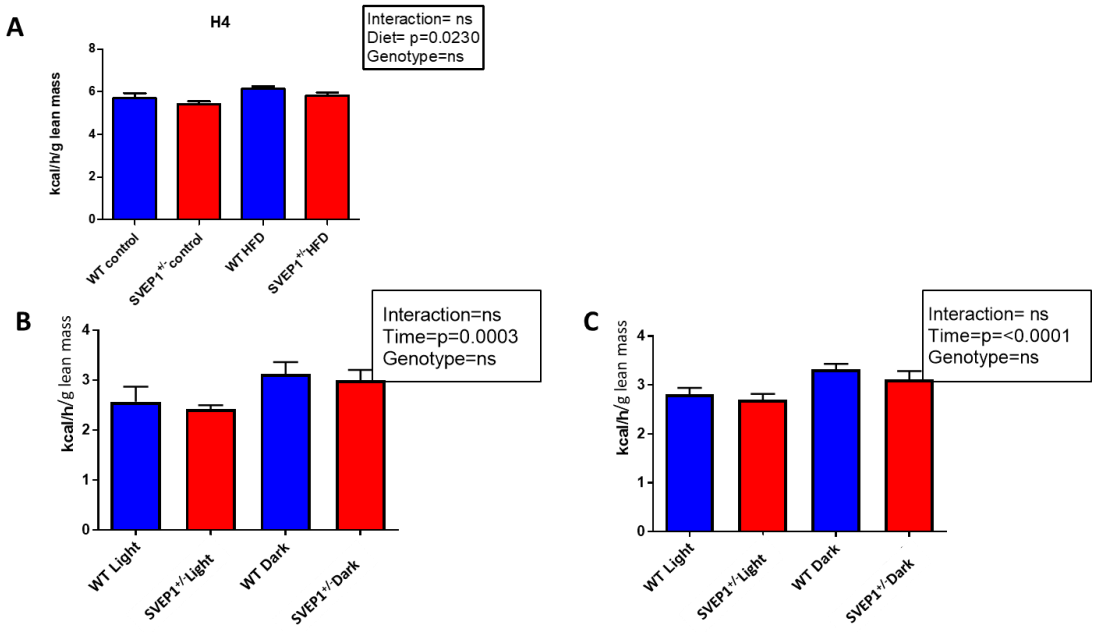

Figure 5 6Calorie utilisation per unit body mass (H4) measured by the phenomaster system.
A= Mean calorie utilisation (H4) in wild type (WT) and hemizygous animals before and after HFD. No differences were noted between the genotypes however a significant increase in H4 was noted after HFD (p=0.0230).
B= Calorie utilisation (H4) on normal chow in light and dark phase in both wild type and hemizygous animals. Calorie utilisation was greater in the dark phase (p=0.0003), but no difference was noted between the genotypes.
C= Calorie utilisation (H4) after HFD in light and dark phase in both wild type and hemizygous animals. Calorie utilisation was greater in the dark phase (p<0001) but no differences were noted between the two genotypes.
Means ±SEM, n=4, 2-way ANOVA.

Activity was monitored using the Phenomaster system to determine if there were any differences in physical activity between the genotypes. The Phenomaster system allows the activity of the mouse to be assessed by counting the number of light beam breaks in the x/y planes over 24 hours.

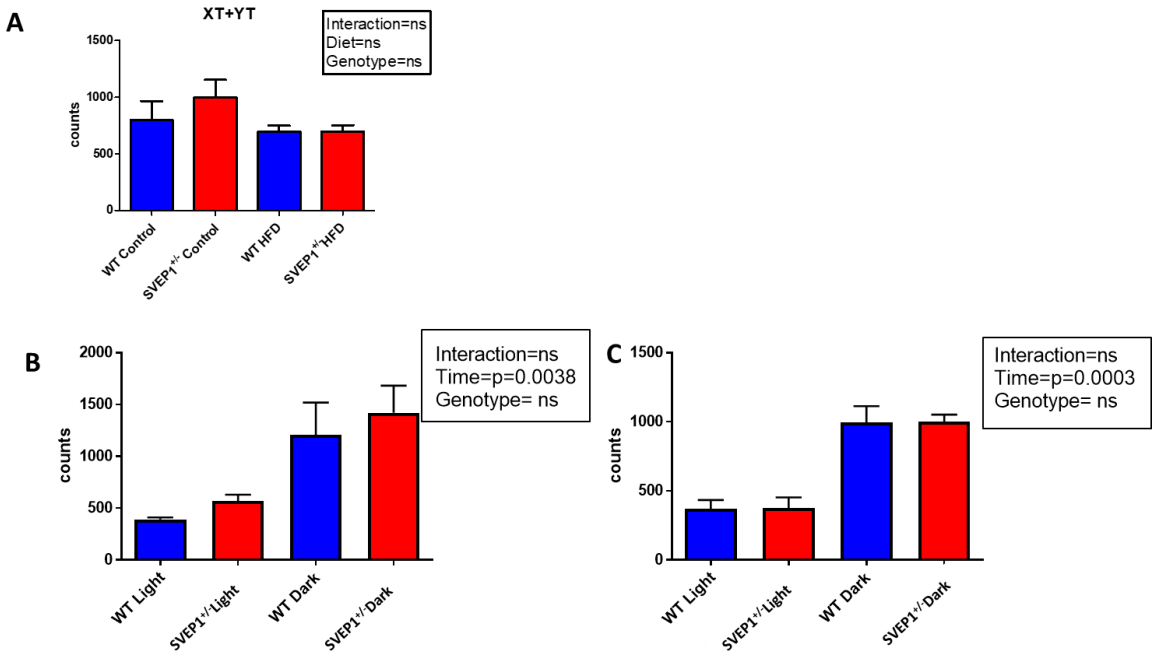

Figure 5 7 Total activity of mice in the x/y planes over 24hrs.
A= average activity over 24hrs of wildtype (WT) and hemizygous mice on control diet and after high fat diet (HFD). After HFD no difference between genotypes was noted. Before HFD there is a trend towards an increase in activity in the hemizygous animals but this was not statistically significant.
B= Activity in the light and dark phases on normal chow in both wild type and hemizygous animals. Animals are significantly more active in the dark phase (p=0.0038). However, there is no statistical difference in activity between genotypes.
C= Activity in light and dark phases on HFD. Animals are significantly more active in the dark phase showing circadian rhythms are intact (p=0.0003), however there is no difference between genotypes after HFD.
Means ± SEM, n=4, 2 way ANOVA.

Over a 24hr period on normal chow the Svep1$^{+/-}$ animals showed a trend towards an increase in activity versus wildtype littermates however this was not significant (Fig 5.7 A). There was no statistical difference between wildtype and Svep1$^{+/-}$ animals after HFD. Animals were significantly more active in the dark phase compared to the light phase (Figure 5 7 B and C) regardless of diet. However there was no significant difference in activity between the genotypes on either diet.

Blood Glucose and Insulin Sensitivity

The second aim of the chapter was to determine if the Svep1$^{+/-}$ mice exhibited altered blood glucose or altered insulin profile compared to wildtype litter mates. To investigate this animals underwent an oral glucose tolerance test (GTT) after being

fasted for 6hrs on normal chow (baseline) and after 6 and 12 weeks of high fat diet. Blood glucose was measured via glucometer.

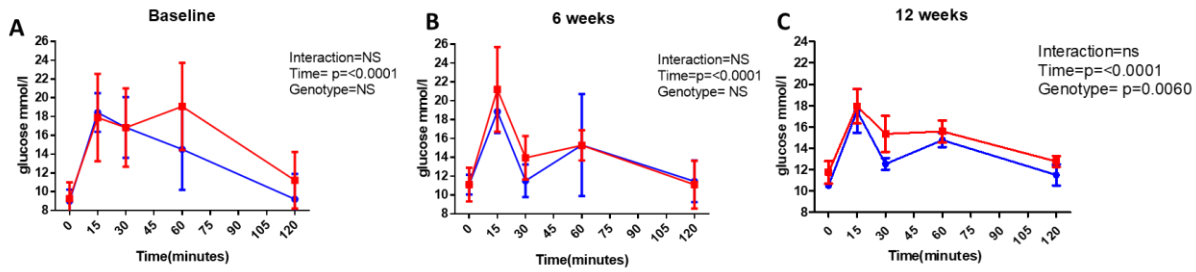

Figure 5 8Glucose Tolerance Test (GTT) at baseline, and after 6 and 12 weeks of high fat diet (HFD) in wild type (blue line) and Svep1+/- (red line) mice.
A= GTT results at baseline. No statistical difference was noted between the genotypes
B= GTT after 6 weeks of HFD. No statistical difference was noted between the genotypes
C= GTT after 12 weeks of HFD. Svep1+/- mice demonstrated decreased glucose tolerance
Means ± SEM, N=4, repeated measures 2 way ANOVA.

No statistical differences in glucose tolerance were seen between the two genotypes on normal chow or after 6 weeks of HFD. However, the Svep1$^{+/-}$ mice showed significantly impaired glucose tolerance after 12 weeks on HFD (Fig 5 8).

During the GTT, plasma was collected to analyse plasma insulin concentration from the two genotypes at baseline, and at the 6 and 12 week time points.

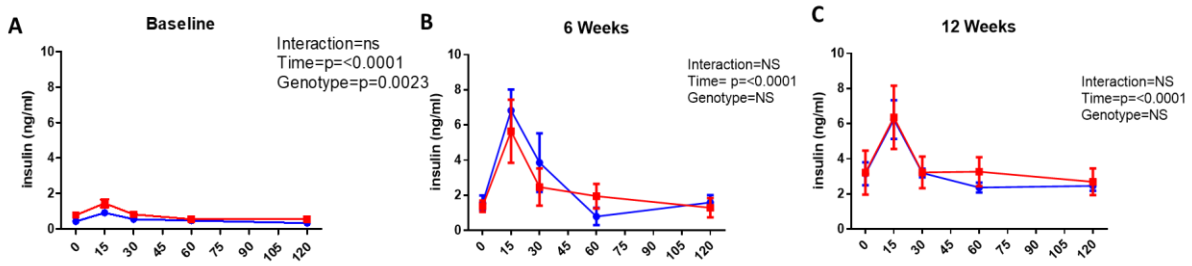

Figure 5 9Insulin ELISA results at baseline, and after 6 weeks and 12 weeks on high fat diet (HFD) in wild type (blue line) and Svep1+/- (red line) mice.
A= Insulin from plasma at baseline before HFD feeding. Hemizygous animals showed significantly increased insulin concentration when compared to wildtype animals (P=0.0023)
B= Insulin concentration from plasma after 6 weeks of HFD, no differences were observed between genotypes however, a higher concentration of insulin is required to normalise blood glucose than at baseline.
C= Insulin concentration in plasma after 12 weeks of HFD, no differences were seen between genotype.
Means ±SEM, N=4, repeated measures 2-way ANOVA.

At baseline both genotypes exhibited small increases in plasma insulin in response to oral glucose load, however there was a significant increase in insulin in Svep1+/- compared with wild-type mice (Fig 5 9). After 6 and 12 weeks of HFD feeding there was a higher plasma insulin concentration after 6 hour fast and a more marked increase in response to glucose load, however no significant difference between the Svep1$^{+/-}$ versus wildtype animals was recorded.

The homeostasis model assessment of insulin resistance (HOMA-IR) was calculated from the fasting blood glucose and plasma insulin concentrations obtained at the start of the GTTs in both genotypes at baseline, 6 and 12 weeks.

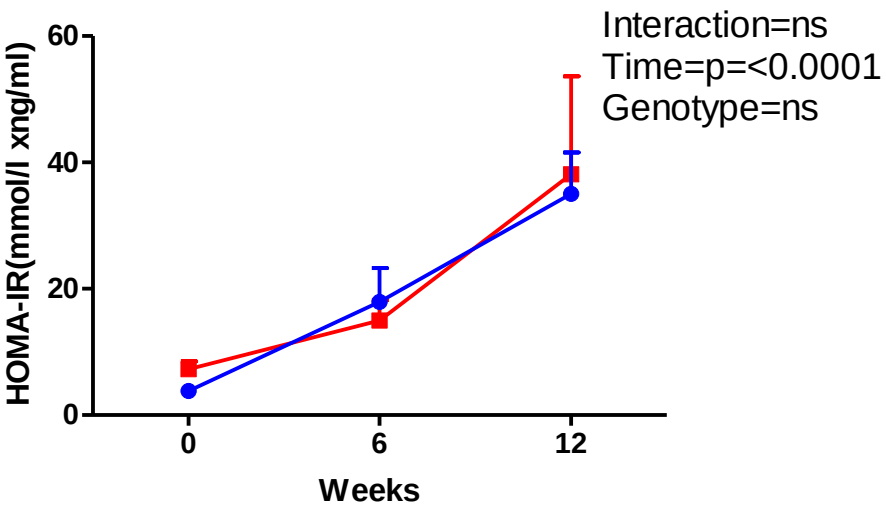

Figure 5 10 HOMA-IR at baseline, and after 6 weeks and 12 weeks of high fat diet in hemizygous animals (red) and wildtype animals (blue).
No difference between genotypes was noted in HOMA-IR values however, HOMA-IR values did increase in response to HFD.
Means±SEM, N=4, 2 way-ANOVA.

In both genotypes, the HOMA-IR values increased progressively over the 12 week experimental period of HFD (Fig 5 10). This suggest that both genotypes have impaired insulin sensitivity on a HFD, however there was no statistical difference between the genotypes.

Metabolic Parameters- RER, VCO_2 and VO_2

The Phenomaster systems employs indirect calorimetry- it records the volume of CO_2 (vCO_2) produced in metabolism by the mice and the volume of O_2 (vO_2) utilised by the animals. These values are then converted to the respiratory exchange ratio (RER) by dividing the vCO_2 by the vO_2. The RER is an indicator of which fuel is being predominantly metabolised by the mice- values of 1, 0.85 and 0.7 are indicative of carbohydrate metabolism, a balance of fat and carbohydrate and predominantly fat metabolism, respectively.

To determine whether there was a difference in fuel preference in the $Svep1^{+/-}$ animals versus wildtype, RER and vO_2 and vCO_2 were recorded by the phenomaster system.

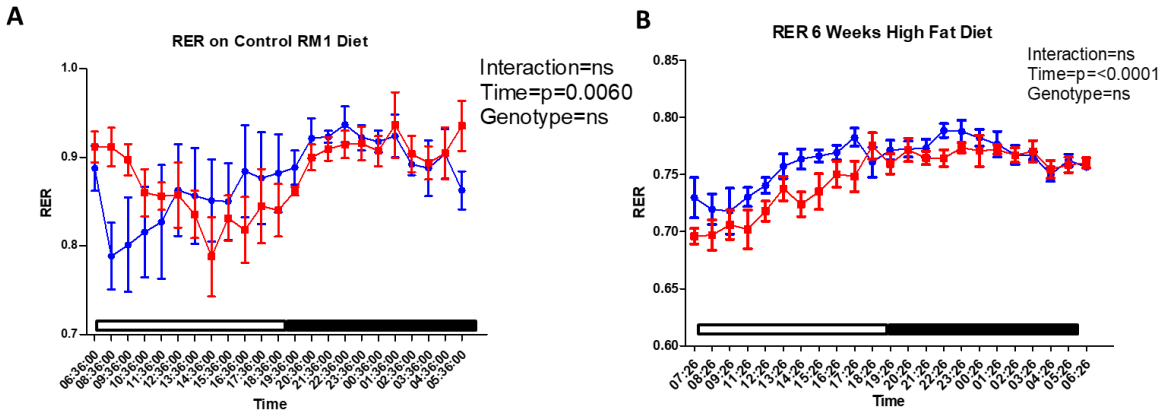

Figure 5 11 Respiratory Exchange Ratio (RER) over the 24hr period in wild type (blue line) and, hemizygous (red line) mice.
A= RER over 24hrs both light and dark phase (indicated by the white and black boxes respectively on the x axis) on normal RM1 chow. No difference was seen between the genotypes.
B= RER values over 24hrs post high fat diet feeding. Hemizygous animals exhibit a trend for lower RER values in the light phase compared to wild type animals, however the overall RER across the 24hr period was not significantly different between the genotypes.
Means±SEM, N=4, repeated measures 2 way-ANOVA.

Animals on chow diet have an average value of 0.85, indicating that they are burning both carbohydrate and fat (Fig 5.11A and 5.12A). This shifts to an average value of 0.75 during HFD indicating that HFD causes animals to predominantly metabolise fat (Fig 5.11B and 5.12A). When the data are separated according to the light and dark phases, an increase in RER when animals are active during the dark phase is observed indicating a switch towards carbohydrate metabolism (Fig 5.11 and 5.12B+C).

RER on normal chow shows no statistical differences over the 24hr period between the genotypes (Fig 5.11A and Fig 5.12B). However, after 6 weeks on HFD Svep1$^{+/-}$ animals have decreased RER values predominantly during the light phase, suggesting that they may be metabolising more fat than wildtype littermates (Fig 5 11B and Fig 5.12C).

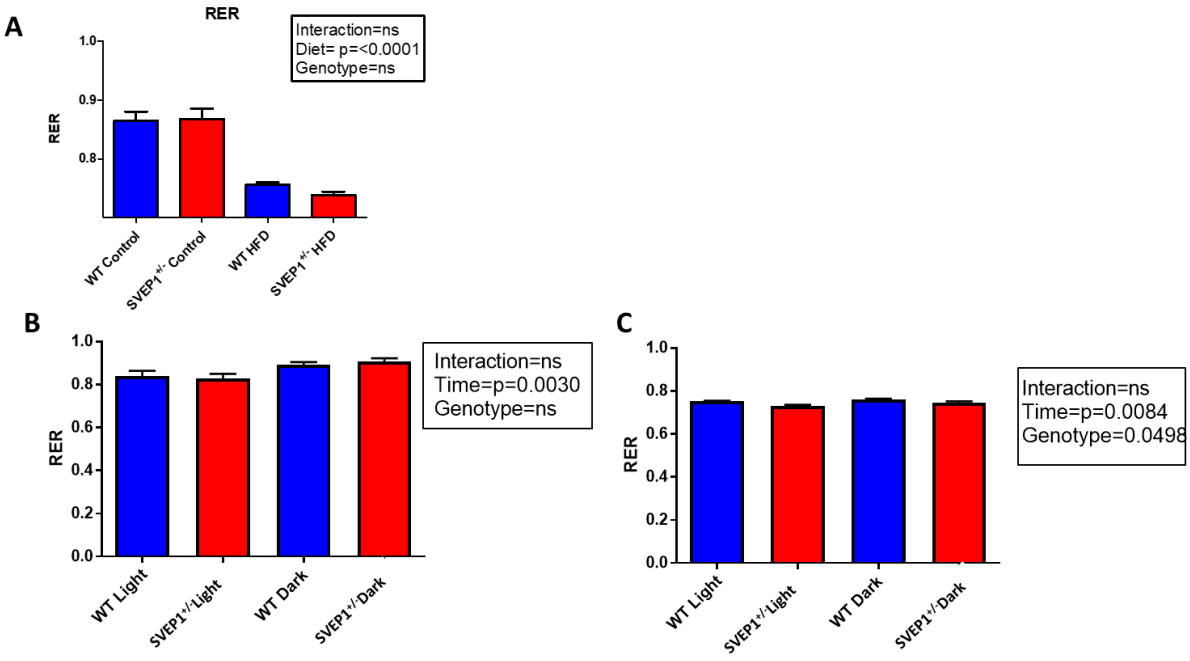

Figure 5 12 Respiratory Exchange Ratio (RER) values on normal chow (control) and high fat diet (HFD) in wild-type (WT) and Svep1+/- mice.
A= average RER data before and after HFD. There is a reduction in RER on HFD, indicating a switch to fat metabolism. No differences can be seen between genotypes, although there is a trend towards lower RER on HFD in the Svep1+/- mice.
B= RER values on normal chow in wild type and hemizygous mice. No difference between genotype can be seen but RER increases in the dark phase suggesting a switch towards carbohydrate metabolism.
C= RER values after 6 weeks on HFD. RER was significantly lower in the Svep1+/- compared with WT mice (p=0.0498)
Means ±SEM, N=4, 2-way ANOVA.

Volume of CO_2 exhaled by the animals is used to calculate the RER values and is employed to assess any metabolic differences between the genotypes.

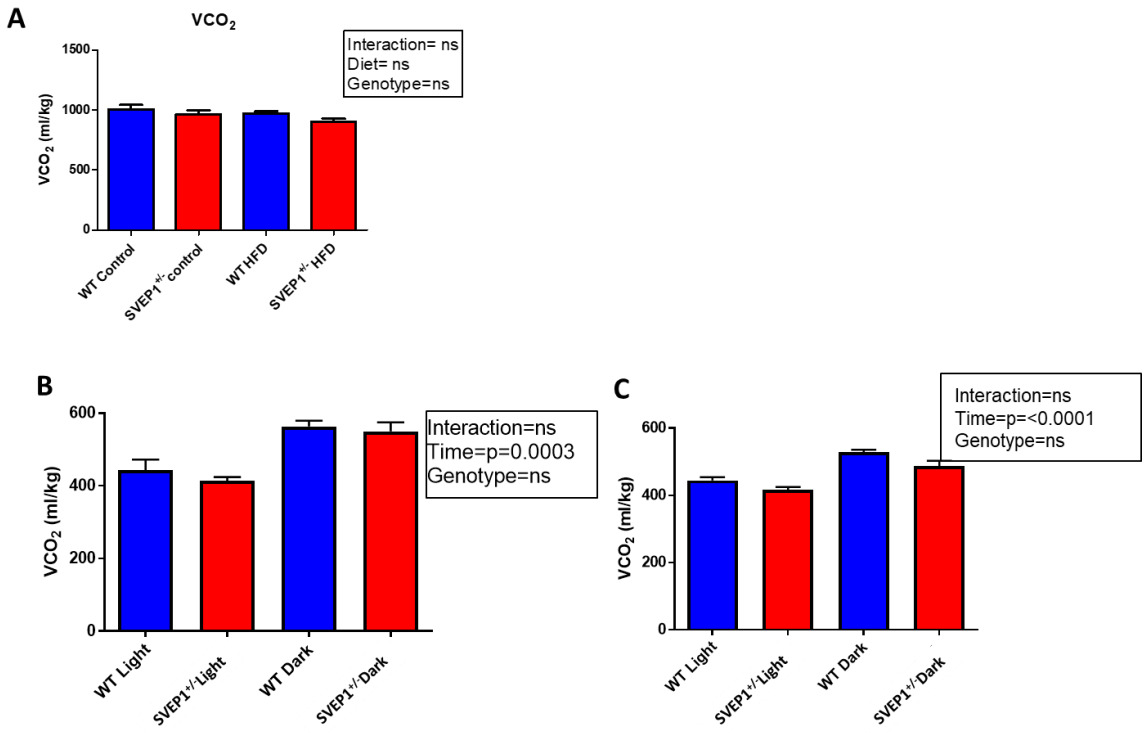

Figure 5 13 VCO_2 production recorded by phenomaster system on normal chow (control) and high fat diet (HFD) in wild-type (WT) and Svep1+/- mice
A= average VCO_2 production of wild type and hemizygous animal before and after 6 weeks HFD. No differences were noted between diets or genotypes.
B= VCO_2 production in wild type and hemizygous animals pre-HFD shows no difference between genotype. When animals were active in the dark phase more CO_2 was produced.
C= VCO_2 produced in wild type and hemizygous animals after 6 weeks HFD showed a trend towards lower VCO_2 production in hemizygous animals t (p=0.0637) .
Means ±SEM, N=4, 2-way ANOVA.

When the 24hr period was broken down into light and dark phases both on control diet and post HFD, this demonstrated an increase in vCO_2 exhaled in the dark phase consistent with the mice being more active in the dark phase (Figure 5 13 B and C). There was a trend towards lower vCO_2 values in hemizygous animals particularly after HFD, though this did not reach statistical significance (p=0.06) (Figure 5 13 C).

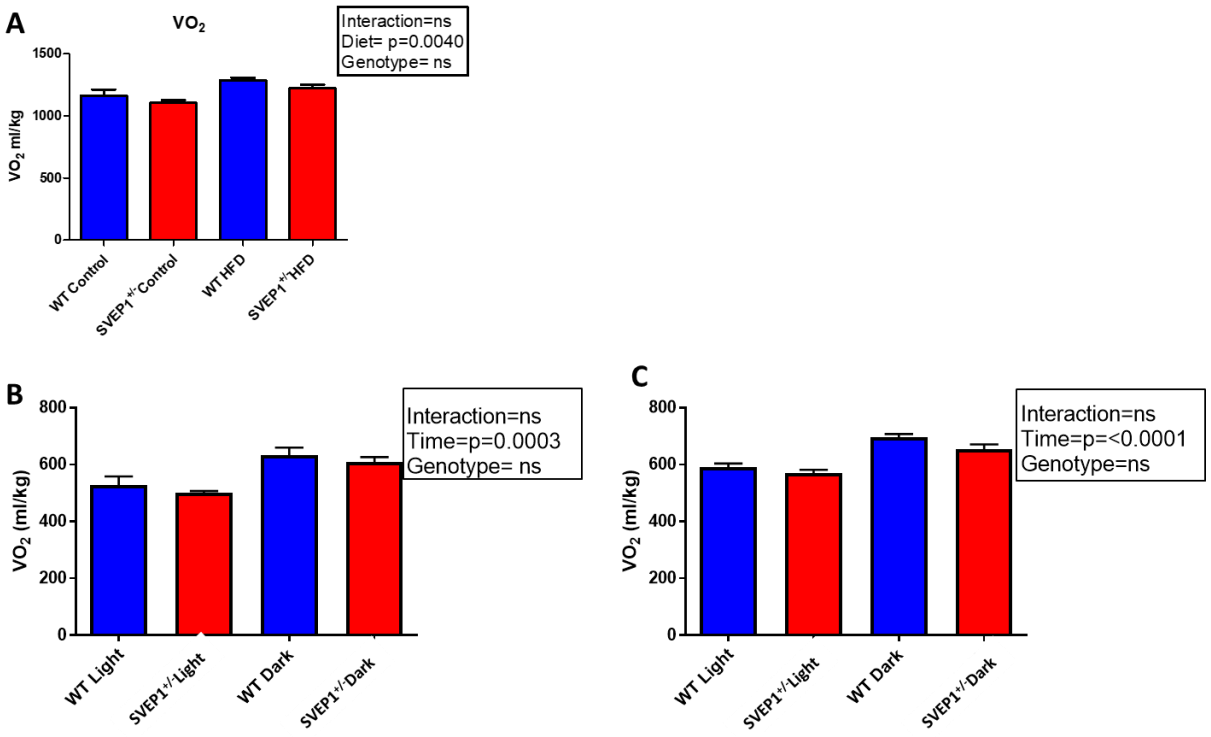

Figure 5 14 VO_2 consumption measured by phenomaster system over 24hrs on normal chow (control) and high fat diet (HFD) in wild-type (WT) and Svep1+/- mice.
A= average VO_2 consumption of wild type and hemizygous mice before and after HFD. There was an increase in VO_2 consumption on HFD, but no difference between genotype was noted.
B= VO_2 consumption in wild type and hemizygous animals before HFD in light and dark phases, showed no genotype differences. When animals were active in the dark phase an increase in O_2 consumption was seen due to animals being active.
C= VO_2 consumption in wild type and hemizygous animals after 6 weeks HFD showed an increase in the dark compared with the light phase but no genotype differences.
Means ± SEM, N=4, 2-way ANOVA.

vO_2 values increased on HFD compared with normal chow (Figure 5 14 A). Splitting the 24hr period into light and dark phases, once again there is an increase in vO_2 in the dark phase consistent with the circadian rhythms of the animals (Figure 5 14 B and C). There were no significant differences in vO_2 values before or after the HFD between the SVEP1 hemizygous animals versus the wildtype littermate controls.

SVEP1 expression in human tissue from Higgins Normal tissue panel

Publically available data from the 'Higgins Normal Tissue Panel' from the Nephroseq database were employed to assess tissue expression of the *Svep1* gene in normal individuals. SVEP1 was most highly expressed in omental and subcutaneous adipose tissue (Figure 5 15). Expression was also found in the kidney (both cortex and medulla), heart, liver, spleen and skeletal muscle. Both spleen and heart expressed SVEP1 more highly than the kidney, where there was more expression of SVEP1 in the renal medulla compared to the renal cortex. Expression of SVEP1 being highest in human adipose tissue could support the gene having a role in metabolism.

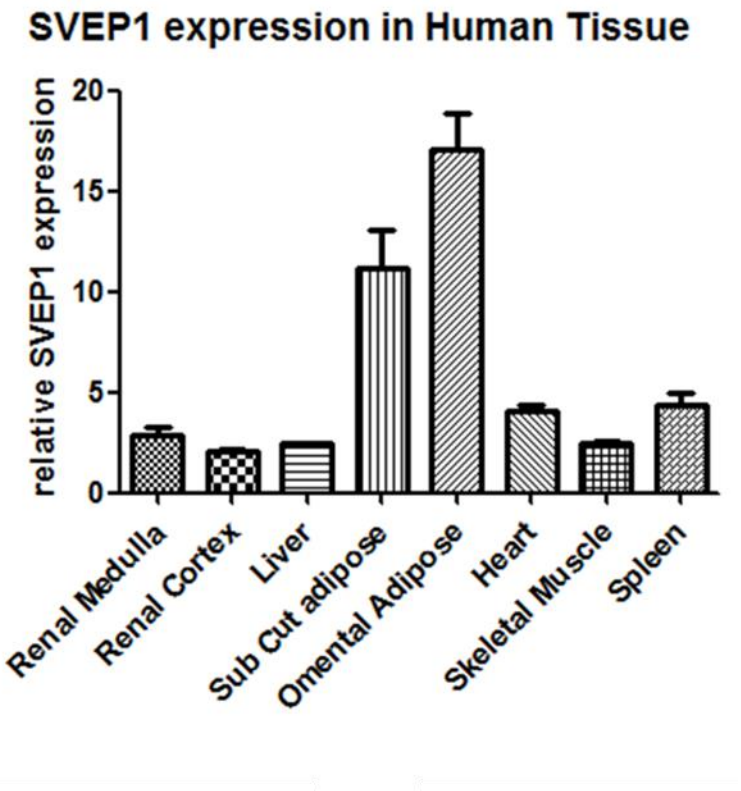

Figure 5 15 SVEP1 gene expression in human tissue.
Using the Higgins normal tissue panel, tissue that was found to highly express SVEP1 was subcutaneous and omental adipose tissue. Other tissues such as the kidney, liver and skeletal muscle were found to express SVEP1 at much lower levels, n=4(Higgins et al 2004).

SVEP1 gene expression was investigated in the SVEP1$^{+/-}$ mice on high fat diet and on normal RM1 chow.

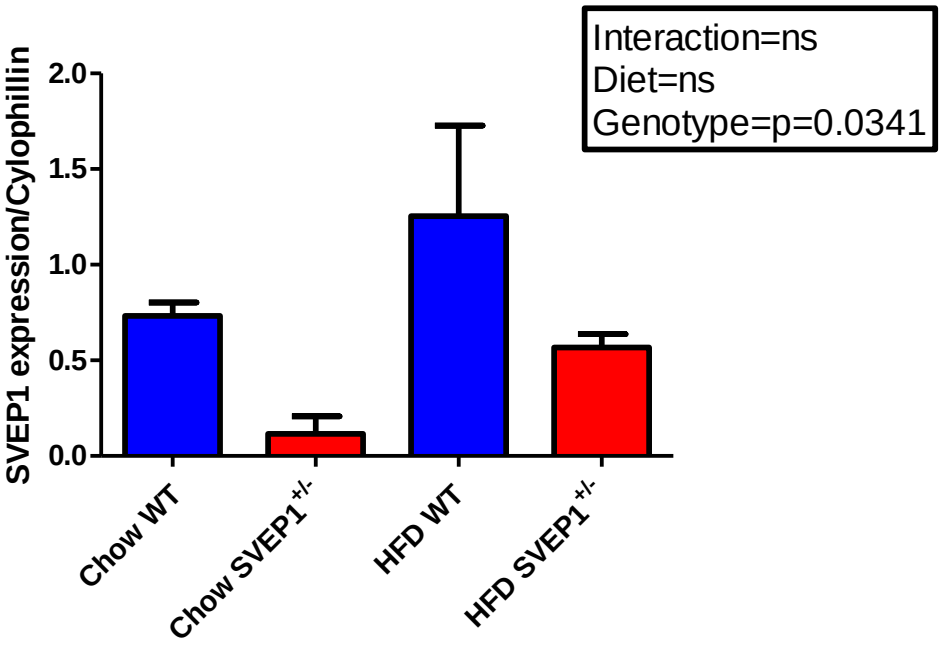

Figure 5 16 SVEP1 expression in subcutaneous fat in animals fed chow diet and HFD in bothwild-type (WT) and SVEP1+/- animals. SVEP1 expression is significantly decreased in SVEP1$^{+/-}$ animals. No differences in SVEP1 expression were seen in respect to diet. Means ±SEM, n=8, 2 way ANOVA.

After 6 weeks HFD SVEP1 expression showed a trend towards increasing compared to animals on a normal RM1 chow diet, however this was not significant (Figure 5 16). SVEP1 was significantly decreased in SVEP1$^{+/-}$ animals compared to wildtype on both normal chow and high fat diet (p=0.0341, Figure 5 16).

5.5 Discussion

SVEP1 hemizygous mice show a potential metabolic phenotype

Stitziel *et al* found that a point mutation- D2702G- in the human Svep1 gene was associated with higher blood pressure and increased risk of type 2 diabetes and coronary heart disease (Stitziel *et al.*, 2016). Therefore the hypothesis of this work was that Svep1$^{+/-}$ mice would exhibit an altered metabolic profile. The Svep1$^{+/-}$ mice exhibited increased blood glucose concentration following oral glucose load after 12 weeks of high fat diet and significantly increased fasting plasma insulin concentration on normal chow. Several additional parameters such as fat depot weights and RER were also different between the genotypes. Hemizygous animals tended to have lighter fat depots, significantly so in subcutaneous fat, and a trend towards lower RER, indicating a trend towards a preference for fat metabolism.

Body composition

SVEP1 hemizygous mice and wildtype animals had similar body weights throughout the study, a significant difference in body weight gain on high fat diet was noted after 6 weeks HFD. There was no difference between genotypes in lean or fat mass as measured by TDNMR. However, there was a trend towards a decreased weight of individual fat depots in the Svep1 hemizygous compared with wild-type animals, which reached significance for the subcutaneous depots. The 2702G variant in the human Svep1 gene predisposes to type 2 diabetes, but it is not associated with risk of obesity. However, the majority of human studies use body mass index as a surrogate measure of obesity and do not test for associations with individual fat depots. In humans adipose tissue SVEP1 mRNA expression correlated positively with adipocyte volume after adjustment for BMI (Kokosar *et al.*, 2016). In woman with Polycystic Ovary Syndrome (PCOS) which presents with hyperinsulinemia, pancreatic β-cell dysfunction, insulin resistance and obesity, SVEP1 mRNA expression is decreased in adipose tissue when compared with control group (Kokosar *et al.*, 2016). This suggests that in humans with increased adiposity or adipose tissue dysfunction there is a reduction in SVEP1 expression. In our animal model study- SVEP1 hemizygous mice

showed a trend towards reducing fat depot weight but specifically subcutaneous fat is significantly reduced.

While the trend for a reduction in fat pad mass in Svep1$^{+/-}$ mice is not significant in all depots, it is interesting to speculate mechanisms by which Svep1 could potentially influence adiposity. SVEP1 is thought to play a role in lymphatic vessel remodelling. Morooka *et al* found that SVEP1 knockout mice die within 30min of birth from respiratory failure. These animals failed to undergo remodelling of the lymphatic plexus- including sprouting new capillaries and formation of collecting lymphatic vessels (Morooka *et al.*, 2017). In SVEP1 knockout animals there was aberrant remodelling of lymphatic capillaries in the intestine and heart (Morooka *et al.*, 2017). Morooka *et al* describe SVEP1 as an extracellular matrix protein which is secreted from mesenchymal cells. Previously it was demonstrated that SVEP1 was a high-affinity ligand for α9β1 integrin which is a well-known cell adhesion receptor involved in lymphangiogenesis (Sato-Nishiuchi *et al.*, 2012). Lymphatic vasculature is known to play a role in lipid absorption and fat metabolism- lymphatics are commonly surrounded by adipose tissue (Wang and Oliver, 2010). It is known that disruption of lymphatic vascular integrity promotes ectopic growth of fat in lymphatic-rich regions due to increased lipid storage in adipocytes and increased differentiation of preadipocytes to mature adipocytes (Harvey *et al.*, 2005). Prox1 is a transcription factor essential for development of lymphatic vessels and Prox1 null embryos are devoid of lymphatic vasculature due to endothelial cells budding from cardinal veins never acquiring a lymphatic phenotype (Harvey *et al.*, 2005). However, Prox1 $^{+/-}$ mice are viable and are considerably heavier than wildtype littermates, with fatty livers and impaired glycaemic tolerance. It would be interesting to determine if there is any disruption of lymphatic vessel integrity in Svep1$^{+/-}$ mice; if integrity was disrupted one would hypothesize that animals with decreased adipose tissue expression of SVEP1 would exhibit an increased adiposity as with the Prox1$^{+/-}$ mice. This is the opposite of the observed trend towards a reduction in fat pad mass in the Svep1$^{+/-}$ mice, however it is possible that the nature of the lymphatic disorder may be different in Svep1$^{+/-}$ and Prox1$^{+/-}$ mice. Such an experiment would not be possible in Svep1$^{-/-}$ mice as adipose tissue is not laid down till after birth and SVEP1$^{-/-}$mice die within 30mins of birth.

Body mass is determined by the balance between calorie intake and utilisation. Hemizygous animals have a slightly lower calorie intake but this is not statistically significant. Similarly, there was no significant difference in the calculated H4, a measure of calorie utilisation, between the genotypes. In keeping with this, activity levels between genotypes is not statistically different although there is a trend towards an increase in activity in the Svep1$^{+/-}$ animals on chow diet.

Blood glucose and insulin sensitivity

Svep1$^{+/-}$ mice exhibited a trend towards increased blood glucose at all time points following oral glucose challenge, however this was not statistically significant until the 12 week time point. This finding is interesting due to the decrease in fat pad mass in the SVEP1$^{+/-}$ animals. One explanation for the reduction in adiposity but reduced insulin sensitivity could be that the SVEP1$^{+/-}$ animals are unable to increase their fat pad mass in response to HFD. It would be interesting to see if these animals were shifting fat towards the liver resulting in fatty liver and increased hepatic insulin resistance which in-turn is leading to an inability to switch off gluconeogenesis. Although only the 12 week time point shows significantly different GTT scores, it could be interesting to carry out a triglyceride assay or oil red O staining on livers from these animals to quantify hepatic fat content. Insulin concentration from plasma samples taken during the GTT increased progressively during HFD in both genotypes. The trend towards an increase in plasma insulin across all time points, exhibited by both genotypes, suggests that the mice were developing insulin resistance but that the pancreas was still functioning effectively. In addition, HOMA-IR values were raised after HFD indicating that 12 weeks of HFD is sufficient to induce insulin resistance on this background.

Plasma insulin levels were significantly greater in SVEP1$^{+/-}$ animals at baseline compared to wildtype animals, however there were no differences between the genotypes in HOMA-IR either at baseline or after insulin resistance had developed on a HFD. Hence, any difference in insulin resistance between the genotypes must be subtle.

RER

Both genotypes had lower RER on HFD than on normal chow, which is consistent with Marvyn *et al's* findings that after 3 days of HFD feeding RER is reduced in both the light and dark phase in C57BL6 mice (Marvyn et al. 2016). Genotype differences in RER are not seen on a chow diet, however there was a decrease in RER in $Svep1^{+/-}$ mice after HFD, suggesting that they may preferentially metabolise fat when it is readily available. This may in part explain the reduced adipose fat depots in the $Svep1^{+/-}$ mice. However, this lower RER in the $SVEP1^{+/-}$ mice is only marginally significant ($p=0.04$), therefore this needs repeated using a larger number of mice before this finding can be robustly concluded.

Experimental Design and N number

An important experimental design consideration which has contributed to all results in this chapter was the low number of mice utilised in each group. The studies were limited to four mice of each genotype due to difficulties in breeding animals and the fact that only 8 Phenomaster cages were available to use in each experimental run. The low number of animals in each group may be contributing to the lack of statistically significant findings in this body of work and conversely some of the positive findings are only marginally significant and must be treated with caution. Hence, a repeat of this experiment is planned, prior to which performing a power calculation to show the number of animals we would need to use to see significant differences is necessary. Using Lehr's formula as described in the previous chapter: basing the power calculation on 20% increase in HOMA-IR value, set at a power of 80% and 5 % significance 10 animals in each group would be necessary to show if there was a metabolic difference in the phenotype.

Disparity between the results of mouse versus human data

The disparity between the relatively modest difference in key metabolic parameters between $Svep1^{+/-}$ and wild-type mice described in this chapter and the 13% increased risk of type 2 diabetes in persons with the 2702G variant of SVEP1 described by Stitziel *et al* may be due to a number of factors. Firstly, as alluded to above, the current

studies are underpowered to detect subtle differences between the genotypes. Secondly, the mice were deficient in a single SVEP1 allele, while the human D2702G variant led to a single amino acid change in the protein structure. One might hypothesize that as the hemizygous mice are deficient for an entire allele of SVEP1 an exacerbated phenotype may be observed. This does not appear to be the case and it may be that the change in amino acid structure induced by the D2072G variant exerts a dominant effect. How the point mutation affects the structure and function of SVEP1 is not yet known therefore the mechanism by which it confers increased risk of diabetes is difficult to assess. The D2702G variant is located in an exon where the amino acid sequence is tightly conserved between humans and mice, therefore one option would be to generate a 'knock-in' mouse in which one normal allele is replaced with the human variant. Further metabolic studies such as those performed above could then be carried out in the knock-in mouse.

The studies presented in this thesis only utilised male mice and therefore masked any sex differences in phenotype between male and female. The omission of using female mice was due to breeding challenges, as previously described. However, in humans, it is well reported in the literature that there is gender specific differences in diabetes mellitus. Woman with diabetes mellitus have not seen a decrease in all-cause mortality and cardiovascular mortality in the last 30 years which has become prevalent in the male population with diabetes mellitus (DM) (Auryan and Itamar, 2008). It has been reported that woman have lower prevalence of isolated impaired fasting glucose and higher prevalence of isolated impaired glucose tolerance based on pathological 75g oral glucose tolerance test than men (Auryan and Itamar, 2008). This leads to woman being diagnosed later with DM. Testosterone has been proven to be protective in men against type 2 diabetes but the opposite effect is seen in woman (Auryan and Itamar, 2008). Oestrogen deficiency in postmenopausal woman has been shown to effect glucose regulation and increase insulin resistance (Auryan and Itamar, 2008). It has also been shown in obese populations that a smaller increase in weight has a more deleterious effect in woman than it does in males in regard to type 2 diabetes incidence (Auryan and Itamar, 2008). Due to the prevalence of gender specific differences in diabetic prevalence and phenotype it would be of great advantage to include a female mouse study to identify if they show a more diabetic phenotype.

5.6 Conclusions and Future Directions

Hemizygous SVEP1 animals exhibit subtle differences in metabolic phenotype compared to wildtype littermates, including reduced adiposity, a preference for fat metabolism and insulin resistance following high fat diet. However, these findings are borderline significance and require validation in an increased number of mice of each genotype. Further future directions would include making the mouse with the human point mutation or a conditional knock out of SVEP1 where SVEP1 can be switched off after development as constitutive global deletion is embryonic lethal.

6. SVEP1 and Regulation of Blood Pressure

6.1 Introduction

Stitziel *et al* reported that a point mutation in the SVEP1 gene - D2702G caused a small, but significant increase in blood pressure in humans. This point mutation results in the substitution of aspartate for glycine and is associated with higher systolic blood pressure- 0.94mmHg higher for each copy of the 2702G allele. The authors did not describe the mechanism behind this increase in blood pressure.

There are no published data regarding blood pressure in Svep1$^{+/-}$ mice. However, given the human data, we hypothesised that mice with only one copy of the Svep1 gene may have differences in blood pressure control compared with wild type mice. If this could be demonstrated, then these mice may be used to investigate the mechanisms by which SVEP1 regulates blood pressure. This hypothesis was assessed by using telemetry analysis of blood pressure in Svep1$^{+/-}$ and wild type mice both on normal chow and on high salt diet.

Chapter Hypothesis

SVEP1$^{+/-}$ mice would show an increase in blood pressure compared to wildtype littermates.

6.1.1 Chapter Aims:

1. To determine if SVEP1$^{+/-}$ mice have altered blood pressure on normal chow compared to wildtype littermates.
2. To determine if SVEP1$^{+/-}$ mice have altered blood pressure when exposed to high salt diet compared to wildtype littermates.

6.1.2 Experimental Plan

The experimental plan is detailed in Figure 6 1 below. Svep1$^{+/-}$ and wild type mice (n=5 in each group) underwent surgery to implant telemetry devices (detailed description in the materials and methods section- surgeries were carried out by Dr Jess Ivy) and were then allowed to recover and placed on normal chow for 3 weeks before high salt diet was initiated. Telemetry data was collected for 3 weeks on normal (RM1)

chow (0.25% sodium) and for 3 weeks on high salt diet (3% sodium) and then animals were culled and tissues removed for future analysis by rtPCR. The data taken forward for further analysis was calculated on readings obtained on 5 consecutive days during the 3rd week to allow for the mice to fully recover after surgery. The high salt data was obtained on 5 consecutive days immediately after switching to high salt diet during the 4th experimental week. Data beyond this time-point were unreliable due to potential software malfunction.

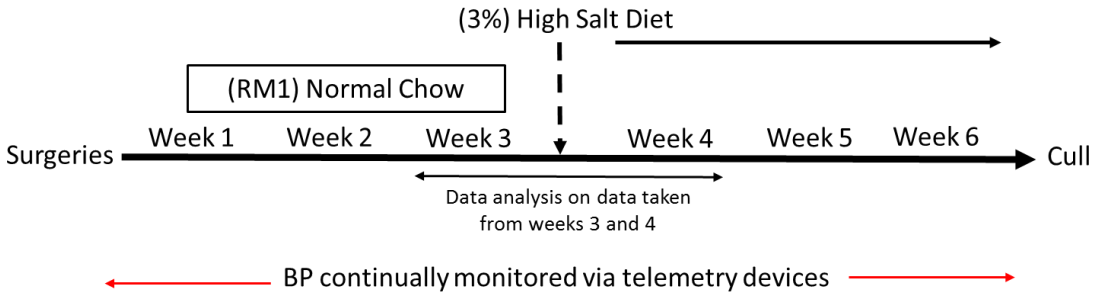

Figure 6 1 Schematic detailing experimental time line of the telemetry study. Animals were implanted with telemetry devices and then monitored on normal chow for 3 weeks. High salt diet was initiated at the start of week 4 and the animals BP was measured for a further 3 weeks on high salt diet. Both genotypes were assessed- wildtype and SVEP1$^{+/-}$ animals. N=5.

6.2 Results

6.2.1 Blood pressure analysis

Mean systolic BP across the 5 day periods before and after the switch to a high salt diet are given in Figure 6 2. No significant differences in systolic BP were observed between animals of either genotype before and after switch to high salt diet (Figure 6 2). However, there was a trend for a higher systolic BP on high salt diet in the wild-type animals only. No statistical difference was noted between genotypes however SVEP1$^{+/-}$ animals showed a trend towards a decrease in SBP on high salt diet compared to wildtype animals.

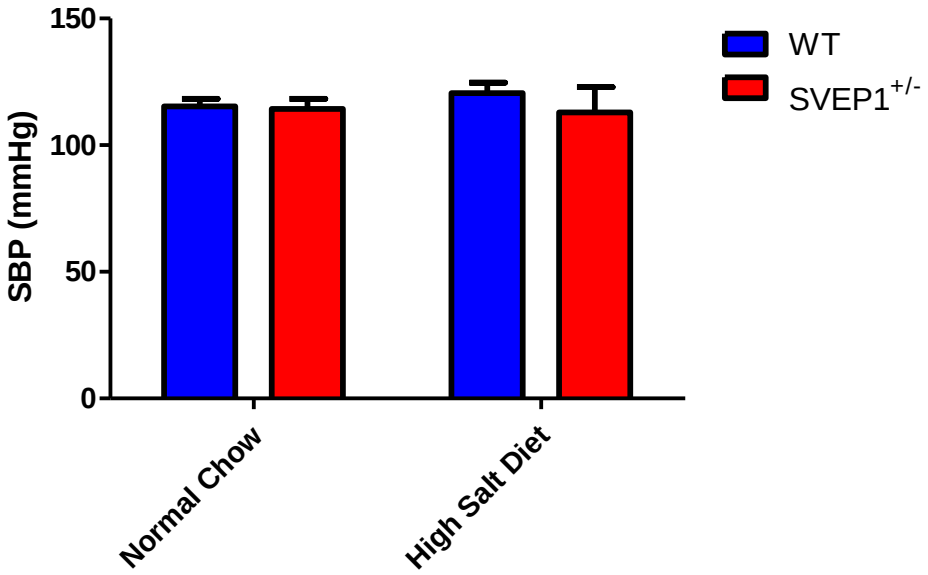

Figure 6 2 Mean Systolic BP (SBP) in wildtype and SVEP1$^{+/-}$ mice on both normal chow and high salt diet.
No statistical differences were noted between high salt diet and normal chow although there was a trend towards an increase in SBP in wildtype animals on a high salt diet. No statistical differences were noted between genotypes.
5 day mean ± SEM, n= 5, 2 way ANOVA.

Blood pressure is known to exhibit a diurnal rhythm, therefore to explore the pattern of BP across the day/night cycle, 6 hour moving averages were calculated.

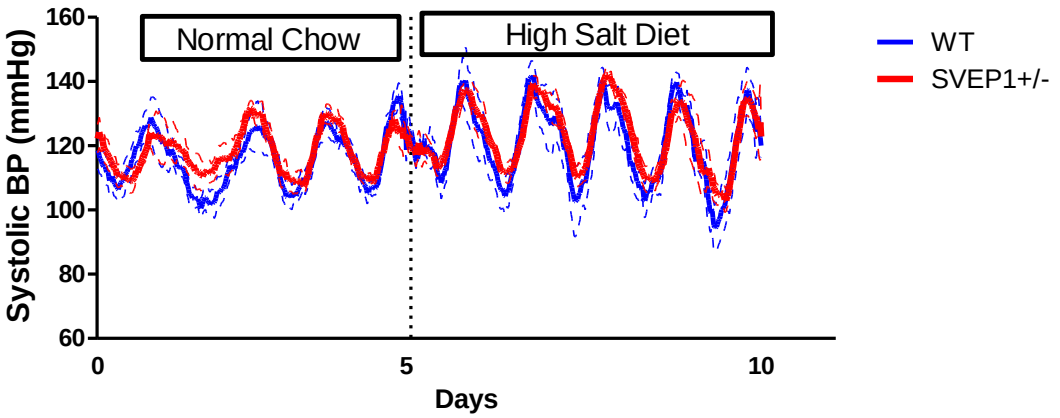

Figure 6 3 Systolic blood pressure in wildtype and SVEP1$^{+/-}$ animals on normal chow and high salt diet. The data were taken over 10 consecutive days in weeks 3 and 4 of the experiment- on normal chow during week 3 post insertion of telemetry devices and in week 4 immediately after the switch to high salt diet. Data are moving 6hr means ±SEM, n= 5.

The 6 hour moving averages over the 10 consecutive 24 hours periods spanning the transition from normal chow to high salt diet are plotted in Figure 6 3. This demonstrates the diurnal variation of blood pressure in both groups.

To further probe the data, mean systolic blood pressure at each time point (not 6hr moving mean) in each animal was calculated across the 5 day periods on normal chow and high salt diet (Figure 6 4). The animals' blood pressure is reduced during their inactive phase and due to the animals being nocturnal this is during the light phase - 7am-7pm. In wild-type animals, the high salt diet appeared to increase the night-time systolic blood pressure with little effect on day-time pressure. This resulted in larger diurnal variation in blood pressure. This effect appeared less marked in Svep1$^{+/-}$ mice.

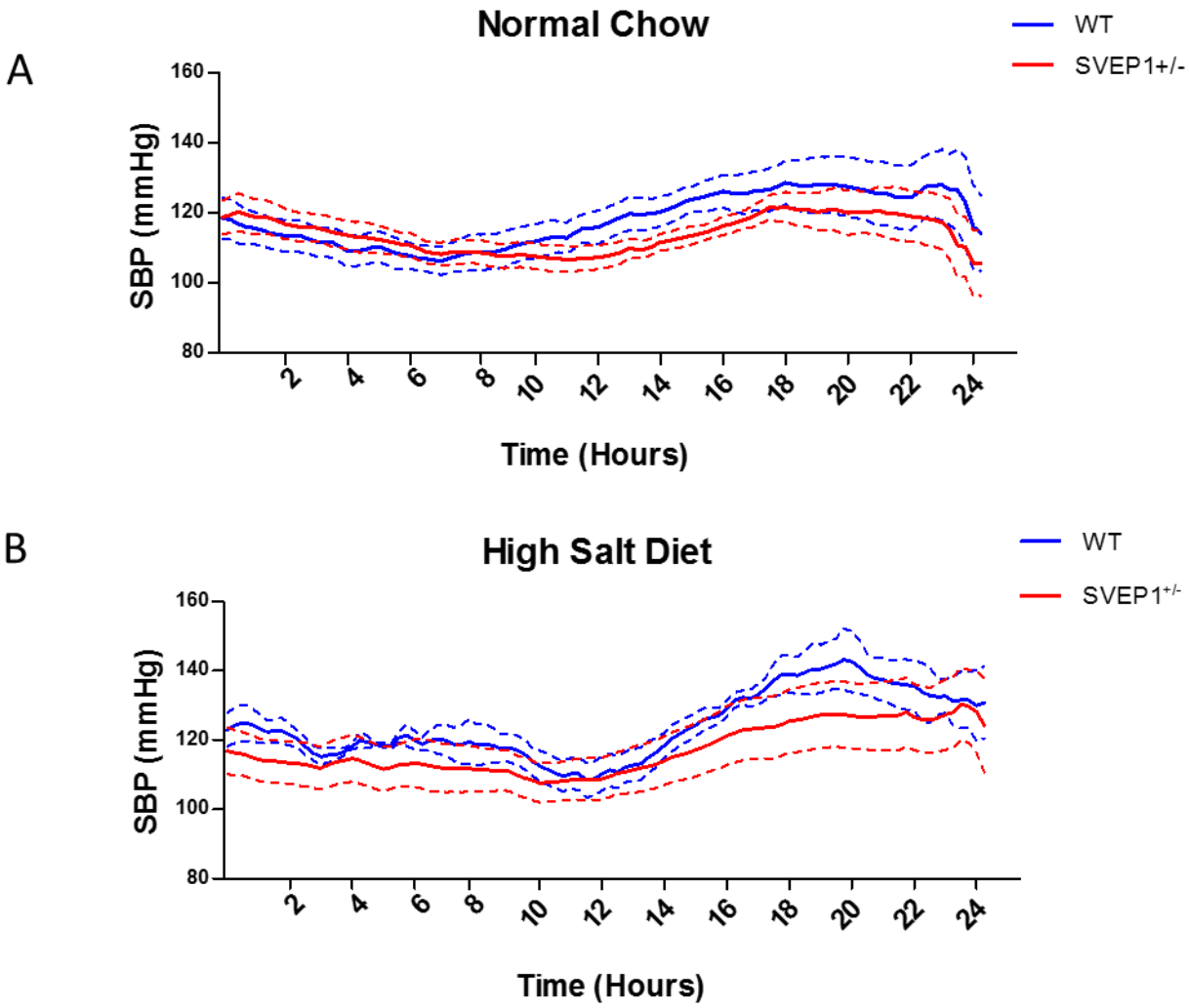

Figure 6 4 Mean systolic blood pressure over 24hrs on both normal chow (A) and high salt diet (B) in SVEP1$^{+/-}$(red) and wildtype animals (blue).
Circadian rhythm of the mice can be seen. During light hours (7am-7pm, zeitgeber=0-12) animals are inactive and therefore blood pressure is lower. During the dark hours (7pm-7am, zeitgebers=12-24) the animals are more active therefore blood pressure is elevated. Data are means +/- SEM, n=5.

There was a significant difference between the trough and peak SBP 6 hour moving mean on both diets- normal chow and high salt diet- but no difference in either trough or peak SBP between the genotypes (Figure 6 5).

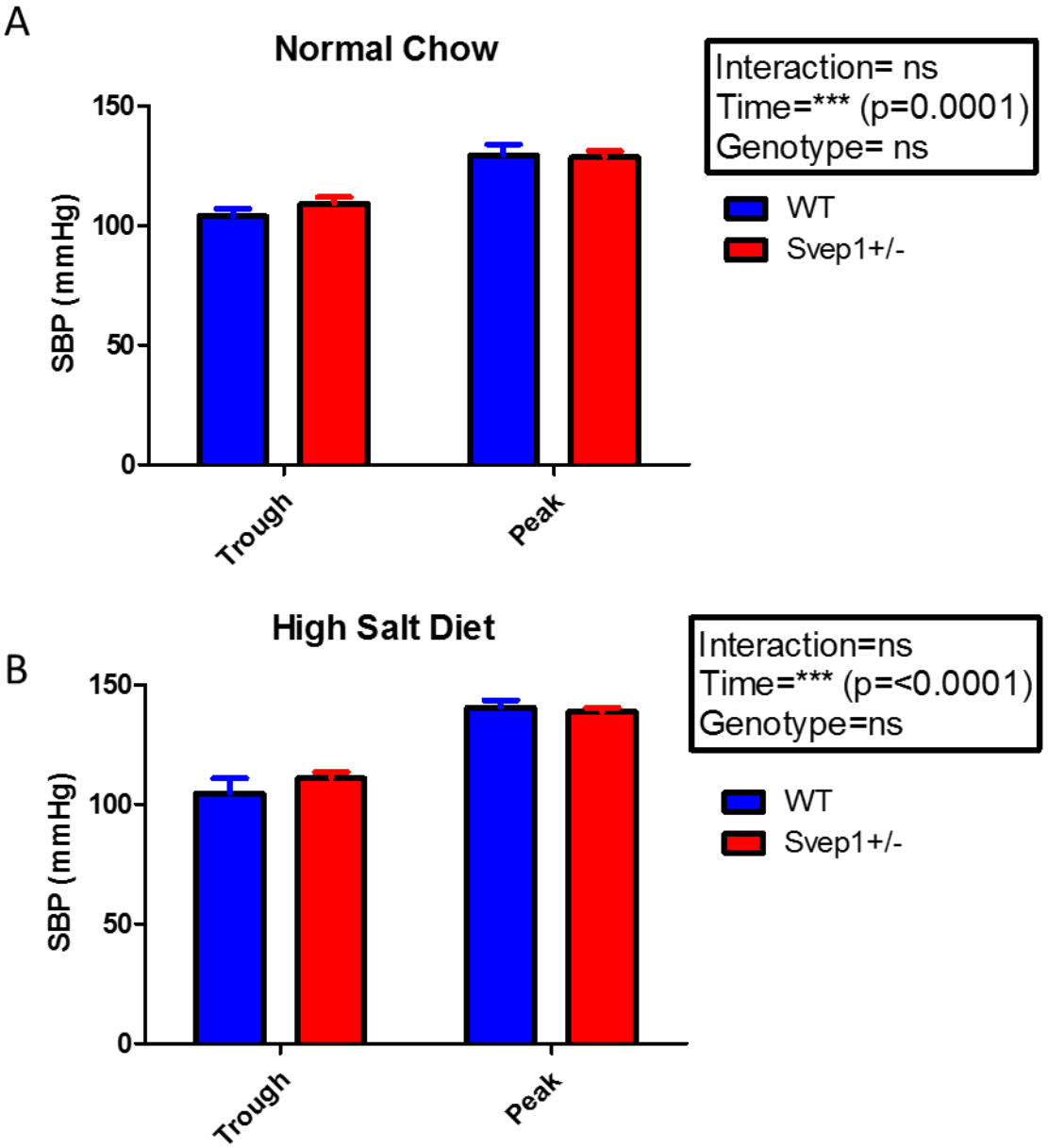

Figure 6 5 Mean trough and peak 6hr moving means of systolic blood pressure (SBP) on (A) normal chow and (B) high salt diet in wildtype (blue) and SVEP1$^{+/-}$ (red) animals. A=Normal chow mean trough and peak SBP calculated from 6hr moving means. A significant difference exists between trough and peak (p=0.0001) SBP but there is no difference between genotype. B= High salt diet mean trough and peak SBP calculated from 6hr moving means. A significant difference was noted between trough and peak (p=<0.0001) SBP but no difference was observed between genotypes. Means ±SEM, n=4-5, repeated measures 2wayANOVA.

There was a significant increase in peak SBP with high salt diet compared to normal chow but no difference in trough SBP (Figure 6 6). No difference between the genotypes in either trough or peak blood pressure on either diet was noted.

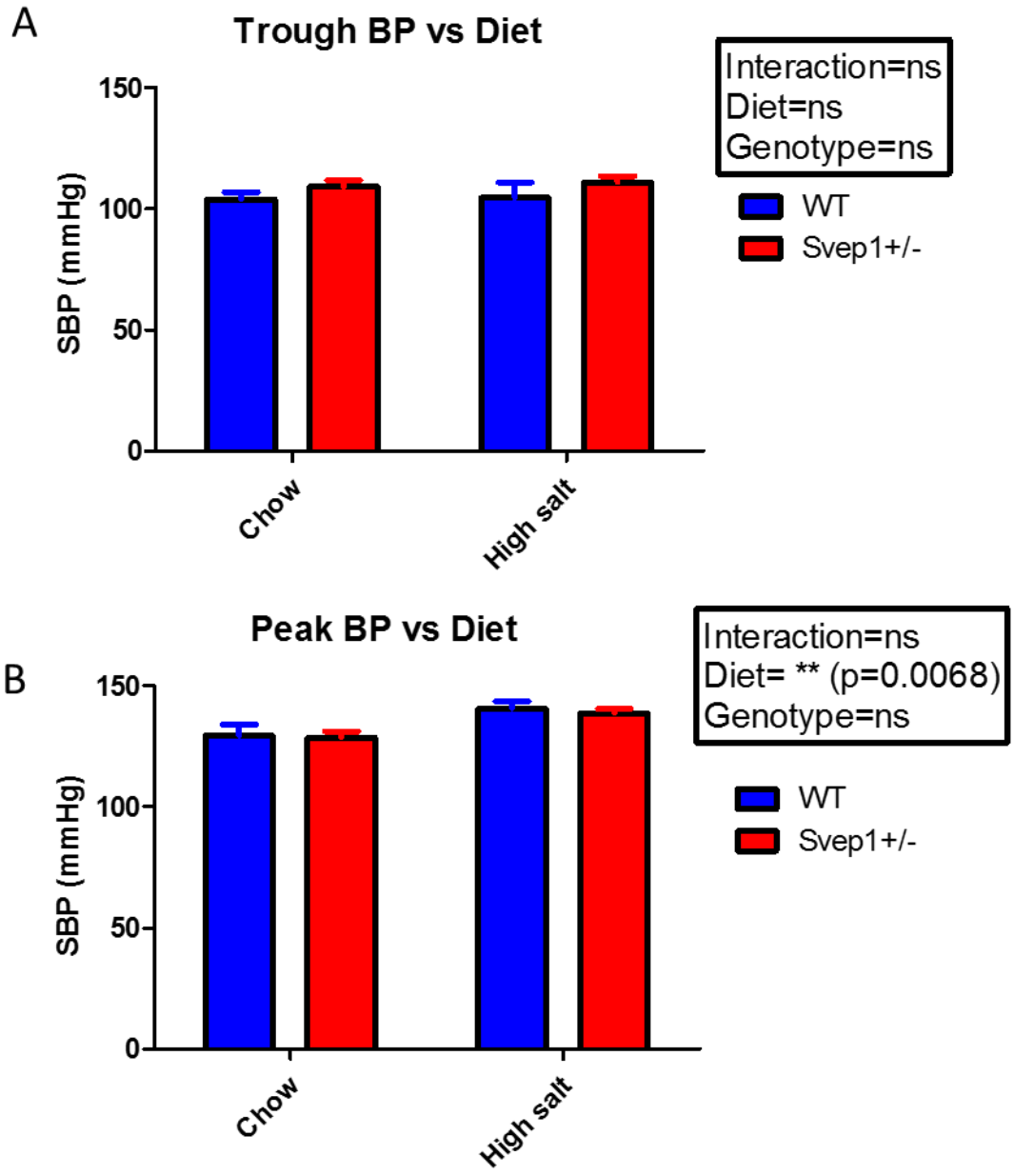

Figure 6 6 Trough and peak systolic blood pressure (SBP) on normal chow and high salt diet in wildtype (blue) and SVEP1$^{+/-}$animals (red). A= Mean trough SBP was not significantly different between diets or genotypes. B= Mean peak SBP was not different between genotypes but was significantly higher on high salt diet vs normal chow (p=0.0068). Means ±SEM, n=4-5, repeated measures 2 way-ANOVA.

The amplitude (peak-trough) of the SBP circadian rhythm was also analysed. The amplitude was higher on high salt diet but there was no difference between genotypes (Figure 6 7).

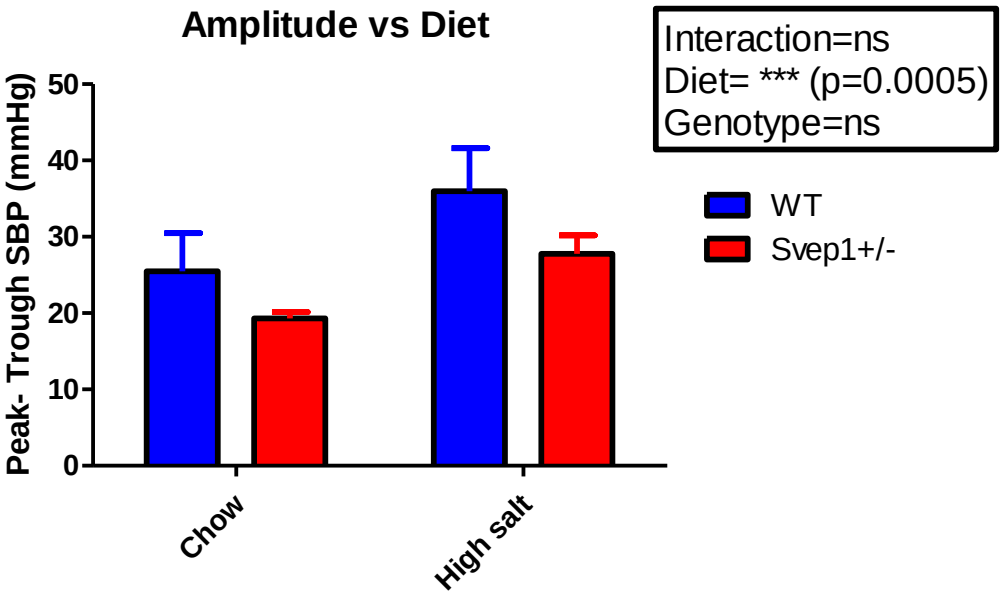

Figure 6 7 Amplitude (peak-trough) of SBP circadian rhythm on normal and high salt diet in wildtype (blue) and SVEP1$^{+/-}$ (red) animals. Amplitude was significantly higher (p=0.0005) on high salt diet but no difference between genotypes was seen. Mean ±SEM, n=4-5, repeated measures ANOVA.

Heart rate was analysed on normal chow and high salt diet in both the SVEP1$^{+/-}$animals and wildtype littermates. Heart rate was increased in SVEP1$^{+/-}$animals compared to wildtype littermates (Figure 6 8). SVEP1$^{+/-}$ animal's heart rate was approximately 100bpm higher than wildtype animals.

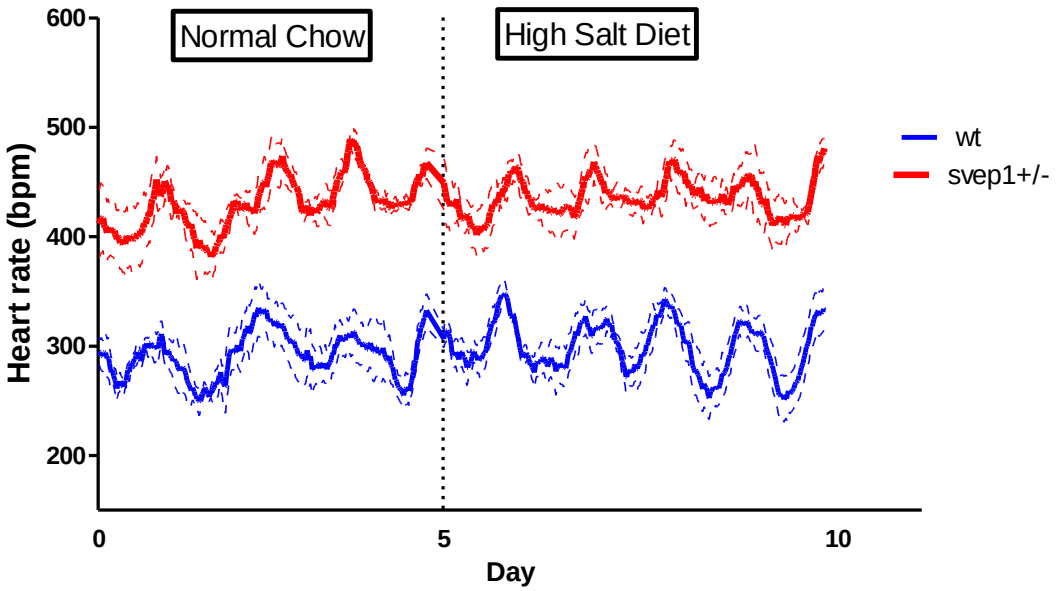

Figure 6 8 Heart rate in beats per minute (bpm) in SVEP1$^{+/-}$ and wildtype animals on normal chow and high salt diet. 6 hour moving means ±SEM, n=5 (dotted line indicated SEM).

Average heart rate between the two genotypes was assessed. SVEP1$^{+/-}$animals showed a significant increase in heart rate compared to wildtype littermates (Figure 6 9, p=0.0002). No statistical difference was seen between normal chow and high salt diet.

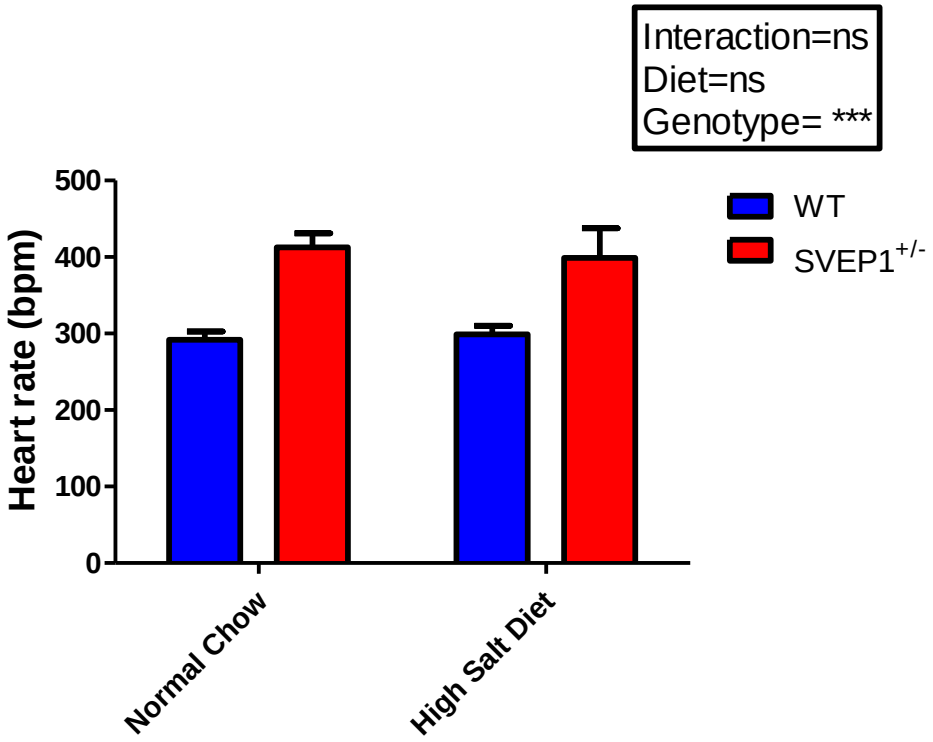

Figure 6 9 Mean Heart Rate in beats per minute (bpm) in both SVEP1$^{+/-}$ and wildtype animals on normal chow and high salt diet.
No differences in mean heart rate were seen between the diets. SVEP1$^{+/-}$animals showed significantly increased heart rate compared to wildtype littermates (p=0.0002).
Means of 5 days ±SEM, n=5, 2 way-ANOVA.

6.3 Discussion

The main conclusions from this chapter are that there were no significant differences in systolic blood pressure between SVEP1$^{+/-}$ animals and wildtype littermates, however SVEP1$^{+/-}$animals showed a significantly increased heart rate before and after high salt diet. High salt diet increased peak (dark phase) but not trough (light phase) systolic blood pressure compared with normal chow.

6.3.1 SVEP1$^{+/-}$ show no difference in blood pressure compared to wildtype littermates

Our hypothesis for this chapter stated that we expected a difference in blood pressure between SVEP1$^{+/-}$ animals and our wildtype littermates given that a point mutation in Svep1 was associated with an increase in blood pressure of 0.94mmHg in humans (Stitziel *et al.*, 2016). However, in our study no difference in blood pressure was seen. A number of factors could explain this difference: the point mutation in humans conferred only a subtle <1mmHg rise in blood pressure. In our study we were left with 5 animals in each group due to surgical deaths while implanting the telemetry devices (n=1 for each genotype) or dysfunction of the devices (n=2 for each genotype) therefore our study is underpowered to detect such a small difference in blood pressure between the genotypes. A more detailed study of the 24hr BP rhythm by cosinor analysis could potentially detect differences- this is alluded to in 6.3.4. . The human variant was a point mutation rather than a loss of one allele- this could cause a different phenotype in the mice. The abnormal protein product produced by the point mutation might have been important in driving the BP increase, rather than the loss of one normal allele.

The literature shows that exposure to high salt diet increases the amplitude of arterial pressure and increases the average mean arterial pressure in mice (Carlson and Wyss, 2000). Our data corroborates this, however there was no differences between the genotypes. Mean arterial pressure (MAP) and heart rate were reported to be stable 7days post-surgery to implant telemetry devices until day 35 (Mattson, 1998). In our study after week 4 the data became unreliable with missing data points which was attributed to software malfunction. Mattson reports blood pressures of 116mmHg in control animals (Mattson, 1998). In animals fed high salt diet blood pressures increase

to 126mmHg (Zhang *et al.*, 2018). These values are similar to those reported in our high salt diet study. Our data also showed evidence of nocturnal dipping which is associated with sleep (Ivy *et al.*, 2016) and corroborates previously undertaken telemetry studies in our lab. Therefore, the telemetry data presented in this chapter corroborates what has been shown in the literature in previous studies utilising high salt diet and radiotelemetry. However, software malfunctions prevented capturing data for the final weeks of the investigation.

In going forward, analysing the data using cosinor analysis to identify any subtle differences in blood pressure over the circadian cycle will identify if further studies in this mouse would be of benefit to determine SVEP1's role in blood pressure regulation. A potentially more useful avenue would be creating the human mutation in the mouse to determine the role the mutation is playing.

6.3.2 C57BL6 and salt resistance/ hypertensive stimuli

C57BL6 mice are thought to be relative salt resistant and this is consistent with the lack of increase in mean systolic blood pressure over 24hrs between the normal chow and high salt diet. The 129/Sv mouse was seen to be more susceptible to hypertension measured by tail cuff plethysmography than the C57BL6 mouse when placed on 1% sodium drinking water for 6 weeks (Hartner *et al.*, 2003). In 2 other studies, arterial BP did not change when C57BL6 mice were administered high sodium (Craigie *et al.*, 2012) and no increase in blood pressure average over 24hrs was noted when animals were placed on a 1% sodium diet for 7 days measured by telemetry (Evans *et al.*, 2016). In our animals an 8 fold increase caused no difference in mean 24 hour systolic blood pressure (RM1 chow contains 0.25% sodium, high salt diet contains 3% sodium). However, other studies have suggested that high salt diet may induce small changes in blood pressure in C57BL6 mice. On placing the C57BL6 mouse on 1% sodium drinking water for 2 weeks blood pressure increased from 89mmHg to 104mmHg (Sugiyama *et al,.* 2000). A high salt diet of 8% sodium was reported to increase blood pressure in the C57BL6 mouse by 10mmHg (measured by telemetry) and induce mild fibrosis (Leenen *et al.*, 2015).

While 24hr SBP was not altered on high salt diet, analysis of peak and trough SBP was performed in SVEP1$^{+/-}$ and wildtype animals to assess whether more subtle changes

may be induced by sodium load. 6hr moving means of peak and trough values along with the amplitude of the SBP diurnal variation have been presented in this chapter. An increase in peak but not trough SBP was observed when animals were switched from normal chow onto a high salt diet. This is congruent with the literature- Combe *et al* report that in C57BL6N mice trough SBP remains the same on normal chow and high salt diet but an increase in peak SBP is observed on high salt diet (8% sodium) compared to normal chow. Interestingly, Combe *et al* reported that heart rate was not affected by the salt challenge (Combe *et al.*, 2016).

Salt sensitivity is an independent risk factor for adverse cardiovascular events in normotensive individuals and is a negative prognostic indicator for clinical progression towards hypertension (Craigie *et al.*, 2012). Current literature suggests that salt sensitivity is driven by abnormally large increases in renal retention of salt. It is thought that salt sensitive individuals have impaired renal ability to excrete salt load which usually causes them to retain more sodium than salt resistant individuals (Morris *et al.*, 2016).

6.3.3 Cosinor Analysis is required to inform a more detailed study of SVEP1$^{+/-}$ mice and blood pressure regulation

The current study uses relatively simple methods for analysis of the telemetry data. However, the most informative way to look at telemetry blood pressure data is cosinor analysis. Cosinor analysis allows calculation of the: 1. mesor -- the mean value based on the distribution of values across cycles of circadian rhythm and is calculated utilising the cosine function; 2. Acrophase - the time point in a cycle during which the cycle peaks- it is the upper part of the sine wave used to measure circadian patterns.; 3. Period – the duration of one circadian cycle. All of these analyses would identify differences in the pattern of blood pressure and heart rate over the circadian period. This would give a more extensive knowledge of any differences between the genotypes which are being masked by averaging the data over 24 hour periods or 6 hour running means.

6.3.4 SVEP1$^{+/-}$ mice have elevated heart rate compared to wildtype littermates

In the SVEP1$^{+/-}$ animals there was a significant increase in heart rate compared to wildtype littermates but no increase in systolic blood pressure. These effects are independent of diet. Elevated heart rate is often associated with elevated blood pressure (Morris *et al.*, 2016). A positive correlation exists between heart rate and peripheral blood pressure however, an inverse relationship has been reported between heart rate and central blood pressure (Morris *et al.*, 2016). In our mice it could be hypothesized that either the stroke volume or peripheral resistance could be altered to allow for the change in heart rate between the two genotypes without an associated increase in blood pressure. An increase in heart rate is associated with increased risk of development of hypertension and diabetes and all-cause mortality (Julius *et al.*, 2012). In the Atherosclerosis Risk in Communities (ARIC) study a higher heart rate and lower heart rate variability were both associated with increased risk of incident diabetes even when controlled for body mass index (BMI) and physical activity (Carnethon *et al.*, 2003). Hence, the increase in heart rate observed in the Svep1$^{+/-}$ mice may be clinically relevant. Heart rate was not reported in the CARDioGRAM consortium, but further studies should be performed to assess whether an increase in heart rate is observed in individuals with the 2702G variant as this could in part explain the increased risk of coronary heart disease in these individuals.

Heart rate is determined by the sinoarterial node which has input from both sympathetic and parasympathetic nervous systems (Sherwood, 2010). Many different factors influence heart rate such as physical activity, increased body temperature, catecholoamines, baroreceptors and thyroid hormones (Sherwood, 2010). Interestingly, data collected in the Phenomaster cages indicated that there was a non-significant trend towards an increase in activity in Svep1$^{+/-}$ compared with mice on normal chow, however this was not observed following a switch to a high fat diet (Fig 5.8). Further investigations into these and other parameters would be necessary to say definitively what is causing the increase in heart rate in the SVEP1$^{+/-}$mice. However, in Coombes et al they report that in normal salt in the dark active phase that C57BL6N animals have a heart rate of 650 beats per minute (bpm) which would suggest that both the SVEP1$^{+/-}$ animals and wildtype littermates have a lower than expected heart rate

compared to C57BL6N animals (Combe *et al.*, 2016). This could be due to the telemetry system not working to its optimum and failing to register every heartbeat.

6.3.5 Future Directions

Key future directions for this body of work include cosinor analysis to determine if there was a difference in circadian patterns between the genotypes in both systolic blood pressure and heart rate. In addition, it would be interesting to follow up the difference in heart rate in the SVEP1$^{+/-}$mice. The increase in heart rate suggests either stroke volume or peripheral resistance are changed in these mice therefore investigations into what is causing the increase in heart rate in these mice could be performed using laser Doppler. Given the concern regarding the fact that the telemetry system was not registering every heart rate, the use of an alternative measure of heart rate such as Doppler would be helpful.

6.3.6 Chapter Conclusions

No differences in blood pressure were identified between SVEP1$^{+/-}$animals and wildtype animals but a significant increase was seen in heart rate in the SVEP1$^{+/-}$ animals both on normal chow and high salt diet.

7. Discussion

The key focus of this thesis was to investigate the role of the SVEP1 gene in the pathophysiology of renal fibrosis, metabolism and blood pressure by utilising heterozygous *B6N(Cg)-Svep1$^{tm1b(EUCOMM)Hmgu}$/J* mice and wild-type littermates.

The major findings of this thesis were that SVEP1 is unlikely to play a critical role in renal fibrosis pathophysiology. SVEP1$^{+/-}$ mice did not show a marked alteration in glucose homeostasis however, there was a trend towards increased blood glucose which was significant at the 12 week time point. SVEP1$^{+/-}$ mice show no increases in blood pressure but have a significantly increased heart rate on both normal chow and high salt diet.

SVEP1 was largely under-represented in the literature, the exact function and cellular location was not known in the kidney. SVEP1 had been described as a cell-cell adhesion protein after being reported to bind α9β1 integrin (Sato-Nishiuchi *et al.*, 2012). Later papers described SVEP1 as playing a crucial role in epidermal differentiation- confocal microscopy showed that SVEP1 is normally expressed in the cytoplasm of basal and suprabasal epidermal cells (Samuelov *et al.*, 2017). Following downregulation of SVEP1 in zebrafish embryos, abnormal epidermal cell-cell adhesion and disadhesion were observed. SVEP1 has also been described to play a role in lymphatic vessel formation (Karpanen *et al.*, 2017) and lymphatic vessel remodelling (Morooka *et al.*, 2017) and deficiencies in lymphatic vessel development may explain the marked subcutaneous oedema observed in Svep1-/- mice and their embryonic lethality.

SVEP1 does not play a major role in the pathogenesis of renal fibrosis

After a literature review and bioinformatic analysis detailed in chapter 4 we hypothesized that the gene may play a role in renal fibrosis. This was mainly due to SVEP1 being highly expressed in mouse fibroblast cell lines and being first reported

in osteoblasts - suggesting that SVEP1 is expressed in cells of a mesenchymal lineage (Shur *et al.,* 2006). Human data from the Nephroseq database showed SVEP1 to be upregulated in human kidney disease- such as diabetic nephropathy and CKD. Furthermore, higher levels of expression of Svep1 in the kidney are associated with poor renal function and the expression of Svep1 correlates with other fibrotic genes, suggesting that *Svep1* was associated with fibrotic renal disease. In addition, rtPCR analysis suggested that renal *Svep1* gene expression was increased in the hypertensive mouse model and archived samples from obstructed murine kidneys, a model of renal fibrosis. Hence we hypothesised that Svep1 may be implicated in the pathogenesis of renal fibrosis. No previous work has been reported which corroborates SVEP1 as having a role in fibrosis in either the kidney or other organs which makes this thesis the primary evidence for the role of SVEP1 in renal fibrosis. From our data there was no difference between the $SVEP1^{+/-}$mice and wildtype mice therefore we concluded that SVEP1 does not play a major role in the pathophysiology of renal fibrosis, though the study was not powered to detect a smaller effect.

The role of SVEP1 in renal fibrosis could be clarified by further work *in vitro*- altering the fibrotic stimulus could identify if SVEP1 affects fibrosis independent of the TGFβ pathway. Alternative stimuli could focus on a hypertensive phenotype by addition of ANG II or PDGF-BB. This *in vitro* work will be greatly enhanced by the localisation of SVEP1 to specific cell types. Utilising a different model of fibrosis such as 5/6 nephrectomy model or the hypertensive mouse model described in chapter 3 could have identified if the UUO model of fibrosis was masking any potential positive effect of downregulating SVEP1. The literature suggests that no other studies investigating SVEP1 in fibrosis have been undertaken in other organs, it may be of interest to investigate the role of SVEP1 in other organs in relation to fibrosis such as the liver. However, SVEP1 is lowly expressed in the liver.

SVEP1- a gene with a potential role in metabolism

A landmark paper by Stitziel *et al* was published while work for this thesis was underway and this greatly influenced the direction of our work. This paper provided insights into the role of SVEP1 in blood pressure and metabolism but there is no mechanistic insight given by the authors- simply that the point mutation D2702G is

associated with both a small increase in blood pressure and an increase in type 2 diabetes risk in humans. This paper is the only evidence available which suggests a role for SVEP1 in metabolism and hypertension.

The metabolic phenotyping of the SVEP1$^{+/-}$ animals showed a significant increase in subcutaneous fat weight in SVEP1$^{+/-}$animals compared with wildtype littermates along with a significant increase in blood glucose at the 12 week GTT. There was a significant increase in insulin concentration from plasma at baseline in the SVEP1$^{+/-}$ animals. The results from the metabolic phenotyping, although not conclusive, hint towards a potential difference between the genotypes however, this study needs to be repeated and adequately powered to give definitive readouts.

SVEP1 hemizygosity causes no difference in blood pressure, but an increase in heart rate compared with wild-type animals

Blood pressure in the SVEP1$^{+/-}$animals and wildtype littermates was measured by telemetry- the gold standard for blood pressure analysis. This study was undertaken due to the evidence in humans that the point mutation D2702G caused an increase in systolic blood pressure of 0.94mmHg for each copy of the allele. No statistical difference was seen in blood pressure between the SVEP1$^{+/-}$animals and wildtype animals, although there was a trend towards a reduction in amplitude of peak to trough systolic blood pressure in the Svep1+/- animals.

The most unexpected finding from this thesis is the significant increase in heart rate in the SVEP1$^{+/-}$compared with wild-type littermates. Many different mechanisms contribute to heart rate regulation, including physical activity, stress, and thyroid status. Of note, data from the Phenomaster cages demonstrated a non-significant trend for increased activity in Svep1+/- mice, which is compatible with the increased heart rate. The cause for this increased physical activity is not clear, but would warrant further investigation if proved in sufficiently powered studies.

Elevated heart rate is often associated with elevated blood pressure (Reule and Drawz, 2012), however this was not evident in our animals. Elevated heart rate is also associated with increased risk of hypertension and increased risk of cardiovascular disease. Heart rate is not considered normally in choosing an antihypertensive therapy.

In the HARVEST study sustained elevations in heart rate over the course of the study were a strong predictor of developing hypertension necessitating pharmacological therapy (Palatini, 2011). The VALUE trial showed elevated baseline and in-trial heart rate was associated with increased risk for cardiovascular events and all-cause mortality- independent of achieved blood pressure (Julius *et al.*, 2012). A positive correlation exists between heart rate and peripheral blood pressure and an inverse relationship between heart rate and central blood pressure (Morris *et al.*, 2016).

Lack of experimental power

This body of work suffered from being underpowered. This was due to poor breeding when the SVEP1$^{+/-}$animals were imported from Jackson Laboratory. The mice were not breeding effectively so gaining the number of mice of the required age and genotype was a struggle for the investigations. Therefore, negative findings could simply be due to the experiments being underpowered. There was a small trend towards a difference in blood glucose between SVEP1$^{+/-}$and wild-type littermates and a significant increase at the 12 week time point suggesting that there may be subtle differences in blood glucose handling in the SVEP1$^{+/-}$ mice. An adequately powered repeat of the metabolism study would elucidate further if this was biologically significant. This trend is supported by the work done by Stitziel *et al* as it would suggest that our SVEP1$^{+/-}$animals are traveling towards insulin resistance which could account for the increased risk of type 2 diabetes seen in humans with the point mutation.

The blood pressure investigation was also underpowered due to the number of animals surviving to the end of the experiment post-surgery. There was no differences between genotype in blood pressure but a difference in heart rate was identified. This negative result in regards to blood pressure could be due to being underpowered as subtle differences are seen when BP data is analysed by peak/trough. Therefore, cosinor analysis will highlight if there is a potential difference and can be used to direct a future appropriately powered experiment.

SVEP1- unanswered questions

One of the most pressing unanswered questions from this thesis is what the human mutation- -D2702G does. One way to address that would be to model the polymorphism *in silico* to determine the effect the point mutation is having on the protein and thus the role this could be playing *in vivo*. Protein modelling could suggest whether the polymorphism is altering the function of the protein by altering protein folding. Utilising tools such as PolyPhen-2 software(Ramensky, 2002) and I-project hope software (Venselaar *et al.*, 2010) could potentially give some indication of the point mutations role.

Polyphen-2 software is used to analyse structural damage due to coding SNPs, it can show how the SNPs effect protein functionality by calculating a score on the basis of characterising the substitution site in reference to a known 3D protein structure (Ramensky, 2002). I-project hope is software that collects structural information from a series of sources and generates a 3D protein structure and analyse the impact of mutations on that protein structure (Venselaar *et al.*, 2010). Running the D2702G mutation through these programs could help elucidate potential mechanisms for the mutation conferring the increasing blood pressure and increased risk of T2D.

During this thesis it was not possible to determine the cellular localisation of SVEP1 in the kidney and answer where in the kidney SVEP1 was expressed. By staining utilising the antibody in the Sato-Nishuchi *et al* paper or by carrying out *in situ* hybridisation the cellular localisation could be identified.

To further address the role of SVEP1 in the kidney, a kidney only knockout mouse could be generated using a SIX2 driver, where SVEP1 would be deleted in the kidney only. This could negate the embryonic lethality of the homozygous knockout by only knocking out the gene in the kidney. An inducible knockout could also be generated to avoid the embryonic lethality of the homozygous knockout by knocking the gene out post development. It would be of interest to phenotype these knockout mice to determine the kidney and whole body phenotype of knocking out SVEP1 in adult mice. Of particular interest would be repeating both the blood pressure and metabolic investigations to determine if the knockout mice exhibit increases in blood pressure or increases in insulin resistance.

Due to the work carried out by Morooka *et al* detailing SVEP1's role in lymphatic development (Morooka *et al.*, 2017) it could be of interest to target the lymphatic system in an inducible knockout as it could be hypothesized that the role of SVEP1 in lymphatic development could be causing the embryonic lethality.

The international mouse phenotyping consortium (IMPC) has carried out phenotyping studies on the B6N(Cg)-Svep1$^{tm1b(EUCOMM)Hmgu}$/J mice in larger cohorts than we were able to produce. They state that the SVEP1 homozygous knockouts *in utero* showed severe oedema at embryonic day 18.5 which supports a lymphatic role for SVEP1.

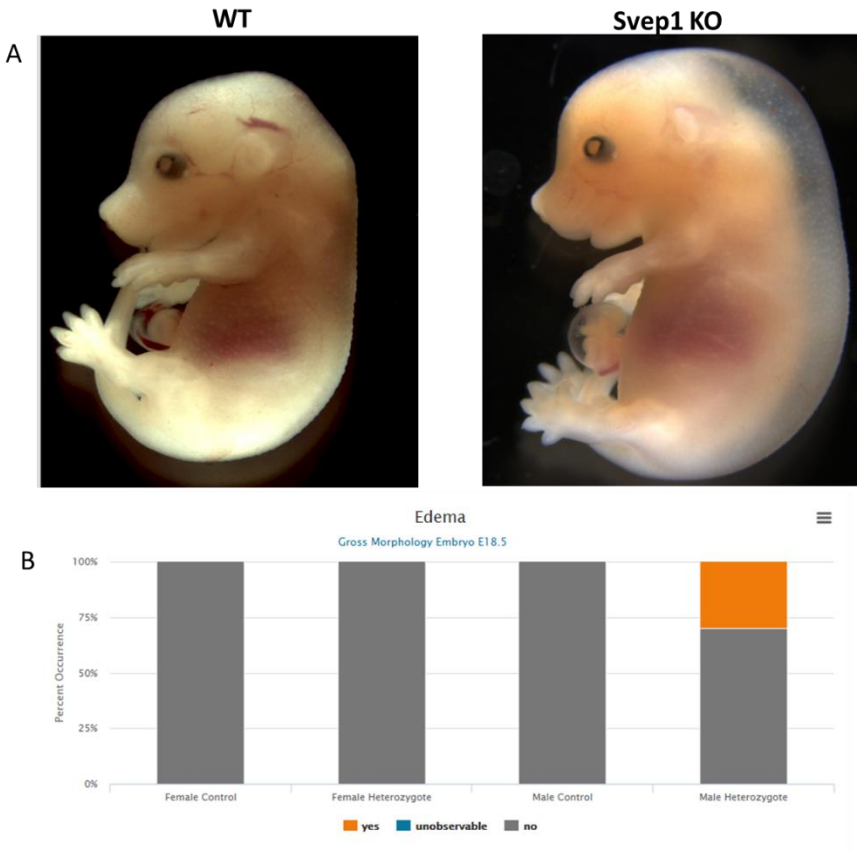

Figure 7 1 Severe oedema is present in Svep1$^{tm1b(EUCOMM)Hmgu}$ homozygous knockout mice (A) at embryonic day 18.5.
The Svep1$^{tm1b(EUCOMM)Hmgu}$ mice had an increase in oedema in the homozygous male animals (B) with 30% hemizygous mice exhibiting oedema at day E18.5.

The B6N(Cg)-Svep1$^{tm1b(EUCOMM)Hmgu}$/J hemizygous mice were reported by the IMPC to have decreased total body fat compared to controls.

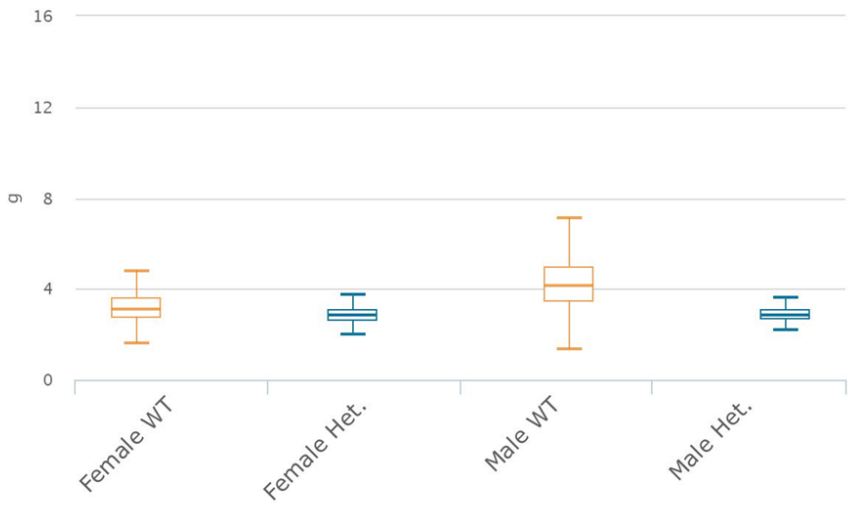

Figure 7 2 Fat mass of Svep1$^{tm1b(EUCOMM)Hmgu}$ mice.
DEXA scanning was carried out by the IMPC on Svep1$^{tm1b(EUCOMM)Hmgu}$ and controls to determine fat mass of the animals. Male hemizygous animals have a reduction in body fat compared to wildtype.

The IMPC also reported on the embryonic lethality of the homozygous phenotype-stating that no homozygous pups were born. This was corroborated in the breeding of our animals.

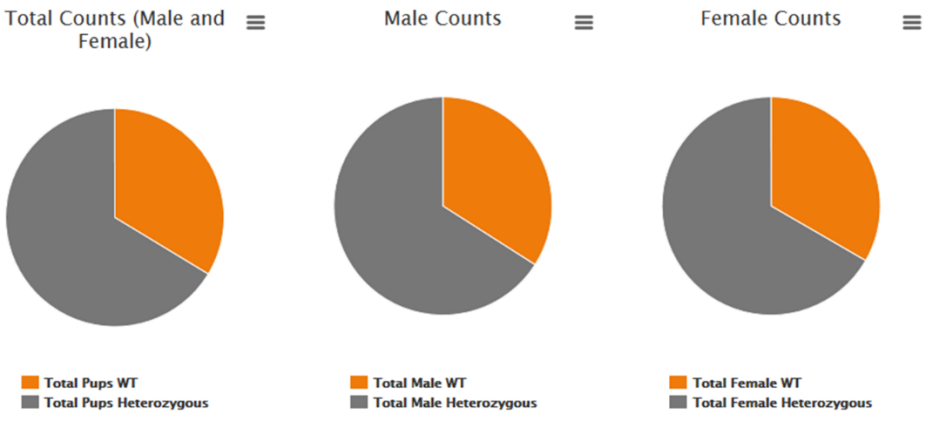

	WT	Hom	Het	Total
Male and Female	33	0	65	98
Male	16	0	31	47
Female	17	0	34	51

Figure 7 3 Svep1$^{tm1b(EUCOMM)Hmgu}$ homozygous mice are embryonic lethal. Svep1$^{tm1b(EUCOMM)Hmgu}$ homozygous mice were never found in live births showing that the homozygous mice must be embryonic lethal.

Utilising the available data from the IMPC, a decrease in adipose tissue of Svep1$^{tm1b(EUCOMM)Hmgu}$ is shown and this could be an interesting to investigate further

with respect to an altered metabolic phenotype. The severe oedema presented in the embryos at day 18.5 could corroborate the role of SVEP1 in lymphatic development (Morooka *et al.*, 2017), this could be another important role for the gene and another integral future direction for this thesis.

SVEP1- future directions

These investigations have just scratched the surface on the role of SVEP1 and its potential role in physiology.

Firstly determining the cellular localisation of SVEP1 in the kidney would be a priority in furthering this body of work. Work has begun in the $PDGFRB^{+}$ mice to isolate $PDGFRB^{+}$ cells to determine if SVEP1 is present in pericytes/fibroblasts. Further identification could be attempted by utilising the $SVEP1^{+/-}$ mice as these animals possess a β-galactosidase reporter. Utilising primers from Jackson Laboratories which have been used to genotype the animals it will be possible to identify which cell types once possessed SVEP1 expression due to the reporter highlighting where the SVEP1 allele has been excised. Immunohistochemistry (IHC) or immunofluorescence (IF) could be attempted utilising the antibody used in the Sato-Nishuchi *et al* paper which showed SVEP1 to stain interstitially- this antibody looks much more promising than commercially available antibodies which we have attempted to optimise without success. Once the cell types which express SVEP1 are identified this would direct a cell-specific knockout of SVEP1 which could be utilised to identify definitive roles for SVEP1 in particular organs and cell types.

The $SVEP1^{+/-}$ mouse exhibited reduced SVEP1 expression rather than a complete knockout. Due to only one allele of *Svep1* being removed this reduction might have been insufficient to cause a change in phenotype. A global knockout is embryonic lethal therefore an inducible knockout would be of great benefit to facilitating the studies knocking out SVEP1 in adults to further our knowledge of SVEP1's role in physiology.

In the $SVEP1^{+/-}$mouse a whole allele was removed which may have important functional differences to the point mutation described in humans in the Stitziel *et al* paper. An interesting future direction would be to introduce the human mutation into

the mouse to determine the effects the point mutation has on a fibrosis, metabolism and blood pressure in mice.

Secondly, repeating the metabolism study to obtain a firmer view on the role SVEP1 contributes to glucose handling and a potential metabolic phenotype. A repeat of this study described in chapter 5 would increase in n number of our study and highlight any significant findings which were missed due to the low n number in this thesis. It would also be of interest to repeat the TSE and TDNMR analysis after 12 weeks HFD. Altering the HFD model could also be achieved by breeding our SVEP1$^{+/-}$ animals to the db/db mouse model of obesity. This would identify any phenotype differences in obesity associated with having a reduction in SVEP1 expression.

Investigating the potential cardiac phenotype displayed by increased heart rate would be a larger study which would provide exciting insights into SVEP1 in cardiac physiology. A repeat of the telemetry analysis to increase n number once cosinor analysis has been carried out on the original data would show us if the differences in heart rate and peak/trough analysis are significant. Analysing the SVEP1$^{+/-}$ mice by cardiac ultrasound to assess heart rate and structural differences could be advantageous. Cardiac ultrasound is used routinely in the clinic and in rodent studies to analyse internal chamber size, pumping capacity and location/extent of any tissue damage. It is also possible from cardiac ultrasound to estimate heart function, cardiac output, ejection fraction and diastolic function- all of which would be useful in investigating a cardiac phenotype in the SVEP1$^{+/-}$ mice. If differences present it would be interesting to analyse adrenal steroid and catecholamine access along with beat-to-beat variation to assess sympathetic nerve activity.

Much remains to learn about this novel gene but clear implications in both human and mouse physiology have been uncovered by this thesis and the current literature on this gene. However, many questions remain to be answered.

8. References

Abe, R. *et al.* (2001) 'Peripheral Blood Fibrocytes: Differentiation Pathway and Migration to Wound Sites', *The Journal of Immunology*, 166(12), pp. 7556–7562. doi: 10.4049/jimmunol.166.12.7556.

Aitken, G. R. *et al.* (2014) 'Change in prevalence of chronic kidney disease in England over time: Comparison of nationally representative cross-sectional surveys from 2003 to 2010', *BMJ Open*, 4(9), pp. 1–12. doi: 10.1136/bmjopen-2014-005480.

Alsaad, K. O. and Herzenberg, A. M. (2007) 'Distinguishing diabetic nephropathy from other causes of glomerulosclerosis: An update', *Journal of Clinical Pathology*, 60(1), pp. 18–26. doi: 10.1136/jcp.2005.035592.

American Diabetes Association (2010) 'Diagnosis and classification of diabetes mellitus', *Diabetes Care*, 33(SUPPL. 1). doi: 10.2337/dc10-S062.

Anderson, S. *et al.* (2009) 'Prediction, Progression, and Outcomes of Chronic Kidney Disease in Older Adults', *Journal of the American Society of Nephrology*, 20(6), pp. 1199–1209. doi: 10.1681/ASN.2008080860.

Andresen, M. C. and Yang, M. Y. (1989) 'Rapid baroreceptor resetting is unaltered by chronic hypertension in rats.', *The American journal of physiology*, 256(4 Pt 2), pp. H1228-35. Available at: http://www.ncbi.nlm.nih.gov/pubmed/2705560.

Appel, L. *et al.* (1997) 'A Clinical Trial of Effects of Dietary Patterns on Blood Pressure', *New England Journal of Medicine*, 336(4641), pp. 1117–1124.

Auryan, S. and Itamar, R. (2008) 'Gender-specific care of diabetes mellitus: Particular considerations in the management of diabetic women', *Diabetes, Obesity and Metabolism*, 10(12), pp. 1135–1156. doi: 10.1111/j.1463-1326.2008.00896.x.

Bidani, A. K. and Griffin, K. A. (2004) 'Pathophysiology of hypertensive renal damage: Implications for therapy', *Hypertension*, 44(5), pp. 595–601. doi: 10.1161/01.HYP.0000145180.38707.84.

Böttinger, E. P. and Bitzer, M. (2002) ‘TGF-Beta signaling in renal disease’, *Journal of the American Society of Nephrology*, 13(10), pp. 2600–2610. doi: 10.1097/01.ASN.0000033611.79556.AE.

Bouzakri, K. and Zierath, H. A. K. and J. R. (2005) ‘Molecular Mechanisms of Skeletal Muscle Insulin Resistance in Type 2 Diabetes’, *Current Diabetes Reviews*, pp. 167–174. doi: http://dx.doi.org/10.2174/1573399054022785.

Breyer, M. D. (2004) ‘Mouse Models of Diabetic Nephropathy’, *Journal of the American Society of Nephrology*, 16(1), pp. 27–45. doi: 10.1681/ASN.2004080648.

Calhoun, D. A. *et al.* (2008) ‘Resistant Hypertension: Diagnosis, Evaluation, and Treatment: A Scientific Statement From the American Heart Association Professional Education Committee of the Council for High Blood Pressure Research’, *Circulation*, 117(25), pp. e510–e526. doi: 10.1161/CIRCULATIONAHA.108.189141.

Carlson, S. H. and Wyss, J. M. (2000) ‘Long-term telemetric recording of arterial pressure and heart rate in mice fed basal and high NaCl diets.’, *Hypertension*, 35(2), pp. E1–E5. doi: 10.1161/01.HYP.35.2.e1.

Carnethon, M. R. *et al.* (2003) ‘Prospective investigation of autonomic nervous system function and the development of type 2 diabetes: The atherosclerosis risk in communities study, 1987-1998’, *Circulation*, 107(17), pp. 2190–2195. doi: 10.1161/01.CIR.0000066324.74807.95.

Chevalier, R. L., Forbes, M. S. and Thornhill, B. A. (2009) ‘Ureteral obstruction as a model of renal interstitial fibrosis and obstructive nephropathy’, *Kidney International*. Elsevier Masson SAS, 75(11), pp. 1145–1152. doi: 10.1038/ki.2009.86.

Combe, R. *et al.* (2016) ‘How does circadian rhythm impact salt sensitivity of blood pressure in mice? A study in two close C57Bl/6 substrains’, *PLoS ONE*, 11(4), pp. 1–14. doi: 10.1371/journal.pone.0153472.

Conway, B. R. *et al.* (2012) ‘Hyperglycemia and Renin-Dependent Hypertension

Synergize to Model Diabetic Nephropathy', *Journal of the American Society of Nephrology*, 23(3), pp. 405–411. doi: 10.1681/ASN.2011060577.

Conway, B. R. *et al.* (2014) 'Tight blood glycaemic and blood pressure control in experimental diabetic nephropathy reduces extracellular matrix production without regression of fibrosis', *Nephrology*, 19(12), pp. 802–813. doi: 10.1111/nep.12335.

Craigie, E. *et al.* (2012) 'Failure to downregulate the epithelial sodium channel causes salt sensitivity in hsd11b2 heterozygote mice', *Hypertension*, 60(3), pp. 684–690. doi: 10.1161/HYPERTENSIONAHA.112.196410.

Crowley, S. D. *et al.* (2006) 'Angiotensin II causes hypertension and cardiac hypertrophy through its receptors in the kidney', *Proceedings of the National Academy of Sciences*, 103(47), pp. 17985–17990. doi: 10.1073/pnas.0605545103.

Daneman, D. (2006) 'Type 1 diabetes', *The Lancet*, 367(9513), pp. 847–858. doi: 10.1016/S0140-6736(06)68341-4.

Debelle, F. D. *et al.* (2002) 'Aristolochic acids induce chronic renal failure with interstitial fibrosis in salt-depleted rats.', *Journal of the American Society of Nephrology : JASN*, 13(2), pp. 431–6. Available at: http://www.ncbi.nlm.nih.gov/pubmed/11805172.

DeFronzo, R. A. (1981) 'The effect of insulin on renal sodium metabolism - A review with clinical implications', *Diabetologia*, 21(3), pp. 165–171. doi: 10.1007/BF00252649.

Dickinson, M. E. *et al.* (2016) 'High-throughput discovery of novel developmental phenotypes', *Nature*. Nature Publishing Group, 537(7621), pp. 508–514. doi: 10.1038/nature19356.

Dinneen SF and Gerstein HC (1997) 'The association of microalbuminuria and mortality in non—insulin-dependent diabetes mellitus: A systematic overview of the literature', *Archives of Internal Medicine*, 157(13), pp. 1413–1418. Available at: http://dx.doi.org/10.1001/archinte.1997.00440340025002.

Duffield, J. S. (2014) ‘Review series Cellular and molecular mechanisms in kidney fibrosis’, *Journal of Clinical Investigation*, 124(6), pp. 2299–2306. doi: 10.1172/JCI72267.a.

Eddy, A. A. *et al.* (2012) ‘Investigating mechanisms of chronic kidney disease in mouse models’, *Pediatric Nephrology*, 27(8), pp. 1233–1247. doi: 10.1007/s00467-011-1938-2.

Eddy, A. a (2000) ‘Molecular basis of renal fibrosis’, *Pediatric Nephrology*, 15(3–4), pp. 290–301. doi: 10.1007/s004670000461.

Edwards, E. W. *et al.* (2014) ‘Top 10 landmark studies in hypertension’, *Journal of the American Society of Hypertension*. Elsevier, 8(6), pp. 437–447. doi: 10.1016/J.JASH.2014.03.333.

Efstratiadis, G. *et al.* (2009) ‘Renal fibrosis.’, *Hippokratia*, 13(4), pp. 224–9. Available at: http://www.pubmedcentral.nih.gov/articlerender.fcgi?artid=2776335&tool=pmcentrez&rendertype=abstract.

Evans, L. C. *et al.* (2016) ‘Vasodysfunction That Involves Renal Vasodysfunction, Not Abnormally Increased Renal Retention of Sodium, Accounts for the Initiation of Salt-Induced Hypertension’, *Circulation*, 133(4), pp. 1–14. doi: 10.1371/journal.pone.0153472.

Farris, A. B. and Colvin, R. B. (2013) ‘Renal Interstitial Fibrosis: Mechanisms and Evaluation in: Current Opinion in Nephrology and Hypertension’, *Current opinion in nephrology and hypertension*, 21(3), pp. 289–300. doi: 10.1097/MNH.0b013e3283521cfa.Renal.

Feng, D. *et al.* (2011) ‘High-fat diet-induced adipocyte cell death occurs through a cyclophilin D intrinsic signaling pathway independent of adipose tissue inflammation’, *Diabetes*, 60(8), pp. 2134–2143. doi: 10.2337/db10-1411.

Fukagawa, M. *et al.* (1999) ‘Chronic progressive interstitial fibrosis in renal disease--are there novel pharmacological approaches?’, *Nephrology, dialysis,*

transplantation : official publication of the European Dialysis and Transplant Association - European Renal Association, 14(12), pp. 2793–2795. doi: 10.1093/ndt/14.12.2793.

Fullerton, B. *et al.* (2016) 'Intensive glucose control versus conventional glucose control for type 1 diabetes mellitus', *Cochrane Database of Systematic Reviews*, (2), p. CD009122. doi: 10.1002/14651858.CD009122.pub2.www.cochranelibrary.com.

Furman, B. L. (2015) 'Streptozotocin-Induced Diabetic Models in Mice and Rats', *Current protocols in pharmacology / editorial board, S.J. Enna (editor-in-chief) ... [et al.]*, 70(September 2015), p. 5.47.1-5.47.20. doi: 10.1002/0471141755.ph0547s70.

Ghazi, L. and Drawz, P. (2017) 'Advances in understanding the renin-angiotensin-aldosterone system (RAAS) in blood pressure control and recent pivotal trials of RAAS blockade in heart failure and diabetic nephropathy', *F1000Research*, 6(0), p. 297. doi: 10.12688/f1000research.9692.1.

Gilbert, E. R., Fu, Z. and Liu, D. (2011) 'Development of a nongenetic mouse model of type 2 diabetes', *Experimental Diabetes Research*, 2011. doi: 10.1155/2011/416254.

Gilgès, D. *et al.* (2000) 'Polydom: a secreted protein with pentraxin, complement control protein, epidermal growth factor and von Willebrand factor A domains.', *The Biochemical journal*, 352 Pt 1, pp. 49–59. doi: 10.1042/0264-6021:3520049.

Goossens, G. H. (2008) 'The role of adipose tissue dysfunction in the pathogenesis of obesity-related insulin resistance', *Physiology and Behavior*, 94(2), pp. 206–218. doi: 10.1016/j.physbeh.2007.10.010.

Gross, J. L. *et al.* (2005) 'Diabetic Nephropathy: Diagnosis, Prevention, and Treatment', *Diabetes Care*, 28, pp. 176–188. doi: 10.2337/diacare.28.1.164.

Gupta, R. *et al.* (2003) 'Mechansims contributing to the development of type 2 diabetes', 44(0), pp. 12–16.

Guyton, A. C. *et al.* (1972) ‘Arterial pressure regulation. Overriding dominance of the kidneys in long-term regulation and in hypertension’, *The American Journal of Medicine*, 52(5), pp. 584–594. doi: 10.1016/0002-9343(72)90050-2.

Hajer, G. R., Van Haeften, T. W. and Visseren, F. L. J. (2008) ‘Adipose tissue dysfunction in obesity, diabetes, and vascular diseases’, *European Heart Journal*, 29(24), pp. 2959–2971. doi: 10.1093/eurheartj/ehn387.

Han, W. K. *et al.* (2002) ‘Kidney Injury Molecule-1 (KIM-1): A novel biomarker for human renal proximal tubule injury’, *Kidney International*, 62(1), pp. 237–244. doi: 10.1046/j.1523-1755.2002.00433.x.

Harada, K. *et al.* (1998) ‘Pressure overload induces cardiac hypertrophy in angiotensin II type 1A receptor knockout mice.’, *Circulation*, 97, pp. 1952–1959. doi: 10.1161/01.CIR.97.19.1952.

Hartner, A. *et al.* (2003) ‘Strain differences in the development of hypertension and glomerular lesions induced by deoxycorticosterone acetate salt in mice’, *Nephrology Dialysis Transplantation*, 18(10), pp. 1999–2004. doi: 10.1093/ndt/gfg299.

Harvey, N. L. *et al.* (2005) ‘Lymphatic vascular defects promoted by Prox1 haploinsufficiency cause adult-onset obesity’, *Nature Genetics*, 37(10), pp. 1072–1081. doi: 10.1038/ng1642.

Hattersley, A. T. and Patel, K. A. (2017) ‘Precision diabetes: learning from monogenic diabetes’, *Diabetologia*. Diabetologia, 60(5), pp. 769–777. doi: 10.1007/s00125-017-4226-2.

Hesketh, E. E. *et al.* (2014) ‘A Murine Model of Irreversible and Reversible Unilateral Ureteric Obstruction’, *Journal of Visualized Experiments*, (94), pp. 1–6. doi: 10.3791/52559.

Higgins, J. P. T. *et al.* (2004) ‘Gene expression in the normal adult human kidney assessed by complementary DNA microarray’, *Molecular biology of the cell*, 15(2), p. 649—656. doi: 10.1091/mbc.e03-06-0432.

Horikawa, Y. *et al.* (1997) ‘Mutation in hepatocyte nuclear factor-1 beta gene (TCF2) associated with MODY.’, *Nature genetics*. United States, pp. 384–385. doi: 10.1038/ng1297-384.

Humphreys, B. D. *et al.* (2010) ‘Fate tracing reveals the pericyte and not epithelial origin of myofibroblasts in kidney fibrosis’, *American Journal of Pathology*. American Society for Investigative Pathology, 176(1), pp. 85–97. doi: 10.2353/ajpath.2010.090517.

Iredale, J. P. (2007) ‘Models of liver fibrosis: Exploring the dynamic nature of inflammation and repair in a solid organ’, *Journal of Clinical Investigation*, 117(3), pp. 539–548. doi: 10.1172/JCI30542.

Ivy, J. R. *et al.* (2016) ‘Glucocorticoids induce nondipping blood pressure by activating the thiazide-sensitive cotransporter’, *Hypertension*, 67(5), pp. 1029–1037. doi: 10.1161/HYPERTENSIONAHA.115.06977.

James, P. *et al.* (2014) ‘2014 evidence-based guideline for the management of high blood pressure in adults: Report from the panel members appointed to the eighth joint national committee (jnc 8)’, *JAMA*, 311(5), pp. 507–520. Available at: http://dx.doi.org/10.1001/jama.2013.284427.

Jenkinson, S. E. *et al.* (2012) ‘The limitations of renal epithelial cell line HK-2 as a model of drug transporter expression and function in the proximal tubule.’, *Pflügers Archiv : European journal of physiology*, 464(6), pp. 601–611. doi: 10.1007/s00424-012-1163-2.

Ju, W. *et al.* (2015) ‘Tissue transcriptome-driven identification of epidermal growth factor as a chronic kidney disease biomarker’, *Science Translational Medicine*, 7(316), p. 316ra193 LP-316ra193. Available at: http://stm.sciencemag.org/content/7/316/316ra193.abstract.

Julius, S. *et al.* (2012) ‘Usefulness of heart rate to predict cardiac events in treated patients with high-risk systemic hypertension’, *American Journal of Cardiology*. Elsevier Inc., 109(5), pp. 685–692. doi: 10.1016/j.amjcard.2011.10.025.

Kalluri, R. and Neilson, E. G. (2003) ‘Epithelial-mesenchymal transition and its implications for fibrosis.pdf’, *Journal of Clinical Investigation*, 112(12), pp. 1776–1784. doi: 10.1172/JCI200320530.

Karpanen, T. *et al.* (2017) ‘An Evolutionarily Conserved Role for Polydom/Svep1 during Lymphatic Vessel Formation’, *Circulation Research*, 120(8), pp. 1263–1275. doi: 10.1161/CIRCRESAHA.116.308813.

Kawada, N. *et al.* (2002) ‘A mouse model of angiotensin II slow pressor response: role of oxidative stress.’, *Journal of the American Society of Nephrology : JASN*, 13(12), pp. 2860–8. doi: 10.1097/01.ASN.0000035087.11758.ED.

Kilkenny, C. *et al.* (2010) ‘Improving Bioscience Research Reporting: The ARRIVE Guidelines for Reporting Animal Research’, *PLoS Biology*. Public Library of Science, 8(6), p. e1000412. doi: 10.1371/journal.pbio.1000412.

Kim, S. and Iwao, H. (2000) ‘Molecular and Cellular Mechanisms of Angiotensin II-Mediated Cardiovascular and Renal Diseases’, *Pharmacological Reviews*, 52(1), pp. 1–4.

Kirchhoff, F. *et al.* (2008) ‘Rapid development of severe end-organ damage in C57BL/6 mice by combining DOCA salt and angiotensin II’, *Kidney International*, 73(5), pp. 643–650. doi: 10.1038/sj.ki.5002689.

Kitada, M., Ogura, Y. and Koya, D. (2016) ‘Rodent models of diabetic nephropathy: Their utility and limitations’, *International Journal of Nephrology and Renovascular Disease*, 9, pp. 279–290. doi: 10.2147/IJNRD.S103784.

Kokosar, M. *et al.* (2016) ‘Epigenetic and Transcriptional Alterations in Human Adipose Tissue of Polycystic Ovary Syndrome’, *Scientific Reports*. Nature Publishing Group, 6(September 2015), pp. 1–18. doi: 10.1038/srep22883.

Laffer, C. L. *et al.* (2016) ‘Hemodynamics and Salt-and-Water Balance Link Sodium Storage and Vascular Dysfunction in Salt-Sensitive Subjects’, *Hypertension*, 68(1), pp. 195–203. doi: 10.1161/HYPERTENSIONAHA.116.07289.

Leask, A. and Abraham, D. J. (2004) ‘TGF-β signaling and the fibrotic response’, *The FASEB Journal*. Federation of American Societies for Experimental Biology, 18(7), pp. 816–827. doi: 10.1096/fj.03-1273rev.

Lebleu, V. S. *et al.* (2013) ‘Origin and function of myofibroblasts in kidney fibrosis’, *Nature Medicine*, 19(8), pp. 1047–1053. doi: 10.1038/nm.3218.

Lee, V. W. and Harris, D. C. (2011) ‘Adriamycin nephropathy: A model of focal segmental glomerulosclerosis’, *Nephrology*, 16(1), pp. 30–38. doi: 10.1111/j.1440-1797.2010.01383.x.

Leenen, F. H. H. *et al.* (2015) ‘Enhanced expression of epithelial sodium channels causes salt-induced hypertension in mice through inhibition of the α2-isoform of Na+, K+-ATPase’, *Physiological Reports*, 3(5), pp. 1–9. doi: 10.14814/phy2.12383.

Leiter, E. H. (1993) ‘The NOD Mouse: A Model for Analyzing the Interplay Between Heredity and Environment in Development of Autoimmune Disease’, *Insitiute for Laboratory Animal Research*, 35(1).

Leong, X. F., Ng, C. Y. and Jaarin, K. (2015) ‘Animal Models in Cardiovascular Research: Hypertension and Atherosclerosis’, *BioMed Research International*, 2015(ii). doi: 10.1155/2015/528757.

Lewington S, Clarke R, Qizilbash N, Peto R, C. R. P. S. C. (2002) ‘Age-specific relevance of usual blood pressure to vascular mortality: a meta-analysis of individual data for one million adults in 61 prospective studies’, *The Lancet*. Elsevier, 360(9349), pp. 1903–1913. doi: 10.1016/S0140-6736(02)11911-8.

Lifton, R., Gharavi, A. and Geller, D. (2001) ‘Molecular Mechanisms of Human Hypertension’, *Cell*, 104, pp. 545–556. doi: 10.1016/S0092-8674(01)00241-0.

Lin, S. L. *et al.* (2008) ‘Pericytes and perivascular fibroblasts are the primary source of collagen-producing cells in obstructive fibrosis of the kidney’, *American Journal of Pathology*. American Society for Investigative Pathology, 173(6), pp. 1617–1627. doi: 10.2353/ajpath.2008.080433.

Dahl, L and Love, R. (1954) ‘Evidence for relationship between sodium (chloride) intake and human essential hypertension’, *A.M.A. Archives of Internal Medicine*, 94(4), pp. 525–531. Available at: http://dx.doi.org/10.1001/archinte.1954.00250040017003.

Lloyd, A. *et al.* (2010) ‘Relation Between Kidney Function, Proteinuria, and Adverse Outcomes’, *Journal of American Medical Association*, 303(5), pp. 423–429.

Long, D. A. *et al.* (2008) ‘Angiopoietin-1 therapy enhances fibrosis and inflammation following folic acid-induced acute renal injury’, *Kidney International*. Elsevier Masson SAS, 74(3), pp. 300–309. doi: 10.1038/ki.2008.179.

Ma, J.-C. *et al.* (2016) ‘Tenascin-C promotes migration of hepatic stellate cells and production of type I collagen’, *Bioscience, Biotechnology, and Biochemistry*. Taylor & Francis, 8451(April), pp. 1–8. doi: 10.1080/09168451.2016.1165600.

Ma, L. J. and Fogo, A. B. (2003) ‘Model of robust induction of glomerulosclerosis in mice: Importance of genetic background’, *Kidney International*, 64(1), pp. 350–355. doi: 10.1046/j.1523-1755.2003.00058.x.

Mancia, G. *et al.* (2013) ‘2013 ESH/ESC guidelines for the management of arterial hypertension: The Task Force for the management of arterial hypertension of the European Society of Hypertension (ESH) and of the European Society of Cardiology (ESC)’, *European Heart Journal*, 34(28), pp. 2159–2219. doi: 10.1093/eurheartj/eht151.

Mariani, L. H. *et al.* (2018) ‘Interstitial fibrosis scored on whole-slide digital imaging of kidney biopsies is a predictor of outcome in proteinuric glomerulopathies’, *Nephrology Dialysis Transplantation*, 33(2), pp. 310–318. doi: 10.1093/ndt/gfw443.

Mathieu, C., Gillard, P. and Benhalima, K. (2017) ‘Insulin analogues in type 1 diabetes mellitus: Getting better all the time’, *Nature Reviews Endocrinology*, 13(7), pp. 385–399. doi: 10.1038/nrendo.2017.39.

Mattson, D. L. (1998) ‘Long-term measurement of arterial blood pressure in conscious mice’, *The American physiological Soceity*, pp. 564–570.

Meigs, J. B. *et al.* (2003) 'The Natural History of Progression From Normal Glucose Tolerance to Type 2 Diabetes in the Baltimore Longitudinal Study of Aging', *Diabetes*, 52(16), pp. 1475–1484. doi: 10.2337/diabetes.52.6.1475.

Meng, X. M., Nikolic-Paterson, D. J. and Lan, H. Y. (2014) 'Inflammatory processes in renal fibrosis', *Nature Reviews Nephrology*. Nature Publishing Group, 10(9), pp. 493–503. doi: 10.1038/nrneph.2014.114.

Mennuni, S. *et al.* (2014) 'Hypertension and kidneys: Unraveling complex molecular mechanisms underlying hypertensive renal damage', *Journal of Human Hypertension*. Nature Publishing Group, 28(2), pp. 74–79. doi: 10.1038/jhh.2013.55.

Morooka, N. *et al.* (2012) 'p53 Localization at Centrosomes during Mitosis and Postmitotic Checkpoint Are ATM-dependent and Require Serine 15 Phosphorylation', *Molecular biology of the cell*. Elsevier Inc., 15(12), pp. 3751–3737. doi: 10.1091/mbc.E03.

Morooka, N. *et al.* (2017) 'Polydom Is an Extracellular Matrix Protein Involved in Lymphatic Vessel Remodeling', *Circulation Research*, 120(8), pp. 1276–1288. doi: 10.1161/CIRCRESAHA.116.308825.

Morris, R. C. *et al.* (2016) 'Vasodysfunction That Involves Renal Vasodysfunction, Not Abnormally Increased Renal Retention of Sodium, Accounts for the Initiation of Salt-Induced Hypertension', *Circulation*, 133(9), pp. 881–893. doi: 10.1161/CIRCULATIONAHA.115.017923.

Mozaffarian, D. *et al.* (2014) 'Global Sodium Consumption and Death from Cardiovascular Causes', *New England Journal of Medicine*, 371(7), pp. 624–634. doi: 10.1056/NEJMoa1304127.

Nahas, M. El and Bello, (2010) 'Chronic kidney disease: the global challenge.', *Lancet*, 365(9456), pp. 331–40. doi: 10.1016/S0140-6736(05)17789-7.

National Kidney Foundation (2002) *K/DOQI Clinical Practice Guidelines for Chronic Kidney Disease: Evaluation, Clasification and Stratification*, *Am J Kidney Dis.* doi: 10.1634/theoncologist.2011-S2-45.

Navar, L. G. (2005) ‘The role of the kidneys in hypertension.’, *Journal of clinical hypertension (Greenwich, Conn.)*, 7(9), pp. 542–549. doi: 10.1111/j.1524-6175.2005.04130.x.

Nie, S. *et al.* (2017) ‘Are There Modifiable Risk Factors to Improve AKI?’, *BioMed Research International*, 2017. doi: 10.1155/2017/5605634.

O’Connor, N. R. and Kumar, P. (2012) ‘Conservative Management of End-Stage Renal Disease without Dialysis: A Systematic Review’, *Journal of Palliative Medicine*, 15(2), pp. 228–235. doi: 10.1089/jpm.2011.0207.

Ohta, Y. *et al.* (2010) ‘Long-term compliance of salt restriction and blood pressure control status in hypertensive outpatients’, *Clinical and Experimental Hypertension*, 32(4), pp. 234–238. doi: 10.3109/10641963.2010.491888.

Omuru, M. *et al.* (2004) ‘Prospective Study on the Prevalence of Secondary Hypertension among Hypertensive Patients Visiting a General Outpatient Clinic in Japan’, *Hypertension Research*, 27(3), pp. 193–202. doi: 10.1291/hypres.27.193.

Palatini, P. (2011) ‘Role of elevated heart rate in the development of cardiovascular disease in hypertension’, *Hypertension*, 58(5), pp. 745–750. doi: 10.1161/HYPERTENSIONAHA.111.173104.

Poosti, F. *et al.* (2015) ‘Precision-cut kidney slices (PCKS) to study development of renal fibrosis and efficacy of drug targeting *ex vivo*’, *Disease Models & Mechanisms*, 8(10), pp. 1227–1236. doi: 10.1242/dmm.020172.

Rajagopalan, S. *et al.* (2002) ‘Angiotensin II-mediated hypertension in the rat increases vascular superoxide production via membrane NADH/NADPH oxidase activation: Contribution to alterations of vasomotor tone’, *Ultrasonics*, 97(1), pp. 1819–1822. doi: 10.1371/journal.pbio.1000412.

Ramensky, V. (2002) ‘Human non-synonymous SNPs: server and survey’, *Nucleic Acids Research*, 30(17), pp. 3894–3900. doi: 10.1093/nar/gkf493.

Regulski, M. osz *et al.* (2015) ‘Chemistry and Pharmacology of Angiotensin-

Converting Enzyme Inhibitors', *Current Pharmaceutical Design*, pp. 1764–1775. doi: http://dx.doi.org/10.2174/138161282066614111216001 3.

Reule, S. and Drawz, P. (2012) 'Heart rate and blood pressure: any possible implications for management of hypertension?', *Current hypertension reports*, 14(6), pp. 478–84. doi: 10.1007/s11906-012-0306-3.Heart.

Rich, S. S. (2006) 'Genetics of Diabetes and Its Complications', *Journal of the American Society of Nephrology*, 17(2), pp. 353–360. doi: 10.1681/ASN.2005070770.

Samuelov, L. *et al.* (2017) 'SVEP1 plays a crucial role in epidermal differentiation', *Experimental Dermatology*, 26(5), pp. 423–430. doi: 10.1111/exd.13256.

Sato-Nishiuchi, R. *et al.* (2012) 'Polydom/SVEP1 is a ligand for integrin alpha 9 beta 1', *Journal of Biological Chemistry*, 287(30), pp. 25615–25630. doi: 10.1074/jbc.M112.355016.

Sherwood, L. (2010) *Human Physiology: From cells to systems 7th Edition*.

Shur, I. *et al.* (2006) 'Molecular and cellular characterization of SEL-OB/SVEP1 in osteogenic cells in vivo and in vitro', *Journal of Cellular Physiology*, 206(2), pp. 420–427. doi: 10.1002/jcp.20497.

Soldatos, G. and Cooper, M. E. (2008) 'Diabetic nephropathy: Important pathophysiologic mechanisms', *Diabetes Research and Clinical Practice*, 82(SUPPL. 1), pp. 75–79. doi: 10.1016/j.diabres.2008.09.042.

Stefanska, A. *et al.* (2016) 'Human kidney pericytes produce renin', *Kidney International*. Elsevier Inc, 90(6), pp. 1251–1261. doi: 10.1016/j.kint.2016.07.035.

Stitziel, N. *et al.* (2016) 'Coding Variation in ANGPTL4, LPL, and SVEP1 and the Risk of Coronary Disease', *New England Journal of Medicine*, 374(12), pp. 1134–1144. doi: 10.1056/NEJMoa1507652.

Sullivan, J. M. *et al.* (1987) 'Hemodynamic characteristics of sodium-sensitive

human subjects', *Hypertension*, 9(4), pp. 398–406. doi: 10.1161/01.HYP.9.4.398.

Sun, Y. B. Y. *et al.* (2016) 'The origin of renal fibroblasts/myofibroblasts and the signals that trigger fibrosis', *Differentiation*. Elsevier, 92(3), pp. 102–107. doi: 10.1016/j.diff.2016.05.008.

Tam, F. (1999) 'Development of scarring and renal failure in a rat model of crescentic glomerulonephritis', *Nephrology Dialysis Transplantation*, 14(7), pp. 1658–1666. doi: 10.1093/ndt/14.7.1658.

Tattersall, R. B. (1974) 'Mild familial diabetes with dominant inheritance.', *The Quarterly journal of medicine*. England, 43(170), pp. 339–357.

Tirschwell, D. (2001) 'Combined therapy with indapamide and perindopril but not perindopril alone reduced the risk for recurrent stroke.', *ACP journal club*, 136(2), p. 51. Available at: http://www.ncbi.nlm.nih.gov/pubmed/11874276.

Townsend, R. R. (2015) 'Management of hypertension in chronic kidney disease', *Nature Reviews Nephrology*, 8(6), pp. 1–9. doi: 10.1007/s11906-006-0029-4.

Turner, R. *et al.* (1998) 'Tight blood pressure control and risk of macrovascular and microvascular complications in type 2 diabetes: UKPDS 38', *Bmj*, 217, pp. 703–713. doi: 10.1016/S0140-6736(98)07037-8.

Venselaar, H. *et al.* (2010) 'Protein structure analysis of mutations causing inheritable diseases. An e-Science approach with life scientist friendly interfaces', *BMC Bioinformatics*, 11. doi: 10.1186/1471-2105-11-548.

Vollmer, R. R. *et al.* (2006) 'Sodium ingestion in oxytocin knockout mice', *Experimental Neurology*, 202(2), pp. 441–448. doi: 10.1016/j.expneurol.2006.07.006.

Wang, Y. and Oliver, G. (2010) 'Current views on the function of the lymphatic vasculature in health and disease', *Genes and Development*, 24(19), pp. 2115–2126. doi: 10.1101/gad.1955910.

Weinberger, M. H. *et al.* (1986) ‘Definitions and characteristics of sodium sensitivity and blood pressure resistance.’, *Hypertension*, 8(6 Pt 2), pp. II127-I134. doi: 10.1161/01.HYP.8.6.

Weir, M. R. and Dzau, V. J. (1999) ‘The Renin-Angiotensin-Aldosterone System: A Specific Target for Hypertension Management’, *American Journal of Hypertension*, 12(12), p. 205S–213S. doi: 10.1016/S0895-7061(99)00103-X.

Weyer C, Antonio Tataranni P, Bogardus C, P. R. (2001) ‘Insulin Resistance and Insulin Secretory Dysfunction Are Independent Predictors of Worsening of Glucose Tolerance During Each Stage of Type 2 Diabetes’, *World Health*, 24(1), pp. 89–94.

Woroniecka, K. I. *et al.* (2011) ‘Transcriptome analysis of human diabetic kidney disease’, *Diabetes*, 60(9), pp. 2354–2369. doi: 10.2337/db10-1181.

Xu, Q. *et al.* (2007) ‘In vitro models of TGF- beta -induced fibrosis suitable for high-throughput screening of antifibrotic agents’, *American Journal of Physiology. Renal Physiology*, 293, pp. F631–F640. doi: 10.1152/ajprenal.00379.2006.

Yasuda, Y. *et al.* (2006) ‘Gene expression profiling analysis in nephrology: Towards molecular definition of renal disease’, *Clinical and Experimental Nephrology*, 10(2), pp. 91–98. doi: 10.1007/s10157-006-0421-z.

Yaturu, S. (2011) ‘Obesity and type 2 diabetes’, *Journal of Diabetes Mellitus*, 01(04), pp. 79–95. doi: 10.4236/jdm.2011.14012.

Yoshioka, M. *et al.* (1997) ‘A novel locus, Mody4, distal to D7Mit189 on chromosome 7 determines early-onset NIDDM in nonobese C57BL/6 (Akita) mutant mice’, *Diabetes*, 46(5), pp. 887–894. doi: 10.2337/diab.46.5.887.

Zacchia, M. (2018) ‘The importance of the thick ascending limb of Henle ’ s loop in renal physiology and pathophysiology’, *International Journal of Nephrology and Renovascular Disease 2018*, 11, pp. 81–92.

Zhang, B. *et al.* (2018) ‘Protective role of AgRP neuron’s PDK1 against salt-induced hypertension’, *Biochemical and Biophysical Research Communications*. Elsevier

Ltd, 500(4), pp. 910–916. doi: 10.1016/j.bbrc.2018.04.192.

Zoccali, C. *et al.* (2017) ‘Chronic Fluid Overload and Mortality in ESRD’, *Journal of the American Society of Nephrology*, (May), p. ASN.2016121341. doi: 10.1681/ASN.2016121341.